

# In-Situ Burning of Crude Oil on Water



A Study on the Fire Dynamics and Fire Chemistry in an Arctic Context

Laurens van Gelderen

PhD Thesis

Department of Civil Engineering  
2017

DTU Civil Engineering Report R-270

# *In-Situ* Burning of Crude Oil on Water

*A study on the fire dynamics and fire chemistry in an Arctic context*

Laurens van Gelderen

Ph.D. Thesis

Technical University Denmark

Department of Civil Engineering

January 2017

Copyright ©, Laurens van Gelderen, 2017

# Preface

This thesis is submitted for the degree of Doctor of Philosophy at the Technical University of Denmark. The Ph.D. study was conducted between January 2014 and December 2016 at the Department of Civil Engineering, under the supervision of:

**Grunde Jomaas**, principal supervisor, Associate Professor, Department of Civil Engineering, Technical University of Denmark, Denmark

**Janne Fritt-Rasmussen**, co-supervisor, Ph.D., Department of Bioscience, Aarhus University, Denmark

**Ali Rangwala**, co-supervisor, Associate Professor, Department of Fire Protection Engineering, Worcester Polytechnic Institute, USA

The following articles have been published or submitted as part of this Ph.D. study:

1. Van Gelderen, L., Brogaard, N. L., Sørensen, M. X., Fritt-Rasmussen, J., Rangwala, A. S., Jomaas, G., 2015. Importance of the slick thickness for effective *in-situ* burning of crude oil. *Fire Safety Journal*, 78: 1-9. DOI: [dx.doi.org/10.1016/j.firesaf.2015.07.005](https://doi.org/10.1016/j.firesaf.2015.07.005)
2. Van Gelderen, L., Malmquist, L.M.V., Jomaas, G., 2015. Crude oil burning mechanisms: A conceptual model review. In *Proceedings of the Thirty-eighth Arctic and Marine Oilspill Program (AMOP) Technical Seminar*, Environment Canada, Vancouver, B.C., p. 385-400.
3. Van Gelderen, L., Malmquist, L.M.V., Jomaas, G., 2017. Vaporization order and burning efficiency of crude oils during *in-situ* burning on water. *Fuel*, 191: 528-537. DOI: [dx.doi.org/10.1016/j.fuel.2016.11.109](https://doi.org/10.1016/j.fuel.2016.11.109)
4. Van Gelderen, L., Fritt-Rasmussen, J., Jomaas, G., 2016. Effectiveness of a chemical herder in association with *in-situ* burning of oil spills in ice-infested water. *Marine Pollution Bulletin*, accepted for publication on 13-12-2016. DOI: [dx.doi.org/10.1016/j.marpolbul.2016.12.036](https://doi.org/10.1016/j.marpolbul.2016.12.036)
5. Van Gelderen, L., Rojas Alva, W.U., Mindykowski, P., Jomaas, G., 2016. Thermal properties and burning efficiencies of crude oils and refined fuel oil. *Abstract accepted for paper presentation at the International Oil Spill Conference, 2017*, draft paper submitted 16-12-2016.

## Supplementary comments

Based on the discussions with the examiner committee during the question and answer session of the Ph.D. thesis defense, the following comments were included in the thesis as supplementary material:

In this thesis, the influence of various parameters on the amount of oil that remains on the water surface, i.e. the burn residue, after *in-situ* burning of crude oil was studied. The results are mainly discussed in terms of the heat balance between heat losses to the water sub-layer and the heat feedback from the flame to the fuel surface. This heat balance determines the amount of energy that is available for evaporation of the various components in the crude oil. Once the evaporation rate is too low to sustain the fire, the flame extinguishes and the oil remaining on the water surface forms the burn residue. In other words, it is the extinction of the fire that controls the residue formation. While this is not explicitly mentioned in the thesis, extinction of the fire should be understood as the underlying governing mechanism in the discussions related to this topic. Minimizing the amount of residue that is formed upon extinction of an *in-situ* crude oil fire is thus a matter of delaying extinction of the fire for as long as possible, through optimization of the burning conditions.

The use of the term “ignitability” in this thesis should be interpreted in a practical context of the ignition of spilled oil on water as oil spill response. As such, successful ignition in this context includes both ignition in its true fire science definition of a fraction of the oil slick and the subsequent series of ignitions that are needed in order to ignite the rest of the oil slick, i.e. the flame spread over the full oil spill following the initial ignition. The ignitability of an oil slick is thus a function of the burning time of the initially ignited oil fraction and the time to ignition of the surrounding oil at the imposed heat flux from the initial fire. Although the practical aspects and spreading of the flame are elaborated on in some instances of the use of the term ignitability, these conditions are not explicitly stated throughout the thesis.

The presented results of emulsified crude oil in this thesis were obtained for a light crude oil that lacked the high concentrations of stabilizing components, such as resins and asphaltenes, needed to form a stable emulsion. These results may therefore not be fully representative of more stable emulsions that could be formed for some of the other oils that were tested in the same experimental setup. In order to be able to put the conclusions presented in this thesis in a broader perspective,

including a wider range of crude oil types, more stable emulsions will be tested in future work with the same experimental setup.

## Abstract

The fire dynamics and fire chemistry of *in-situ* burning of crude oil on water was studied in order to improve predictions on the suitability of this oil spill response method. For this purpose, several operational parameters were studied to determine the factors that control the burning efficiency of *in-situ* burning, i.e. the amount of oil (in wt%) removed from the water surface by the burning process. The burning efficiency is the main parameter for expressing the oil removal effectiveness of *in-situ* burning as response method and is thus relevant for suitability predictions of *in-situ* burning as oil spill response method. The parameters studied were the initial slick thickness of the oil, the vaporization order of burning crude oil, the ignition of fresh and weathered crude oils on water, the influence of the burning area, the effect of the water layer below the burning oil and the use of chemical herders in ice-infested water to thicken spread oil slicks.

All the experimental work, except for the crude oil herding studies in ice-infested water, was conducted in several small and intermediate scale setups with oil pool diameters between 0.1 m and 1.1 m. The main apparatus used in this study featured a water basin (water volume of  $1.0 \times 1.0 \times 0.50 \text{ m}^3$ ) in which a 0.34 m high Pyrex glass cylinder with a diameter of 0.16 m was placed to contain the oil samples. Several fresh crude oils, refined oils, and pure oils, which were used as reference fuels, were burned in this setup to study the surface temperature, burning rate, flame height, burning efficiency and chemical composition of the burn residue as a function of the oil type, the initial slick thickness and other experimental conditions.

The results showed that crude oils burned distinctively different from pure oils and refined fuel oils, as no steady state burning behavior was observed for the crude oils. Whereas the pure reference oils burned with relatively constant surface temperatures, burning rates and flame heights, the surface temperature increased and the burning rate and flame height decreased over time for the crude oils. Through a comparison with predictions of these parameters from vaporization order models for multicomponent fuels, it was shown that the components in a crude oil vaporize in the order of decreasing volatility. This volatility controlled vaporization order was confirmed by a principal component analysis of the chemical composition of the residues as a function of the burning efficiency. The differences in chemical composition between the 85 *m/z* ion chromatographs, which include the *n*-alkanes ( $\text{C}_9\text{-C}_{31}$ ), clearly showed that the abundance of light components decreased with increasing burning efficiency.

A mathematical analysis of the heat transfer mechanics of oil pool fires on water showed that the net heat feedback to the fuel surface depends on the pool diameter due to the heat losses to the water layer. Due to the fact that burning crude oils follow a volatility controlled vaporization order, these heat losses furthermore increase as a function of the burning time. By supporting this mathematical analysis with experimental results, it was shown that the burning area is the most important parameter of the burning efficiency for crude oil burning on water, with larger pool areas leading to higher burning efficiencies. This size dependency of the burning efficiency was attributed to the increased heat feedback to the fuel surface for large scale pool fires, as compared with small scale fires, that could cancel out the heat losses to the water. Small scale burning experiments subjected to an incident heat flux from a conical heater confirmed that an increased incident heat flux increased the burning efficiency of both fresh and weathered crude oils. At incident heat fluxes representative of large scale fires (diameter  $\geq 2$  m), however, the burning efficiency did not reach the high efficiencies ( $\geq 90\%$ ) reported for large scale *in-situ* burning operations. It was therefore deduced that the high burning efficiencies observed in large scale crude oil fires on water are not only caused by an increased heat feedback, but by other factors inherent to large scale fires as well. Further studies on the fire dynamics of large scale crude oil fires on water should be conducted to identify the factors associated with a large pool diameter that are responsible for the high burning efficiencies.

The initial slick thickness was primarily of importance to the ignition of oil slicks in the small scale experiments. Once a minimum ignitable thickness that accommodated for the heat losses to the water layer was reached, the results suggested that further increasing the slick thickness has little influence on the burning behavior of crude oil on water. The thickening of simulated crude oil spills in ice-infested water with a chemical herder, a surfactant that rapidly spreads over a water surface, also indicated that the slick thickness is only a minimum requirement for ignition. Crude oil spread on water with 2/10-7/10 ice coverages in small ( $1 \text{ m}^2$  water surface) and intermediate ( $19 \text{ m}^2$  water surface) scale experiments was successfully thickened from non-ignitable oil spill thicknesses of 0.1-2 mm to ignitable herded thicknesses of 3-7 mm. During the herding process, however, the crude oil slicks were observed to fracture as a function of the ice coverage. This fracturing process complicated and inhibited ignition of small slicks, even though the herded oil slicks theoretically had an ignitable slick thickness. The resulting burning efficiencies were therefore lower than expected based on the burning areas. Herders thus successfully facilitated *in-situ* burning of oil in ice-infested waters, but ignitability issues of fractured oil slicks should be addressed to improve burning efficiencies of herded oil slicks.

Ignition studies of fresh and weathered crude oils and a fresh heavy refined oil under a conical heater showed that the critical heat flux for weathered oils and heavy oils with little volatile components was 5-10 kW/m<sup>2</sup>. At higher incident heat fluxes ( $\geq 20$  kW/m<sup>2</sup>), ignition was very rapid for fresh and weathered oils and the weathering state (evaporated or emulsified) did not significantly affect the ignition or burning efficiency. These results correspond well with the reported need for large ignition sources to ignite and spread flames on weathered oils on water. Once ignited, however, the weathering state is not expected to influence the burning efficiency for large scale fires, which is in accordance with the postulated theory on the size dependency of the burning efficiency.

The boilover phenomenon, i.e. the explosive burning of crude oil, was shown to be a function both of the superheating of water and the chemical composition of the burning oil. Cooling of the water layer below the burning oil, by introducing a current in the water body, prevented boilover from occurring for oil burned in the small scale water basin. Boilovers were also observed during the burning of a heavy crude oil with a substantial light fraction without a water layer, however, which suggests that water is not essential for boilover occurrence. Further studies are required to determine the conditions under which these boilovers without a water layer can occur.

Overall, the results showed that the studied operational parameters, apart from the pool diameter, only have a limited effect on the efficiency of *in-situ* burning as oil spill response method. This strongly suggests that high burning efficiencies are inherent to operational scale crude oil fires on water. Operational and environmental conditions such as the weathering state of the oil and the initial slick thickness only influence the ignitability of the oil. Once ignition and flame spread on a large oil slick are successful, high burning efficiencies are expected simply due to the scale of the fire. As such, the main parameter that determines the suitability of *in-situ* burning as oil spill response method becomes the ignitability of the oil. This ignitability parameter is depending on complex fire dynamics aspects, but can be expressed in terms of the heat flux that the ignition source needs to be able to provide to the oil surface to ignite the oil. From an operational point of view, predicting the suitability of *in-situ* burning can thus be reduced to answering the question whether the strength of the required ignition source to ignite the spilled oil is practically feasible.

# Table of Contents

Preface.....	iii
Abstract .....	iv
Acknowledgements .....	xiii
Nomenclature.....	xv
Abbreviations.....	xvi
1 Introduction.....	1
1.1 Oil in the Arctic .....	1
1.2 Marine oil spill response in the Arctic .....	2
1.3 <i>In-situ</i> burning .....	6
1.3.1 Background.....	6
1.3.2 Operational challenges.....	7
1.3.3 Environmental impact .....	9
1.3.4 Knowledge gap .....	10
1.4 Research objective.....	10
1.5 Research overview.....	11
1.5.1 Oil slick thickness .....	13
1.5.2 Ignition.....	13
1.5.3 Burning area .....	14
1.5.4 Vaporization order of crude oil .....	14
1.5.5 Water influence and boilover.....	16
1.5.6 Chemical herders in ice-infested water.....	17
1.5.7 Residue, smoke and water fraction composition.....	17
1.6 Outline of the thesis .....	18
2 Theoretical background.....	19

2.1	Liquid pool fires .....	19
2.1.1	Ignition and flame spread.....	19
2.1.2	Combustion efficiency .....	21
2.1.3	Diameter and fire dynamics .....	22
2.1.4	Heat transfer mechanics.....	24
2.2	Crude oil chemistry.....	27
2.2.1	Chemical composition of crude oils.....	27
2.2.2	Physical properties of hydrocarbons .....	30
2.2.3	Chemical analysis of crude oils .....	32
2.3	Weathering of crude oils .....	33
2.3.1	Evaporation .....	34
2.3.2	Emulsification .....	34
2.3.3	Weathering in cold climates .....	36
2.4	Multicomponent fuel combustion models.....	37
2.5	Chemical herders.....	40
3	Materials and methods .....	43
3.1	Crude Oil Flammability Apparatus.....	43
3.1.1	Burning rate setup .....	45
3.1.2	Crude oils, refined oils and reference oils.....	46
3.1.3	Water .....	47
3.1.4	Vaporization order of crude oil .....	47
3.1.5	Residue composition as a function of the burning efficiency .....	48
3.1.6	Influence of initial slick thickness .....	49
3.2	Crude oil herding setup .....	50
3.2.1	Chemical herder .....	53
3.3	Cone setup for ignition studies.....	53

3.4	Burning efficiency studies.....	55
3.4.1	Burning efficiency as a function of the oil composition .....	55
3.4.2	Burning efficiency as a function of the pool diameter .....	56
3.5	Chemical composition of in-situ burning byproducts .....	58
3.5.1	Smoke composition test .....	60
3.5.2	Residue and water fraction composition tests.....	60
4	Results and Discussion.....	63
4.1	Observational results.....	63
4.2	Vaporization order.....	64
4.2.1	Modeling of burning parameters .....	65
4.2.2	Experimental results .....	67
4.2.3	Residue composition as a function of the burning time .....	72
4.2.4	Influence on heat transfer mechanics and burning efficiency .....	77
4.2.5	Sub-conclusion.....	79
4.3	Initial slick thickness .....	80
4.3.1	Regression rate .....	80
4.3.2	Burning rate .....	83
4.3.3	Burning efficiency .....	86
4.3.4	Flame height .....	89
4.3.5	Sub-conclusion.....	91
4.4	Crude oil herding in ice-infested water .....	91
4.4.1	Slick thickness .....	91
4.4.2	Hered oil slick distribution.....	93
4.4.3	Ignition of herded oil .....	98
4.4.4	Burning efficiency .....	99
4.4.5	Sub-conclusion.....	102

4.5	Ignition.....	103
4.5.1	Ignition time .....	103
4.5.2	Heat release rate .....	107
4.5.3	<i>In-situ</i> burning results.....	110
4.5.4	Sub-conclusion.....	111
4.6	Boilover.....	111
4.6.1	COFA setup and burning rate setup .....	112
4.6.2	Modified COFA setup.....	114
4.6.3	Cone setup.....	115
4.6.4	Sub-conclusion.....	117
4.7	Burning efficiency .....	118
4.7.1	Oil types in COFA setup .....	118
4.7.2	Scaling in ice cavities .....	120
4.7.3	Cone setup.....	123
4.7.4	Sub-conclusion.....	126
4.8	Composition analysis of byproducts.....	127
4.8.1	Smoke analysis test .....	127
4.8.2	Water fraction test .....	129
4.8.3	Residue composition test .....	129
4.8.4	Sub-conclusion.....	131
5	Conclusion .....	133
5.1	Result highlights .....	133
5.2	Summary of experimental results .....	133
5.3	Research objective.....	136
5.4	Recommendations for future work.....	137
	Bibliography.....	139

## Acknowledgements

Throughout my Ph.D. study I have been supported, both financially and personally, and interacted with many great people and institutions. I would like to thank all of them for giving me the opportunity to conduct my Ph.D. studies and the great experience that the past three years have been. In particular I want to thank the following:

The Danish Council for Independent Research (Det Frie Forskningsråd), which funded my Ph.D. study as a part of the DDF – 1335-00282 grant.

Grunde Jomaas, my supervisor, for his guidance, research intellect and motivating me throughout my Ph.D. study. He was an excellent supervisor from whom I learned a lot and I am grateful for having had the opportunity to conduct my Ph.D. study under his supervision.

Janne Fritt-Rasmussen, my co-supervisor, for her guidance, enthusiasm and sharp reader eyes that always helped to improve my work.

Ali Rangwala, my co-supervisor, for his guidance and hospitality during my external research stay at his research group at the Worcester Polytechnic Institute in Massachusetts. Working at his research group was a very educational and interesting experience.

Rolff Ripke Leisted, Bjørn Skjønning Andersen and Pierrick Mindykowski, without whom my time in the office would not have nearly been as fun and educational. Each of them helped me greatly with theoretical and practical problems and I have been lucky to have had such awesome colleagues.

Hamed Farmahini Farahani, my colleague with whom I worked closely together at WPI and who later joined our research group at DTU for his external stay. Working with him was fun and he was one of the main persons who made my external stay a memorable experience.

Ulises Rojas Alva, Eirini Adamopoulou, Marc Martorell, Barbara Falatova and Jinlong Zhao for their help with my experimental work, some of which I could not have done without them.

Linus Malmquist, Peter Christensen and Jan Christensen from the Copenhagen University for their enthusiasm, positive attitude and assistance with many of the chemical analyses conducted during my work.

Professor C.K. Law, Mr. Delin Zhu and the research group at Princeton University for their warm welcome, hospitality and great help during my brief stay at their research group for experimental work.

Kristian Schiang-Franck from Nordsjællands Brandskole ([www.nsbs.dk](http://www.nsbs.dk)), who allowed me to use the facilities of the NSBS to conduct some of my experimental work.

Mikael Emil Olsson from DTU Environment, who helped me with the chemical analysis of my last samples during the final weeks of my Ph.D. study.

The Otto Mønsted fond and COWI fonden for co-funding one of my experimental setups, my research stays and some of my conference participations.

Mærsk, Statoil, Trumf Bunker and Desmi for providing me with the crude oils, refined fuel oil and the chemical herder that were used in this study.

My parents, who encouraged and helped me to undertake this project and always welcomed me with open arms whenever I returned to their home in the Netherlands for a visit.

Mette, my loving girlfriend, on whom I could always count and who supported me, especially in the last months, and without whom this whole experience would have been less complete.

## Nomenclature

$a$	Absorptivity (-)	$\dot{Q}_{ref}$	Radiative reflection from fuel (kW)
$B$	Mass Transfer Number (-)	$\dot{Q}_{re-rad}$	Re-radiation from the fuel surface (kW)
$c_p$	Specific Heat Coefficient (J/(kg·K))	$r$	Regression rate (mm/s)
$D$	Diameter (m)	$t$	Time (s)
$g$	Gravitational Constant (m/s <sup>2</sup> )	$T$	Temperature (K)
$\Delta H_c$	Heat of Combustion (kJ/kg)	$T_b$	Boiling point (K)
$\Delta H_{eff}$	Effective Heat of Combustion (kJ/kg)	$T_s$	Surface temperature (K)
$\Delta H_g$	Heat of Gasification (kJ/kg)	$y_{s,i}$	Initial slick thickness (mm)
$\Delta H_v$	Latent Heat of Vaporization (kJ/kg)		
$k$	Thermal Conductivity (W/(m·K))	<b>Greek symbols</b>	
$k\beta$	Fuel Specific Constant (m <sup>-1</sup> )	$\alpha$	Thermal diffusivity (m <sup>2</sup> /s)
$L_f$	Flame Height (m)	$\gamma$	Surface tension (mN/m)
$\dot{m}$	Burning Rate (g/s)	$\gamma_N$	Water-liquid surface tension (mN/m)
$\dot{m}_\infty$	Maximum Burning Rate (g/s)	$\rho$	Density (g/ml)
$\dot{m}''$	Burning Rate per Unit Area (g/(s·m <sup>2</sup> ))	$\pi$	Spreading pressure (mN/m)
$m/z$	Mass-to-Charge Ratio (g/(mol·Q))	$\chi_c$	Combustion Efficiency (-)
$Pe_m$	Peclet Number for Mass Diffusion (-)	$\chi_s$	Heat feedback fraction (-)
$\dot{q}_{inc}''$	Incident Heat Flux (kW/m <sup>2</sup> )		
$\dot{Q}$	Heat Release Rate (kW)	<b>Subscripts</b>	
$\dot{Q}_{conf}$	Heat losses from fuel to confinement (KW)	$\infty$	Ambient (air)
$\dot{Q}_{conv}$	Convection from flame to fuel (kW)	$f$	Flame
$\dot{Q}_{evap}$	Energy used to evaporate fuel (kW)	$F$	Fuel
$\dot{Q}_{grad}$	Energy used to heat fuel layer (kW)	$ig$	Ignition
$\dot{Q}_{loss}$	Heat losses from fuel to water (kW)	$l$	Liquid
$\dot{Q}_{net}$	Total net heat from flame to fuel (kW)	$lw$	Water-liquid interface
$\dot{Q}_{rad}$	Radiation from flame to fuel (kW)	$w$	Water

## Abbreviations

---

AMAP	Arctic Monitoring Assessment Programme	GC	Gas Chromatography
ANS	Alaska North Slope	IFO	Intermediate Fuel Oil
COFA	Crude Oil Flammability Apparatus	IR	Infrared
DLV	Diffusion-Limited Vaporization	MS	Mass Spectrometry
DUC	Danish Underground Consortium	NEBA	Net Environmental Benefit Analysis
EFV	Equilibrium Flash Vaporization	PAH	Polycyclic Aromatic Hydrocarbon
EPPR	Emergency Prevention, Preparedness and Response	REBCO	Russian Export Blend Crude Oil
		TD	Thermal Desorption

---

# 1 Introduction

## 1.1 Oil in the Arctic

The Arctic is commonly defined as the area above the circle of latitude known as the Arctic Circle (66° 33' north of the equator), although alternative definitions of the Arctic territory are also used (see e.g. AMAP (2010a)). There are eight states that lie partially within the Arctic Circle, namely the United States of America, Canada, Greenland (part of the Danish Kingdom), Iceland, Norway, Sweden, Finland and Russia, of which all but Sweden contain marine territories in the Arctic. These eight countries make up the member states of the Arctic Council, an intergovernmental forum that is “promoting cooperation, coordination and interaction among the Arctic States, Arctic indigenous communities and other Arctic inhabitants on common Arctic issues, in particular on issues of sustainable development and environmental protection in the Arctic” (Council, 2016).

Due to climate change, particularly in the past three decades, the Arctic has become more accessible to shipping routes and oil exploration and production (ACIA, 2005; AMAP, 2012). Exploration activities and production of oil in the Arctic have increased steadily since the 1980s, from a total oil activity area of < 40,000 km<sup>2</sup> to a total area of > 400,000 km<sup>2</sup> in 2004 (AMAP, 2010a). Oil related activities in the Arctic have continued to increase in the past decade, among others through oil exploration licenses, for example offshore around Greenland (MLSA, 2016) and north of Alaska (BSEE, 2012, 2015). The Arctic is of remaining interest to oil producers because it has been estimated that a large amount of the undiscovered oil (13%) and gas (30%) is to be found within the Arctic Circle (Gautier et al., 2009). Lacking exploration results, high costs and low oil prices, however, caused oil producers to withdraw from Arctic exploration activities in the past five years (see e.g. Jacobsen (2015) and Shell (2015)). The oil exploration in US, Canadian or Greenlandic Arctic waters is not expected to recommence until after 2020 (EPPR, 2015). Still, Norwegian and Russian Arctic waters remain active (EPPR, 2015) and Norway recently issued new licenses for exploration in a newly opened area of the Barents Sea (MPE, 2016). With the current activities ongoing and increasing activity expected from 2020 onward, potential oil spills in the Arctic marine environment will therefore remain a pollution risk in the foreseeable future.

The occurrence of an oil spill in the Arctic marine environment is an acknowledged risk associated with the oil related activities in the Arctic (AMAP, 2010a). According to the latest assessment of the Arctic Monitoring and Assessment Programme (AMAP), oil production in the Arctic accounted for approximately 10% of the total

world oil production (AMAP, 2010a). In order to minimize the risk and impact of an oil spill in the Arctic, the “Agreement on Cooperation on Marine Oil Pollution Preparedness and Response in the Arctic” was drafted by the Arctic Council state members in 2013 and ratified in 2016 (Arctic Council, 2013, 2016). This agreement clearly signifies that the risk of an oil spill is not only acknowledged in scientific reports but is also of importance to the international stake-holders in the Arctic.

Oil spills can cause severe environmental damage and have costly socio-economic consequences, in both the short- and long-term (Chang et al., 2014). The acute toxicity of oil disrupts ecosystems because it results in (mass) mortalities of birds, mammals, fish and other organisms that come into contact with the oil during the first days after a spill (e.g. Peterson et al. (2003)). Oil can furthermore persist in the environment for a very long time (decades), in particular in sediments (Short et al., 2004; AMAP, 2010b). Long-term effects from chronic exposure to persisting oil have been shown to reduce the growth rate of affected populations (Peterson et al., 2003) and thereby also reduce the recovery rate from any acute toxicity effects.

In the Arctic, the microbial and chemical degradation of oil is slower than in other climates because of the low temperatures, ice and darkness, which causes oil to be even more persistent in this type of environment (AMAP, 1998, 2010b; Shigenaka, 2011). The Arctic ecosystem is also considered to be more vulnerable to oil contamination because its recovery rate is typically slower than in warmer climates (AMAP, 1998). AMAP (2010b) assessed that in particular the marine environment of the Arctic is vulnerable to oil pollution, although knowledge on the long-term consequences from such an oil spill is currently limited. It is thus important that if an oil spill occurs in this sensitive environment, the response is as fast and efficient as possible.

## **1.2 Marine oil spill response in the Arctic**

In the Arctic environment, responding to an oil spill on water is stated to be much more challenging than in more temperate climates (Fitzpatrick, 1985; AMAP, 2010a; Nuka, 2010; EPPR, 2015). For example, low temperatures complicate the use of mechanical equipment, darkness reduces the visibility, the logistic infrastructure is very limited and ice-infested waters make it harder to access the spill location. On the other hand, ice can also aid response methods by inhibiting the spreading of oil and reducing wave activity, which, combined with the low temperatures, slow the weathering process of spilled oil (e.g. SL Ross and DF Dickins (1987); Brandvik et al. (2004); Brandvik et al. (2010c)). Weathering of oil describes the chemical and physical

processes that oil undergoes once spilled, such as evaporation of its lighter components and emulsification with water (Section 2.3) (Mackay et al., 1983). These processes typically reduce the available time window, or window-of-opportunity, during which response methods can be effectively applied (Nordvik, 1995; Nordvik et al., 2003). Arctic conditions thus pose additional challenges for oil spill response operations, but can also have a positive side effect by increasing the window-of-opportunity for effective responses.

The current established oil spill response methods are 1) mechanical recovery, 2) dispersants and 3) *in-situ* burning. Mechanical recovery typically features the use of skimmers that collect the oil from the water surface and store it for disposal at a later moment, occasionally supported by booms to contain the oil (see e.g. Fingas (2011c)). Dispersants are chemicals that are applied to the oil to aid with dispersing the oil from the water surface into the water column in the form of small droplets (see e.g. National Research Council (2005)). Finally, *in-situ* burning burns the oil off the water surface and turns the oil into soot and gaseous combustion products that will diffuse in the air (see e.g. Buist et al. (1999)).

Of these three methods, mechanical recovery is the primary response method used by the Arctic Council member states (Arctic Council, 2013). The other methods are mostly considered as alternative methods in specific situations, if they are at all considered. Finland and Sweden have specifically stated that dispersants could not be used as response methods and only Canada, Denmark and the US have considered *in-situ* burning as an alternative response method (Arctic Council, 2013; Potter et al., 2013).

The main advantage of mechanical recovery is that it fully removes the oil from the local environment, whereas the other methods have polluting side effects in other areas of the environment. Dispersants increase the oil concentration in the water column, which increases the exposure of marine species to the oil and possibly increases its toxicity. The smoke plumes from *in-situ* burning pollute the air with toxicants such as CO, SO<sub>2</sub> and NO<sub>x</sub> (Day et al., 1979; Ross et al., 1996) and the formed soot could cause pollution of nearby soil, snow, ice or water after it deposits ( e.g. Clarke and Noone (1985); AMAP (2010b)). The downsides of mechanical recovery, however, are that it is expensive (Allen and Ferek, 1993), generates a large volume of waste (Fingas, 2011c), requires a lot of equipment and has a relatively low removal rate of oil from the water surface (Federal Interagency Solutions Group, 2010). Dispersants are easier to apply and can cover larger areas faster via aircraft, although this method can be imprecise and requires nearby dispersant stock and infrastructure for the aircrafts (EPPR, 2015). *In-situ* burning is the cheapest response option (Allen and Ferek, 1993) and the simplest to apply, but has a limited removal rate as well (Federal Interagency Solutions Group, 2010) and ignition of the

oil can be challenging (e.g. Bech et al. (1993); Fritt-Rasmussen et al. (2012)). Clearly, none of these response methods are perfect and each has its advantages and disadvantages. While mechanical recovery is the preferred response method, the other methods can also be effective (additional) responses to oil spills, depending on the situation.

In the latest review on oil spill response methods in the Arctic, the Arctic Council Emergency Prevention, Preparedness and Response (EPPR) working group stated that mechanical recovery is mainly limited to small spills (EPPR, 2015). For large scale spills, in particular in ice-infested waters or remote areas, the expected mechanical recovery rate is not sufficient to make a significant impact on the spilled oil volume. For these types of scenarios, the use of dispersants or *in-situ* burning is considered to be a viable alternative (Chevron, 2011; National Research Council, 2014).

In order to use either dispersants or *in-situ* burning as alternative response method to a marine oil spill, a Net Environmental Benefit Analysis (NEBA) may be required (e.g. in the Greenlandic and the Norwegian Arctic (Arctic Council, 2013)). A NEBA is a method to assess the suitability of a response method by comparing its expected net impact on the environment to the net impact of other response options or intentionally refraining from a response (Baker, 1995; Fritt-Rasmussen et al., 2013b). Recently, this method has been frequently suggested as the basis for the decision making process on the environmentally most suitable response method in case of an oil spill (Potter et al., 2012; Fritt-Rasmussen et al., 2013b; National Research Council, 2014; EPPR, 2015). The NEBA was developed in the aftermath of the Exxon Valdez oil spill in 1989 in Alaska. Monitoring of the environmental recovery showed that some of the used response methods, although effectively removing oil from shorelines, were in fact more harmful to the environment than the oil (Shigenaka, 2014). A NEBA is as such a more realistic approach to responding to oil spills that acknowledges that the negative environmental impact from an oil spill cannot be prevented. Instead, the focus for oil spill responses is to minimize the negative impact on the environment by choosing the best (combination of) response methods for the given situation.

Recent studies on the use of dispersants in Arctic conditions have shown the potential of this oil spill response method in the Arctic environment. Crude oil has been effectively dispersed in cold and ice-infested waters (Nedwed et al., 2007; Mullin et al., 2008; Brandvik et al., 2010c) and Arctic marine microorganisms were shown to be capable of biodegrading chemically dispersed oil (Margesin and Schinner, 2001). However, the use of dispersants in the Arctic was stated to be “still highly controversial” by the EPPR (2015, p. 103).

Two of the main remaining concerns regarding the use of dispersants are the toxicity of the dispersant and dispersed oil, and the application and efficiency of dispersants in high (> 5/10) ice coverages. Lee et al. (2013) stated that toxicity experiments should take into account the rapid dilution of chemically dispersed oil in the water column at sea, which typically results in oil concentrations of 1-100 ppm (see also Bejarano et al. (2014)). Research has shown that for these concentrations the chemically dispersed oil was not acutely more toxic than natural dispersed oil (Gardiner et al., 2013; Adams et al., 2014). The dispersant only showed acute toxicity at concentrations several orders of magnitude larger than those expected at sea. However, other research has shown that chemically dispersed oil did have increased acute toxicity and sub-lethal effects compared to naturally dispersed oil in these low concentrations (Almeda et al., 2014). As such, the toxicity of dispersants remains debatable.

In high ice coverages (> 5/10), the dampening effect of ice on the wave energy reduced the effectiveness of dispersants and additional mixing energy was required to obtain high dispersion efficiencies (e.g. Spring et al. (2006); Brandvik et al. (2010c); Daling et al. (2010)). The application of the dispersant also requires more precision to avoid the pollution of ice floes (EPPR, 2015). Aircrafts, typically the fastest method to cover a large area, were assessed to be accurate up to 2/10-3/10 ice coverages (Lewis and Daling, 2007). Helicopters, which are more maneuverable than aircrafts but have a lower dispersant capacity, could be accurate up to an ice coverage of 5/10 and higher ice coverages would require dispersant application by ice class ships. While applicable in higher ice coverages, the use of dispersants would thus require additional equipment to provide mixing and loses the advantage to cover large areas of spilled oil in a short amount of time.

*In-situ* burning, on the other hand, has been stated to be a particularly suitable response method in high ice coverages, and as such for the Arctic environment (Buist et al., 2013; EPPR, 2015). A high ice coverage inhibits the spreading of oil on water (Free et al., 1981; Tebeau et al., 1984; SL Ross and DF Dickins, 1987) and reduces the weathering rate of the spilled oil (Brandvik et al., 2010c), which are two processes that make oil spilled on water more difficult to ignite (Buist et al., 1999). Rather than being an inhibiting factor, the presence of ice may thus in fact aid *in-situ* burning as an oil spill response method. In combination with the relatively simple logistic requirements (Allen and Ferek, 1993), *in-situ* burning has therefore been mentioned as the most promising oil spill response method in ice-infested water (AMAP, 2010a; Nuka, 2010; Buist et al., 2013). An overview of *in-situ* burning as response method to oil spills in Arctic waters is presented in the following section.

## 1.3 *In-situ* burning

### 1.3.1 Background

The recorded use of *in-situ* burning as response method to marine oil spills dates back to an oil spill in Canada in 1958 (McLeod and McLeod, 1972), but has only been attempted sporadically on accidental oil spills since then (Buist et al., 2013). The best known examples of *in-situ* burning of incidentally spilled oil are from the Exxon Valdez spill in 1989 (Allen, 1990) and more recently from the Macondo spill after the Deepwater Horizon incident in 2010 (Allen et al., 2011). In particular the *in-situ* burning operations conducted during the Macondo spill demonstrated the potential of this response method, as an estimated 260,000 barrels of oil were successfully burned off the water surface (Federal Interagency Solutions Group, 2010; Allen et al., 2011).

Since the use of *in-situ* burning in 1958, a large amount of research has also shown that oil on water can be burned with high burning efficiencies ( $\geq 90\%$ ) in a variety of conditions (e.g. Allen (1990); Guénette et al. (1994); Potter (2010b); Buist et al. (2011)). The burning efficiency is the main parameter that is used to express the effectiveness of *in-situ* burning as an oil spill response method. Herein, the burning efficiency is defined as the amount of oil (in wt%) that is removed from the water surface during the burning. The remaining amount of oil on the water surface is called the residue, which, if it does not sink (Buist et al., 1997), can be collected mechanically to remove it from the environment or is otherwise left untreated on the water surface.

The current focus of *in-situ* burning related activities is on the Arctic, because *in-situ* burning could be the most suitable response method available in remote or ice-infested Arctic waters (AMAP, 2010a; Nuka, 2010; Buist et al., 2013). The two most recent international research projects that included *in-situ* burning, “JIP in Ice” (2006-2009) (Sørstrøm et al., 2010) and “Arctic Response Technology” (2012-2016) (Mullin, 2012), both focused on the Arctic environment. Due to the lack of practical experience with oil spills responses in the Arctic, these types of experimental research projects have been the main information sources for oil spill response guides in Arctic waters (e.g. EPPR (2015)).

Of all the possible interactions between oil, water and ice in the Arctic (AMAP, 1998, p. 672), the oil can appear in two distinct types of interactions with water and ice that are relevant in terms of *in-situ* burning. The first appearance is on sea where spilled oil is surrounded by a large body of water and the ice coverage influences the extent to which the oil will spread out. The second appearance is in melt pools of oil that was trapped under ice and surfaced during the melting season (NORCOR, 1975). In melt pools, the oil is contained by the

surrounding ice and spreading of the oil is controlled by further melting of the ice. The interactions between the oil, water and ice can be notably different for oil on sea and oil in melt pools (e.g. differences in water current, oil spreading and ice coverage), which can affect the *in-situ* burning of oil (see Section 1.5). It is therefore relevant to distinguish between oil on sea and oil in melt pools when studying *in-situ* burning of oil on water. This study focused on *in-situ* burning of oil on open water and ice-infested water and all further discussions in this thesis are related to these two oil spill appearances, unless specifically mentioned otherwise.

### 1.3.2 Operational challenges

There are several weather and practical challenges related to *in-situ* burning as a response method that can limit its applicability or effectiveness. In order for oil on water to be ignitable and produce a self-sustaining fire, the oil slick must be at least 1-2 mm thick to sufficiently insulate the burning oil surface from the heat losses to the underlying water (Brzustowski and Twardus, 1982; Buist et al., 1999). On open water, oil spreads out to thicknesses well below 0.1 mm and mechanical or chemical (Section 1.5.6) measures are required to gather and thereby thicken the oil. The conventional, mechanical method to collect and thicken a spread oil slick for *in-situ* burning purposes is by use of a fire-resistant boom (Allen and Ferek, 1993). A fire boom is a floating, flexible barrier which is 'towed' by two boats in a U-shape configuration, within which spread oil is collected to increase its thickness. While this method can be effectively used on open sea, it has proven challenging in ice-infested water (Potter, 2010a). Ice that is collected within the boom area reduces the amount of oil that can be collected and above 3/10 ice coverages the ice starts lifting up the boom so that oil leaks out of the contained area. Booms are furthermore heavy and can be difficult to handle without the appropriate equipment (Potter, 2010a), which can present challenges in remote Arctic areas with limited available equipment.

Ice can, however, also aid *in-situ* burning of oil on water, as mentioned earlier, because it inhibits the spreading of oil (e.g. SL Ross and DF Dickins (1987)). In high ice coverages of > 6/10, spilled oil is naturally contained by the ice and likely maintains a readily ignitable thickness without the need for additional measures to thicken the oil (SL Ross and DF Dickins, 1987; Brandvik et al., 2006; Sørstrøm et al., 2010). High ice coverages can therefore be considered to be a positive environmental factor that supports *in-situ* burning as response method to a marine oil spill and further simplify the required logistics for *in-situ* burning. This positive natural containment effect from high ice coverages is the main reason why *in-situ* burning is considered to be the most

suitable oil spill response method for marine oil spills in the Arctic environment (e.g. Buist et al. (2013); EPPR (2015)).

Apart from the slick thickness, the ignition and spreading of the fire is also dependent on the wave and wind conditions and the state of the oil. Oil ignition has been reported to be unachievable in wind speeds over 10 m/s and swell waves prevented the ignition of water-in-oil emulsions (Bech et al., 1993; Guénette et al., 1995). Weathering of oil (see Section 2.3) also greatly reduces its ignitability (also known as flammability) and depending on the oil type, weather conditions and ice coverage oil, weathering can prevent ignition within a few hours to a few days (e.g. Brandvik et al. (2010a); Fritt-Rasmussen et al. (2012)). This limited time window to ignite spilled oil is one of the main constraints to effectively applying *in-situ* burning as response spill method (Buist, 2003). The EPPR (2015) stressed that because of these limited windows-of-opportunity, it is important to implement efficient regulatory frameworks that allow for rapid decision making on the most suitable response method.

As mentioned in Section 1.2, the Arctic environment poses some unique logistic challenges such as difficulties with accessing spill sites in high ice coverages, darkness, cold temperatures and limited infrastructure (Fitzpatrick, 1985; AMAP, 2010a; Nuka, 2010; EPPR, 2015). In addition, the overall removal efficiency of boomed oil by *in-situ* burning can be very low compared to the spilled oil volume. During the Macondo spill, the *in-situ* burning operations had access to several tens of vessels and multiple fire booms and were capable of performing 376 burns over a time span of two and a half months (Allen et al., 2011). The amount of oil removed by *in-situ* burning was estimated to be around 5% of the total amount of spilled oil (Federal Interagency Solutions Group, 2010). For reference, 3% of the total amount of spilled oil was recovered mechanically and 16% was dispersed with chemical dispersants. The single test burn that was conducted during the Exxon Valdez spill similarly removed only about 0.2% of the total amount of spilled oil (based on Allen (1990); Allen and Ferek (1993)). Considering the limited infrastructure and challenges with booming oil in ice-infested water, it seems highly unlikely that fire booms can be an effective method to facilitate *in-situ* burning of spilled oil in the Arctic. *In-situ* burning of oil collected by chemical surfactants (Section 1.5.6) or naturally contained in high ice coverages could potentially lead to higher removal percentages, but the available experience is limited to experimental scale spill sizes (Brandvik et al., 2010a; Buist et al., 2011).

### 1.3.3 Environmental impact

A variety of studies have addressed the toxicity and related impact on the environment of the byproducts of *in-situ* burning over the past two decades. The current consensus observed in these studies is that the *in-situ* burning of oil on water does not increase the toxicity to the environment compared to the unburned oil. Water fractions below *in-situ* burning oil have been tested for toxicity (Daykin et al., 1994; Blenkinsopp et al., 1997; Gulec and Holdway, 1999; Faksness et al., 2012) and were shown to have similar toxicity as the water fraction of untreated oil and lower toxicity than (chemically) dispersed oil. Research on the burning residue focused on the composition and physical properties of residues from different crude oils (Blenkinsopp et al., 1997; Buist et al., 1997; Garrett et al., 2000; Fritt-Rasmussen et al., 2013a) and toxicity of the residue (Blenkinsopp et al., 1997; Gulec and Holdway, 1999). Physical effects of burn residues (see e.g. Fritt-Rasmussen et al. (2016)), however, have only received limited study and the environmental impact of sunken residues are also poorly understood (Fritt-Rasmussen et al., 2015). The need for more information on the chemical composition and toxicity of residues as a function of the burning efficiency was also addressed in the latest review on *in-situ* burning residues (Fritt-Rasmussen et al., 2015).

Studies on the smoke plumes of crude oil fires have focused on the parameters that influence the smoke formation (Evans et al., 1988; Evans et al., 1992; Mulholland et al., 1996), concentrations of gaseous and particle emissions in smoke plumes (Day et al., 1979; Benner et al., 1990; Ross et al., 1996; Sartz and Aggarwal, 2016), and plume trajectories (McGrattan et al., 1993; McGrattan et al., 1997). The results showed that the main health risk is related to the small particulate matter (with a diameter < 10 µm) in the smoke plume. Concentrations of gaseous toxic components were found to be of no concern outside the near vicinity of the fire (Fingas et al., 1994b). The total amount of polycyclic aromatic hydrocarbons (PAHs), which are generally considered to be carcinogenic components (Santodonato et al. (1981) in Nisbet and LaGoy (1992)), created by the fire was also less than the amount of PAHs consumed by the fire (Benner et al., 1990; Fingas et al., 1994b; Westphal et al., 1994). Modeling of the plume trajectory showed that the concentration of particulate matter was already within acceptable concentrations on ground level at > 5-10 km downwind of the fire (McGrattan et al., 1993; McGrattan et al., 1997). In remote Arctic locations, the health effects from the smoke plume should thus be negligible. However, the environmental effects from precipitating soot and particulate matter on ice or mammals are not known, although soot precipitation was stated to be negligible based on visual observations (EPPR, 2015). The overall contribution to climate change from the smoke plume emissions was also considered to be negligible compared to other greenhouse gas sources (EPPR, 2015).

### **1.3.4 Knowledge gap**

The above overview of *in-situ* burning shows that there is a large amount of (practical) knowledge available on this response method, also for an Arctic setting. The majority of the performed studies, however, focused on the operational issues concerning *in-situ* burning. These practical issues were primarily related to the feasibility of *in-situ* burning for a set of experimental conditions in terms of whether or not the oil could be ignited and the burning efficiency of the tested oil (e.g. SL Ross and DF Dickins (1987); Bech et al. (1993); Fingas et al. (1994a); Guénette et al. (1995); Brandvik et al. (2010a); Potter (2010b); Fritt-Rasmussen et al. (2012)). The fundamentals of the fire science behind the burning of a multicomponent fuel such as crude oil on water, on the other hand, have been relatively less studied. For example, the current theoretical understanding of *in-situ* burning of oil on water is insufficient to explain the wide range of burning efficiencies (32-99%) that has been reported in literature (Guénette and Wighus, 1996; Potter, 2010b; Fritt-Rasmussen et al., 2012; Farmahini Farahani et al., 2015b). This lack of theoretical understanding is reflected in literature by statements on the uncertainties related to burning efficiency and the resulting residue for the *in-situ* burning of oil on water (e.g. Holland-Bartels and Pierce (2011); Fritt-Rasmussen et al. (2015)). Without the capability to accurately predict the burning efficiency of *in-situ* burning as response method to an oil spill, the net impact on the environment from this response will be difficult to assess. As a result, performing a NEBA and subsequently making an informed decision on whether *in-situ* burning will be a suitable response method for a specific situation will then be very challenging.

## **1.4 Research objective**

In this study, the fire dynamics and the fire chemistry of *in-situ* burning of crude oil on water related to a number of operational parameters (Section 1.5) were studied within the broader context of a NEBA. A better understanding of the fundamentals that govern the net impact on the environment of *in-situ* burning would improve the accuracy of the NEBA that assesses the suitability of *in-situ* burning as oil spill response method. The net impact on the environment of *in-situ* burning is a balance between the environmental effects from the byproducts of the fire (negative) and burning efficiency (positive). The byproducts of *in-situ* burning of oil on water fire consist of the smoke plume, the residue and the oil fraction dissolved in the water column. Improving the understanding of which and how much of these byproducts are formed and what the burning efficiency will be would thus add valuable knowledge to the expected net impact on the environment. This

study mainly focused on the burning efficiency, which was studied through quantitative and qualitative (chemical) analysis of the residue. As such, the research objective of this study can be formulated as follows:

*The objective of this study is to improve the forecasting of the suitability of in-situ burning that is used in the decision making on oil spill responses, by analyzing the influence of operational parameters on the quantity and chemical composition of byproducts resulting from in-situ burning of crude oil on water.*

## **1.5 Research overview**

In this section the operational parameters that were studied to fulfill the stated research objective are presented. A graphical overview of these parameters is shown in the general context of an *in-situ* burning of crude oil operation in ice-infested water in Fig. 1.1. The columns on the left indicate how the parameters are connected to the overall decision making process. For the purposes of this study, the decision making process was divided into a practical component (*can in-situ burning be performed?*) and an environmental component (*is it beneficial for the environment?*). These components are not independent of each other, but separating them makes it easier to put the research in this study into the broader context of *in-situ* burning operations.

The majority of the studied parameters are related to the operational side of *in-situ* burning, i.e. how *in-situ* burning is conducted and what is expected to happen once the oil is burning. All these parameters have an influence on the burning efficiency, as discussed in the sub-sections below, and in terms of the research objective thus address the quantity of the residue byproduct. These operational parameters furthermore have an indirect influence on the environmental component because the chemical composition of the byproducts is a function of the burning efficiency.

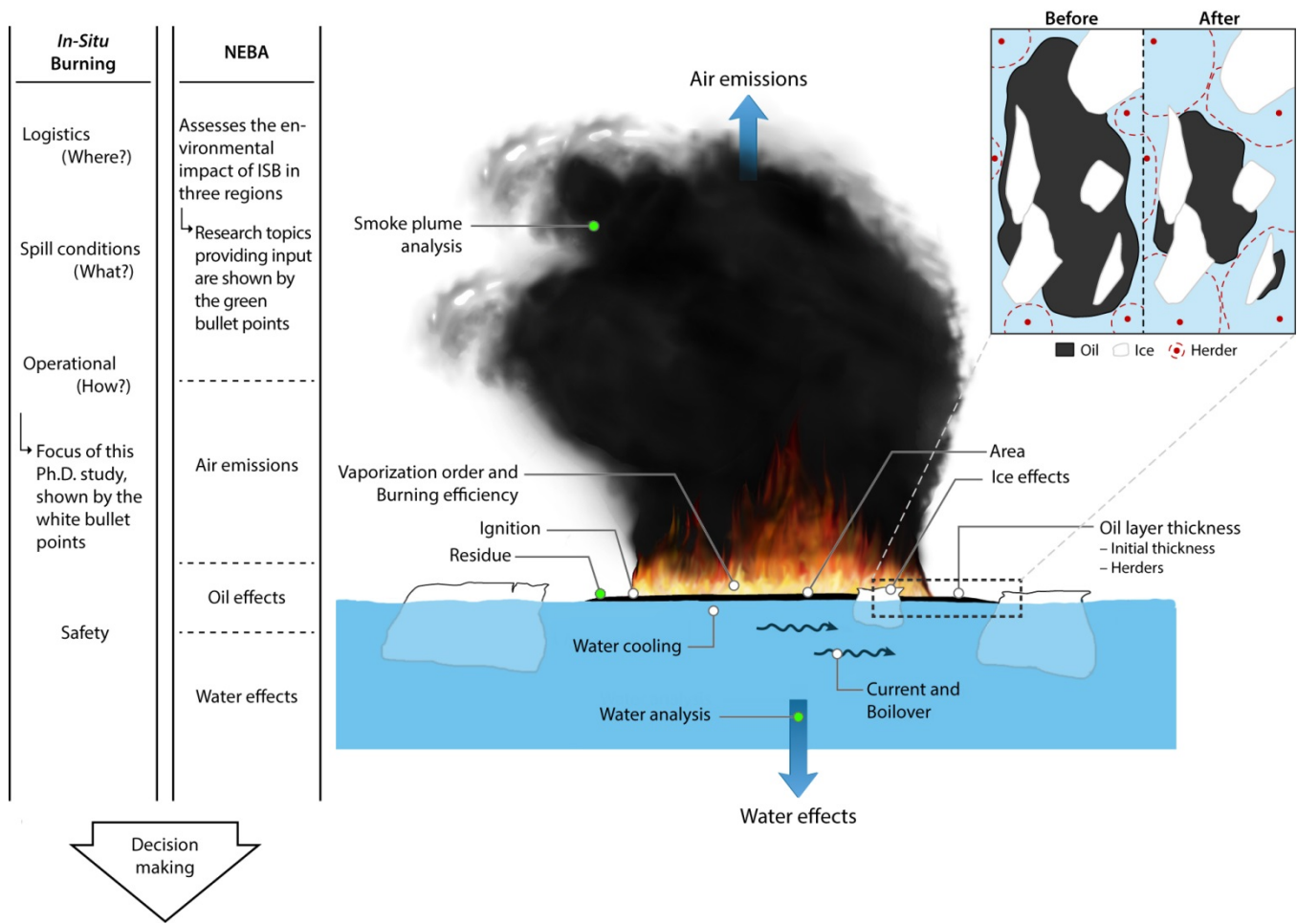


**Figure 1.1.** Overview of the studied *in-situ* burning parameters and their relation to the decision making process.

The environmental column is presented in terms of a NEBA, i.e. the net impact of *in-situ* burning of oil on water on the environment. This column is separated into three regions (air, water surface and water column) that are each affected by one of the three byproducts from *in-situ* burning. Studying the chemical composition of these byproducts will improve the input parameters that are used to determine the environmental impact in each of the affected regions as a part of a NEBA. The combination of the chemical composition of the byproducts and the operational parameters thus addresses both the positive environmental impact of *in-situ* burning (burning efficiency) and its negative impact (byproduct composition). The selected parameters are therefore considered to be able to fulfill the stated research objective.

### 1.5.1 Oil slick thickness

In addition to a minimal required thickness to support ignition, the slick thickness has also been known to influence burning parameters such as the burning efficiency, burning rate and residue formation (Garo et al., 1994; Buist et al., 1999; Buist et al., 2013). The most recent correlation between the slick thickness prior to ignition, i.e. the initial slick thickness, and the final residue thickness is based on a general “rule of thumb” (Buist et al., 1999; Buist et al., 2013). It states that for an initial slick thickness of < 40 mm, an oil slick would burn until it reaches a thickness of approximately 1 mm and for initially thicker slicks up to 100 mm the residue reaches a thickness of up to 6 mm. This rule suggests that the burning efficiency is predominantly a function of the initial slick thickness, with thicker initial slicks result in higher burning efficiencies. However, this rule is not consistent with experiments featuring oil slicks of > 10 mm thick that showed very low burning efficiencies (as low as 32%) (e.g. Fritt-Rasmussen et al. (2012); Farmahini Farahani et al. (2015b)). Therefore, the influence of the initial slick thickness on the burning efficiency, regression rate, mass burning rate and flame height was studied to improve the knowledge on the correlation between the slick thickness and the efficiency of *in-situ* burning. The results of this study are presented in Section 4.3.

### 1.5.2 Ignition

*In this thesis the term ignitability is used instead of the term flammability, which is used in fire science, to describe how difficult an oil slick is to ignite because ignitability is more common in the field of in-situ burning.*

The efficiency of an *in-situ* burning operation depends heavily on the ignitability of the oil slick. Once spilled, oil weathers as it loses its volatile components, mixes with water to form water-in-oil emulsions and spreads out, decreasing the slick thickness. These events all contribute to a more difficult to ignite oil slick (Buist, 2003). However, the degree to which weathering (evaporation and emulsification) and the slick thickness complicate the ignition of different oil types in terms of their thermal properties is not well established for most oils. Previous ignition studies have either focused on the thermal properties (Chen et al., 2014), the weathering of crude oils (Fritt-Rasmussen and Brandvik, 2011; Fritt-Rasmussen et al., 2012) or a combination of evaporation and the ignition delay time (Wu et al., 2000). A parametric study on the ignition of crude and refined oil in various weathering states in terms of their thermal properties would improve the understanding of the thermal requirements for igniting difficult to ignite oils. Therefore, the ignition time, surface temperature upon ignition, heat release rate, peak of the heat release rate and burning efficiency were studied as a function of the

external heat flux, weathering state and slick thickness for a light crude oil, a heavy crude oil and a heavy fuel oil. The results of this study are presented in Section 4.5.

### **1.5.3 Burning area**

The burning area is a parameter known to influence burning rate and smoke production of *in-situ* burning of crude oil (Koseki and Mulholland, 1991; Mulholland et al., 1996) and pool fires in general (Hottel, 1958; Babrauskas, 1983). Compared to operational scales, laboratory experiments on crude oil fires typically feature pool diameters that are one or two orders of magnitude smaller, in the range of 0.1-1 m. In this range, the burning rate and smoke production vary greatly with the diameter and results can be expected to deviate from operational scale measurements.

The known relations between the burning area and pool fire dynamics, however, cannot account for the observed burning area dependency of the burning efficiency. Small scale laboratory studies (Garo et al., 1996; Brandvik et al., 2010b; Fritt-Rasmussen et al., 2012; Farmahini Farahani et al., 2015b) have repeatedly reported lower burning efficiencies than large scale field studies (Allen, 1990; Guénette and Wighus, 1996; Brandvik et al., 2010a; Potter, 2010b). The burning efficiencies in the small scale studies varied between 30-90%, whereas a minimum burning efficiency of 95% was reported for the large scale studies. Apart from the burning area, no parameters were found to be related to the differences in burning efficiencies between the small and large scale studies. For *in-situ* burning to be a suitable oil spill response method, it is important to ensure that the lower range of burning efficiencies can be avoided during full scale operations. Throughout this Ph.D. study, experiments have been performed under similar conditions at different sizes to confirm the relationship between the burning area and burning efficiency observed in literature. The fire chemistry of *in-situ* burning of crude oil was studied in order to determine the parameters that govern the burning efficiency and as such establish the influence of the burning area, as described in the following section. The results on the parameters governing the burning efficiency, including the burning area, are presented in Section 4.7.

### **1.5.4 Vaporization order of crude oil**

For a multicomponent fuel such as a crude oil (see Section 2.2), the burning efficiency is determined by the type and the quantity of components that evaporate from the burning fuel, i.e. the vaporization process. Many

of the physical parameters that influence the vaporization have been studied and their effects on the ignitability and burning efficiency of crude oil are well-known. Examples include the regression rate (Torero et al., 2003), heat losses to the water (Brzustowski and Twardus, 1982), emulsification (Guénette et al., 1995; Walavalkar and Kulkarni, 2001), evaporative losses (Guénette et al., 1995; Wu et al., 2000) and weather conditions (Guénette et al., 1995). However, the studied parameters could not be used to explain the observed dependency of the burning efficiency on the burning area.

One aspect of crude oil that has remained relatively less studied in relation to combustion is its multicomponent nature. The aforementioned studies focused on the quantity and rate of the vaporization process and not the chemical composition that determines the type of components that can evaporate. Crude oils consist of thousands of different hydrocarbons, each with their own specific density, viscosity, flashpoint, boiling point, etc. (AMAP, 2010b; Fingas, 2011a). The order in which these components evaporate during combustion is here referred to as the vaporization order. Although several models have been suggested in literature for the vaporization order of multicomponent fuels (Petty, 1983; Buist et al., 1997; Law, 2006), there has not been a single generally acknowledged model for crude oil combustion. Combined with the physical parameters that determine the vaporization quantity and rate, knowing the vaporization order would result in a good understanding of the vaporization process. This will in turn improve the general understanding of the burning efficiency and could provide new insight on the relation between the burning area and burning efficiency.

The vaporization order models from literature were used to make qualitative predictions for four burning parameters: the surface temperature, burning rate, flame height and the residue composition. Experimental data from fresh crude oil and alkane burning experiments were then compared to the model predictions to determine the best fitting model for the vaporization order of crude oil. In order to confirm the suggested model, a series of burn experiments was conducted in which burning crude oil was manually extinguished at burning efficiency intervals of 10-15%. The resulting residue samples were analyzed by chemometrics, a statistical analysis of chemical data (Christensen et al., 2005; Christensen and Tomasi, 2007; Malmquist et al., 2007), to identify relevant changes in the chemical composition of the residues over time. Using the established model, the obtained burning efficiencies were analyzed for the tested scale and large scale results from the literature. The results of this study are presented in Section 4.2.

### 1.5.5 Water influence and boilover

The main difference between a regular pool fire and *in-situ* burning is the water body below the burning oil. The two most notable effects of the water are that it acts as a heat sink and can start boiling below the oil slick and cause an explosive effect known as the boilover phenomenon. As a heat sink, the water causes the required minimum thickness for ignition and unburned residue (Brzustowski and Twardus, 1982) and reduces the burning rate (Arai et al., 1990). The cooling effect of the water layer below the oil was monitored during the studies on the influence of the slick thickness, ignition and vaporization order to account for any effects it could have had on the results.

The boilover phenomenon is typically attributed to the superheating of the water directly below the burning oil (Arai et al., 1990; Garo et al., 1994). Because the oil layer isolates the water from the air, the water cannot vaporize at its normal boiling point and becomes superheated, to the point where it reaches a temperature of 120-150 °C. At this point (heterogeneous) nucleation will occur, which leads to the violent boiling of the water (Blander and Katz, 1975) that forces water vapor through the oil slick. This violent boiling also throws liquid oil droplets in the flames, leading to the explosive character of a boilover. The burning rate, flame height and heat release rate greatly increase during a boilover (Evans et al., 1988; Garo et al., 1994; Guénette et al., 1994) and oil droplets are being ejected outside of the burning area. The effects of this phenomenon on operational scales are not known, but could potentially complicate cleanup of the residue and safety measures would need to account for the sudden increase of the fire intensity.

Boilovers are observed predominantly during (laboratory) experiments in controlled test volumes (e.g. Evans et al. (1988); Arai et al. (1990); Garo et al. (1994); Farmahini Farahani et al. (2015b)) and have not been observed during any *in-situ* burning operations or experiments on moving water (Buist et al., 2013), such as on sea. It was suggested that the currents refresh the water below the oil layer so that the water never reaches the boiling temperatures to start a boilover (Buist et al., 2013). If this theory is correct, the boilover phenomenon would not be relevant to most *in-situ* burning operations on open water and could thus be neglected in risk or impact assessments. To test this theory, the boilover tendency of burning crude oil was studied on still water, on moving water, without water and as a water-in-oil emulsion without water. The results of this study are presented in Section 4.6.

### 1.5.6 Chemical herders in ice-infested water

An alternative tool to thicken spread oil slicks instead of fire booms is a chemical “herder”. Herders are a chemical surfactant that spreads out rapidly over a water surface and when applied around an oil slick will ‘push’ the oil into a smaller surface area, i.e. herding the oil. As the surface area decreases, the slick thickness of the oil must increase. Herders are of particular interest in water with a medium (3/10-7/10) ice coverage because fire booms have only been effectively used in ice coverages up to 3/10 (Potter, 2010b) and the ice inhibits the spreading of the oil above a 7/10 ice coverage (SL Ross and DF Dickins, 1987; Brandvik et al., 2006). Experiments have shown that herders could effectively increase the slick thickness in this range of ice coverages (3/10-7/10) to 3-8 mm, which are sufficient for ignition (SL Ross, 2007). During the herding of oil in ice-infested waters, however, oil slicks were observed to break up into multiple slicks after the herder had been applied (SL Ross, 2007). This fracturing of the oil slick would inhibit flame spreading, since flames cannot spread between separate oil slicks. Considering that one of the main uses of herders is to facilitate *in-situ* burning, the burning efficiency should not be reduced by fracturing of the oil slick during the herding process.

There is currently very little knowledge on how the formation of multiple oil slicks would influence *in-situ* burning and the achieved burning efficiency. Previous studies reporting the fracturing of herded oil slicks focused on the herded slick thickness and did not study the *in-situ* burning of these fractured slicks (SL Ross, 2007). Fracturing of an oil slick may be due to the presence of ice on the water surface, since the formation of multiple slicks has not been observed in open waters under similar calm weather conditions (SL Ross, 2012). It is therefore important to map the effects of ice on the herding process in order to determine the ice conditions under which herders can effectively facilitate *in-situ* burning of oil. As such, the pre- and post-herding slick thickness, surface distribution and burning efficiency of a crude oil on ice-infested water were studied as a function of the ice coverage. Herding of oil in ice-infested water was studied in both small and intermediate scale experiments to investigate whether the results can be extrapolated to full scale scenarios. The results of this study are presented in Section 4.4.

### 1.5.7 Residue, smoke and water fraction composition

A variety of studies have addressed the composition and toxicity of the smoke plume, residue and oil fraction dissolved in the water column, i.e. the formed byproducts, as a result of *in-situ* burning (e.g. Daykin et al. (1994); Ross et al. (1996); (Faksness et al., 2012); Fritt-Rasmussen et al. (2013a)). These studies typically

focused on the composition of one of these three byproducts and the residue and water fraction compositions were only measured after the fire was extinguished. Combining the results for each byproduct may give an impression of the overall toxic effects from the *in-situ* burning byproducts, but only if they were based on samples originating from a similar burning efficiency and oil type. The chemical composition of the residue was shown to be a function of the burning efficiency (Fritt-Rasmussen et al., 2013a), which implies that the composition of the other byproducts should also be a function of the burning efficiency. Depending on the burning efficiency, the toxicity of each byproduct and thus the overall toxic impact of *in-situ* burning may differ. Toxicity studies should therefore be aware of the burning efficiency from which the tested samples originate, as this can have an influence on the results.

A comprehensive study of the chemical composition of each of the three byproducts as a function of the burning efficiency, and thus time, however, does not exist. A new experimental setup that allows for the simultaneous study of the water fraction, the residue and the smoke plume emissions from *in-situ* burning of crude oil on water was therefore developed. Initial experiments were conducted to evaluate and test the potential of the new setup to provide a complete chemical balance between the three byproducts as a function of the burning efficiency. The new experimental setup is introduced in Section 3.5 and the initial results are presented in Section 4.8.

## **1.6 Outline of the thesis**

In Chapter 2 an overview is provided on the background of *in-situ* burning and the theoretical concepts that are relevant to crude oil burning on water for this thesis. The presented information is supplementary to the introduction and the above discussed experimental parameters and aids the interpretation of the presented results in Chapter 4. Then, Chapter 3 describes the materials and the experimental equipment used in this study and the methodology of the experimental work. Chapter 4 presents the results and discusses the results in terms of the research objective. Finally, Chapter 5 presents the conclusions of this study and provides recommendations for further studies.

## 2 Theoretical background

This chapter presents the theoretical concepts related to the burning of a crude oil on water. Sections 2.1 and 2.2 are relevant for the general understanding of the presented results throughout this thesis. Some of the sub-sections in these sections have a more direct relation to some of the result sections, which is indicated at the end of each of these sub-sections. Section 2.3 discusses the weathering of crude oil, both in general and in an Arctic context, which is mainly relevant for the results on the ignition of weathered oils (Section 4.5). Then, Section 2.4 presents the vaporization order models for multicomponent fuels, which are used to determine the vaporization order for crude oils in combination with the experimental results in Section 4.2. Finally, Section 2.5 discusses the functioning mechanisms of chemical herders, which is relevant to the results on the herding of crude oil in ice-infested water (Section 4.4).

### 2.1 Liquid pool fires

The fire dynamics of *in-situ* burning of oil fall in the category of pool fires, which features flaming combustion of a non-premixed, liquid fuel. Liquid fuels are by definition non-premixed fuels, which means that the fuel is not mixed with an oxidizer prior to ignition. The oxidizer will thus come from an external source, which is commonly the oxygen in air. Combustion is an exothermic chemical reaction in the gas phase between a fuel and oxidizer that results in heat and combustion products and may produce a flame, as is seen for liquid pool fires.

#### 2.1.1 Ignition and flame spread

Ignition of any given fuel requires that the gaseous concentration ratio of fuel and oxidizer lies between the lower and upper flammability limits, i.e. there should be sufficient fuel and oxidizer present in the mixture to be ignitable (Zabetakis, 1965; Drysdale, 2016). For liquid fuels, this means that the evaporation rate from the fuel must be sufficient to result in a gaseous fuel concentration in air above the lower flammability limit. The minimum temperature of a liquid fuel at which its evaporation rate will exceed the lower flammability limit, and the fuel thus becomes ignitable, is called the flashpoint. Introducing an ignition source, such as a spark or

flame, to the gaseous mixture of fuel and oxygen of a liquid fuel at its flashpoint will then trigger the ignition and start the flaming combustion of the fuel.

Once a fuel is ignited, the initial flame can either result in a self-sustaining fire or extinguish shortly after the combustible gases in the initial fuel-oxygen mixture have been burned. In order for the fire to be self-sustainable, the evaporation rate from the (liquid) fuel source must be equal to or higher than the reaction rate of the fuel with the oxygen in the reaction zone (i.e. the flame sheet). The temperature of the fuel that corresponds to this evaporation rate is called the fire point (Glassman and Dryer, 1981). For hydrocarbon fuels, the fire point can be several tens of degrees higher than the flashpoint (Glassman and Dryer, 1981), which indicates that additional heating may be required after ignition to produce a self-sustaining fire.

After ignition, the spreading of the flame over the fuel surface depends on whether the surrounding fuel temperature is above or below the flash- or fire point. Because extinction of the flame has the same result for *in-situ* burning purposes (i.e. no burning) whether the flame spreads on the surface or not, only the scenarios for self-sustaining fires are discussed here. For fuel temperatures above the flash- and fire point, the flame will spread rapidly over the fuel surface and result in a fully developed pool fire. For fuel temperatures below the flash- or fire point, the flame will first need to heat up the fuel and create a combustible mixture of fuel gas and oxygen above the fuel before the flame can spread further. The flame propagation will thus be notably slower, and if the heat feedback from the flame (Section 2.1.4) is not sufficient to heat up the fuel to its flash- or fire point, it may not propagate at all. This scenario is particularly relevant for heavily weathered oils with high flashpoints and indicates that the initial ignition of such weathered oils may not guarantee successful *in-situ* burning of the oil (i.e. a high burning efficiency).

The time it takes to ignite a fuel subjected to a heat source depends on whether the fuel is thermally thin or thermally thick (Quintiere, 1981; Wu et al., 2000; Torero, 2016). Thermally thin fuels are fuels that, when heated up from one side, have a uniform temperature distribution inside the fuel towards the opposite side of the fuel (Çengel and Ghajar, 2011). For example, for a pool fire on water, when the fuel surface is heated, a thermally thin fuel would have a uniform temperature between the fuel surface and the fuel-water interface. Thermally thick fuels, on the other hand, are fuels that do not heat up uniformly but will show a temperature gradient inside the fuel when subjected to a heat source (Çengel and Ghajar, 2011). Using the same example of a pool fire on water heated at the surface, a thermally thick fuel would have a higher temperature at the fuel surface than at the fuel-water interface.

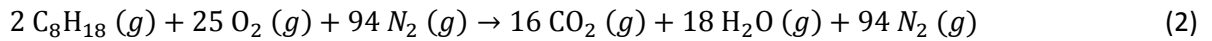
Crude and refined oils are typically assumed to be thermally thick fuels (e.g. Garo et al. (1999a); Wu et al. (2000); Chen et al. (2014)). For thermally thick fuels, Wu et al. (2000) showed that the time to ignition ( $t_{ig}$ ) can be calculated using Eq. (1):

$$t_{ig} = \frac{\pi}{4} \cdot k\rho c_p \cdot \left( \frac{T_{ig} - T_{\infty}}{a \cdot \dot{q}_{inc}''} \right)^2 \quad (1)$$

Here,  $k$  is the thermal conductivity,  $\rho$  is the density,  $c_p$  is the specific heat,  $T_{ig}$  is the surface temperature upon ignition,  $T_{\infty}$  is the ambient temperature,  $a$  is the absorptivity of the fuel and  $\dot{q}_{inc}''$  is the incident heat flux (in kW/m<sup>2</sup>), which is the (radiant) heat source used to heat up the fuel. Typically, the absorptivity is assumed to be equal to unity, but Wu et al. (2000) found that this was not representative for crude oils and therefore retained the absorptivity in the above equation. By expressing the ignition time of a fuel in the form of  $1/\sqrt{t_{ig}}$  as a function of the incident heat flux, a linear correlation will be observed between the ignition time and the incident heat flux. The intercept of this linear function with the x-axis ( $1/\sqrt{t_{ig}} = 0$ ) shows the minimum heat flux required for ignition, i.e. the critical heat flux ( $\dot{q}_{crit}''$ ). When the surface temperature upon ignition of a fuel is known, Eq. (1) can also be used to calculate the thermal inertia ( $\sqrt{k\rho c_p}/a$ ) of the fuel. The thermal inertia gives a measure of how difficult it is to heat up a fuel, i.e. the higher the thermal inertia, the more heat needs to be applied to heat up the fuel (Quintiere, 2006). The critical heat flux and thermal inertia are two common fuel properties that are used as a measure of how difficult it is to ignite a fuel (see e.g. Torero (2016)) and as such allow for comparison of the ignitability between different fuels. The theoretical concepts discussed in this section were specifically used to analyze the ignitability results of fresh and weathered oils (Section 4.5.1).

### 2.1.2 Combustion efficiency

The ratio between the fuel and oxidizer, known as the stoichiometry, determines the efficiency of the combustion, i.e. the extent to which the fuel is being oxidized in the fire (Gottuk et al., 1992). The optimal stoichiometry of a fuel depends on its molecular formula. For example, for hydrocarbons, such as  $n$ -octane in its gaseous state ( $C_8H_{18}(g)$ ), the complete combustion products are carbon dioxide ( $CO_2$ ) and water ( $H_2O$ ). The combustion reaction in Eq. (2) shows the required amount of oxygen ( $O_2$ ) to fully convert the  $n$ -octane to its combustion products. The inclusion of nitrogen ( $N_2$ ) indicates that the reaction is conducted in air.



The coefficients in front of each molecule indicate the mole ratio between each of the reactants (left) and the resulting products (right). Thus, for every mole of *n*-octane, twelve and a half moles of oxygen are required to result in complete combustion. When the fuel concentrations in the fuel-oxidizer mixture in the reaction zone increase above the ideal stoichiometric ratio, the mixture becomes fuel rich and the combustion efficiency reduces. Because there is not enough oxygen available to oxidize all the fuel atoms, other byproducts such as carbon monoxide (CO) and soot (C) are then formed (Gottuk et al., 1992; Tewarson et al., 1993). This is the case for hydrocarbon (oil) pool fires because the oxygen in the air outside the flames cannot mix sufficiently with the gaseous fuel within the flames before the fuel reacts in the flame sheet. For large fires, the incomplete combustion results in the formation of the characteristic black smoke plumes, such as for *in-situ* burning of oil on water.

### 2.1.3 Diameter and fire dynamics

The size of a pool fire, expressed in terms of the pool diameter ( $D$ ), is one of the most defining parameters of its fire dynamics. Blinov and Khudiakov (1957) found that the burning rate per unit area ( $\dot{m}''$ ) of liquid pool fires changes as a function of the diameter for different flow regimes (from Hottel (1958)) (Fig. 2.1). For  $D < 5$  cm, the flame is in the laminar flow regime and  $\dot{m}''$  decreases with increasing diameter. For  $0.05 < D < 1$  m, the flames are in the laminar-turbulent transition regime and  $\dot{m}''$  increases with increasing diameter. Finally, for  $D > 1$  m, the flames are in the turbulent regime and  $\dot{m}''$  is constant. Similar values and dependency of  $\dot{m}''$  as a function of the diameter in the laminar-turbulent transition and turbulent flow regimes have been shown for pool fires on water in experimental studies (see e.g. Koseki and Mulholland (1991); Evans et al. (1992); Garo et al. (1994); Shi et al. (2016)). Figure 2.2 gives an impression of the flames in different flow regimes and the corresponding smoke plumes as a function of the diameter.

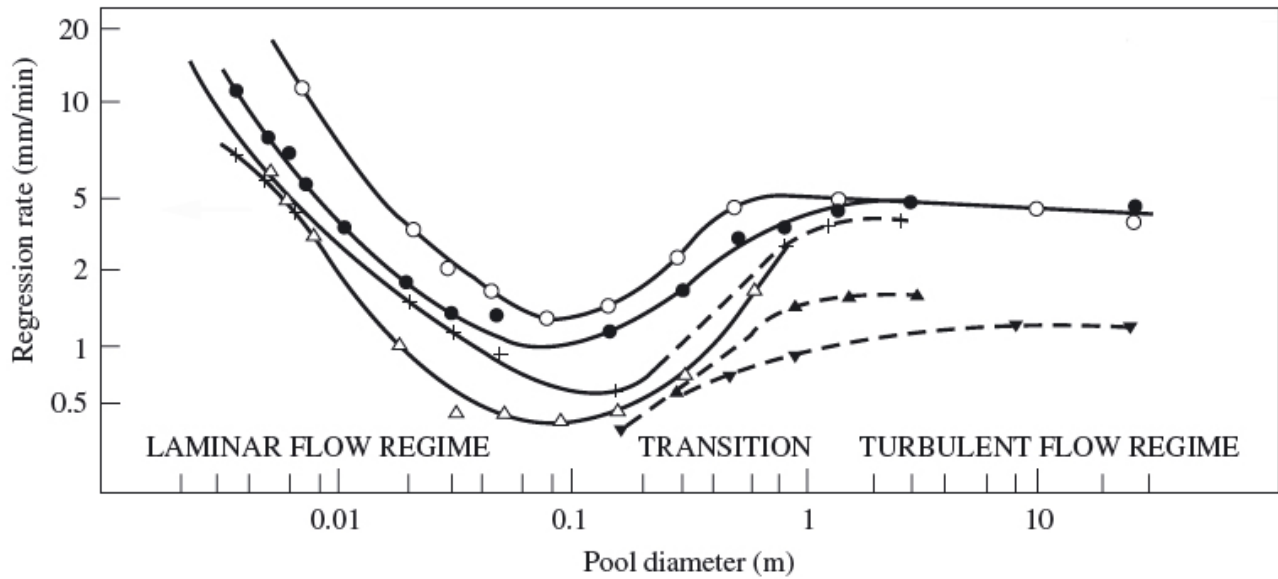


**Figure 2.1.** Regression rate of liquid pool fires as a function of diameter. Annotated symbols indicate gasoline (○), tractor kerosene (●), solar oil (△), diesel (+), petroleum (▲) and mazut oil (▼). Adapted from Drysdale (2011), based on Hottel (1958) and Blinov and Khudiakov (1957).



**Figure 2.2.** Examples of the flame type and smoke production for a laminar candle flame ( $D = 7$  mm), a laminar-turbulent small scale fire ( $D = 0.16$  m), a turbulent intermediate scale fire ( $D = 1.5$  m) and a turbulent operational scale fire ( $D > 10$  m). Operational scale photo (right) by Elastec (Allen, 2016).

Babrauskas (1983) showed that for  $D > 0.2$  m, the correlation between  $\dot{m}''$  and the diameter could be described using Eq. (3), where  $\dot{m}_{\infty}$  is the maximum burning rate and  $k\beta$  is a fuel specific constant (based on Zabetakis and Burgess (1961)).

$$\dot{m}'' = \dot{m}_{\infty} \cdot (1 - e^{-k\beta D}) \quad (3)$$

For any given fuel, the burning rate can then be used to determine the heat release rate ( $\dot{Q}$ ) using Eq. (4):

$$\dot{Q} = A \cdot \dot{m}'' \cdot \chi_c \cdot \Delta H_c \quad (4)$$

Here,  $A$  is the area of the fuel,  $\chi_c$  is the combustion efficiency factor that accounts for the incomplete combustion of the fuel and  $\Delta H_c$  is the heat of combustion of the fuel. The formation of soot and CO, as compared to CO<sub>2</sub>, releases less energy and hence the heat of combustion needs to be multiplied by  $\chi_c$  to reflect the effective heat of combustion ( $\Delta H_{eff}$ ). For soot producing and fuel rich fires,  $\chi_c$  is typically between 0.4-0.7 (Tewarson, 1982; Gottuk et al., 1992; Drysdale, 2011) and has been shown to depend on the diameter (Koseki and Mulholland, 1991). When the heat release rate and diameter are known, the flame height ( $L_f$ ) can be estimated using Eq. (5), as described by Heskestad (1983):

$$L_f = 0.235 \cdot \dot{Q}^{2/5} - 1.02D \quad (5)$$

In this equation, the flame height is defined as the height at which the flames are present 50% of the time.

From the above equations, it becomes evident that the diameter is an important parameter for pool fires. It is the only actual variable that determines the burning rate, heat release rate and flame height of a pool fire because all other parameters are constant for a given fuel. It is therefore important that results from experimental studies in the laminar-turbulent transition regime are adjusted accordingly when they are extrapolated to the turbulent regime of operational scales.

#### 2.1.4 Heat transfer mechanics

The main heat transfer mechanics for a confined pool fire on water are shown in Fig. 2.3, (adapted from Hamins et al. (1994)). Energy to the fuel is provided by the heat feedback from the flame and therefore depends on the size of the flame. The total net energy ( $\dot{Q}_{net}$ ) transferred to the fuel consists of the incoming

convective ( $\dot{Q}_{conv}$ ) and radiative ( $\dot{Q}_{rad}$ ) heat from the flame, minus any reflection from the fuel surface ( $\dot{Q}_{ref}$ ) (Eq. (6)) (Hamins et al., 1995). The net incoming energy is divided amongst the energy used to evaporate the fuel ( $\dot{Q}_{evap}$ ), heating of the bulk of the fuel as a consequence of the thermal gradient between the fuel surface and the oil-water interface ( $\dot{Q}_{grad}$ ), re-radiation from the fuel surface ( $\dot{Q}_{re-rad}$ ) and conductive heat losses to the water-cooled confinement ( $\dot{Q}_{conf}$ ) and the water below the fuel ( $\dot{Q}_{loss}$ ). Re-radiation from the pool surface is typically small compared to  $\dot{Q}_{evap}$  and is therefore considered to be negligible (Hamins et al., 1994). Usually, the conductive heat losses are also considered to be small but due to the presence of water as a heat sink the  $\dot{Q}_{loss}$  term becomes more prominent (Arai et al., 1990). Because the confinement area exposed to hot fuel is generally small compared to the area of the fuel-water interface for oil pool fires on water, the conductive heat losses predominantly consist of  $\dot{Q}_{loss}$ . Thus, the two main mechanics that reduce the energy available at any given time for evaporation of the liquid fuel are  $\dot{Q}_{grad}$  and  $\dot{Q}_{loss}$  (Eq. (7)).

$$\dot{Q}_{net} = \dot{Q}_{conv} + \dot{Q}_{rad} - \dot{Q}_{ref} \quad (6)$$

$$\dot{Q}_{evap} = \dot{Q}_{net} - \dot{Q}_{grad} - \dot{Q}_{loss} \quad (7)$$

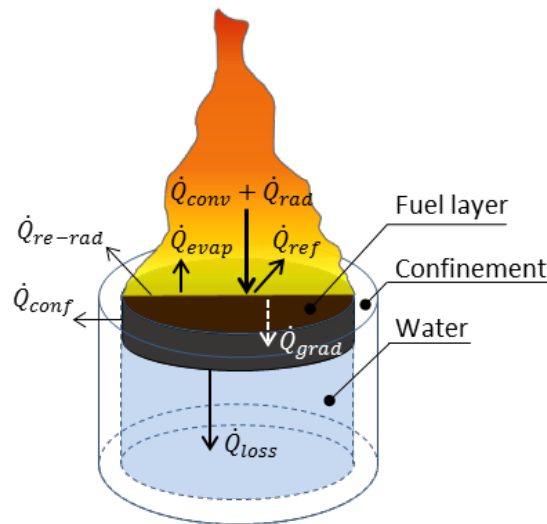


**Figure 2.3.** Schematic of the main heat transfer mechanics for a confined oil pool burning on water, adapted from Hamins et al. (1994). For *in-situ* burning purposes, the confinement could be a boom, ice or herder, which is in turn surrounded by a large water body.

Hamins et al. (1995) showed that the ratio between  $\dot{Q}$  and  $\dot{Q}_{net}$  is independent of the burning rate for pool fires without an underlying water layer. This is a relevant correlation because it indicates that the energy available for evaporating a fuel is mainly depending on its intrinsic parameters, rather than external factors such as the pool diameter. By assuming that all heat losses are insignificant, all of the incoming heat is used to evaporate the fuel at the fuel surface ( $\dot{Q}_{evap}$ ) and heating of the bulk of the fuel ( $\dot{Q}_{grad}$ ). The energy needed to evaporate the fuel depends on its latent heat of vaporization ( $\Delta H_v$ ) and the burning rate. The energy used to heat up the bulk of the fuel depends on its specific heat, the difference between the surface temperature ( $T_s$ ) and the ambient temperature, and the burning rate ( $\dot{m}$ ). The effective heat of gasification ( $\Delta H_g$ ) was defined as a combination of these terms (see also Spalding (1955, 1962)), resulting in Eq. (8):

$$\dot{Q}_{net} = \dot{Q}_{evap} + \dot{Q}_{grad} = \dot{m} \cdot \Delta H_v + \dot{m} \cdot c_p \cdot (T_s - T_\infty) = \dot{m} \cdot (\Delta H_v + c_p \cdot (T_s - T_\infty)) = \dot{m} \cdot \Delta H_g \quad (8)$$

The heat feedback to the fuel can also be expressed as a function of  $\dot{Q}$  and a heat feedback fraction ( $\chi_s$ ), as shown in Eq. (9):

$$\dot{Q}_{net} = \chi_s \cdot \dot{Q} \quad (9)$$

Using the expression for  $\dot{Q}$  from Eq. (4) for complete combustion of the fuel ( $\chi_c = 1$ ), the heat feedback fraction was then rewritten to finally yield Eq. (10). Although this equation was developed for pool fires with a steady fuel surface level and not for a regressing fuel layer, the mass loss rates in the  $\dot{Q}_{net}$  and  $\dot{Q}$  terms are not expected to differ significantly for *in-situ* burning of oil on water. Equation (10) is therefore expected to be valid for the oil pool fires on water discussed in this thesis as well.

$$\chi_s = \frac{\dot{Q}_{net}}{\dot{Q}} = \frac{\dot{m} \cdot \Delta H_g}{\dot{m} \cdot \Delta H_c} = \frac{\Delta H_g}{\Delta H_c} \quad (10)$$

For a pool fire on water, however, the conductive heat losses to the water layer ( $\dot{Q}_{loss}$ ) cannot be assumed to be negligible and should be taken into account in the above equations. Combining Eq. (7) and (8) then results in Eq. (11):

$$\dot{Q}_{net} = \dot{Q}_{evap} + \dot{Q}_{grad} + \dot{Q}_{loss} = \dot{m} \cdot \Delta H_g + \dot{Q}_{loss} \quad (11)$$

Substituting this expressing for  $\dot{Q}_{net}$  into Eq. (10) then gives Eq. (12):

$$\chi_s = \frac{\dot{Q}_{net}}{\dot{Q}} = \frac{\dot{m} \cdot \Delta H_g + \dot{Q}_{loss}}{\dot{m} \cdot \Delta H_c} = \frac{\Delta H_g}{\Delta H_c} + \frac{\dot{Q}_{loss}}{\dot{m} \cdot \Delta H_c} = \frac{\Delta H_g}{\Delta H_c} + \frac{\dot{Q}_{loss}''}{\dot{m}'' \cdot \Delta H_c} \quad (12)$$

Since  $\dot{Q}_{loss}$  is not depending on the burning rate, but rather on the mass of the water volume that is heated up, the burning rate cannot be removed from this term. As such, Eq. (12) shows that the heat feedback fraction is depending on the burning rate (per unit area) for oil pool fires on water. When  $\dot{m}''$  increases, the heat loss term becomes less significant, which suggests that heat losses to the water layer are less relevant for large scale than small scale *in-situ* burning operations or experiments. Literature data report that the burning rate per unit area can increase by as much as a factor 6 between  $D = 0.1$  m and  $D = 1$  m (Koseki and Mulholland, 1991) (see also Fig. 2.1). It is therefore important to take the scaling of conductive heat losses to the water layer into consideration when analyzing *in-situ* burning results among different scales. The heat transfer equations derived in this section were used in particular to analyze the influence of the vaporization order on the burning efficiency for different scales of crude oil fires on water (Section 4.2.4).

## 2.2 Crude oil chemistry

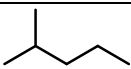
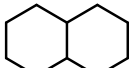
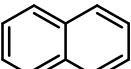
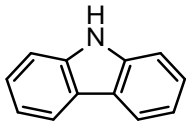
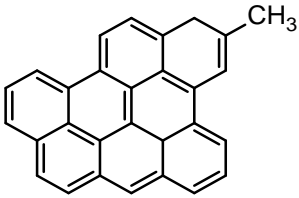
### 2.2.1 Chemical composition of crude oils

As mentioned in the introduction, crude oils consist of thousands of different components. The vast majority of these components are hydrocarbons ( $C_xH_y$ ) in various molecular structures, from small alkanes such as hexane ( $C_6H_{14}$ ) to large asphaltenic components consisting of multiple aromatic  $C_6$ -rings. In addition to pure hydrocarbons, crude oils can also contain hydrocarbons with heteroatoms, such as nitrogen, oxygen and sulfur, and low concentrations of trace metals. The countless possible combinations of all these chemical components make that each crude oil is a unique chemical mixture. Crude oils have therefore been categorized based on the abundance of chemical structure types or their physical properties, rather than on precise chemical structures.

The main chemical structure classifications of hydrocarbon molecules (including heteroatoms) in crude oils are shown in Table 2.1 (Sørheim and Moldestad, 2008; AMAP, 2010b; Fingas, 2011a). This table does not provide a

complete overview of all the chemical structures found in crude oils, but only focuses on the structures that are commonly used for the categorization of crude oils (see also Fan et al. (2002) and Fingas (2011a) for an alternative categorization method). Based on these structure classifications, Moldestad and Lewis (2006, in AMAP 2010b) categorized crude oils in four categories (paraffinic, naphthenic, waxy and asphaltenic), as shown in Fig. 2.4 (adapted from Sørheim and Moldestad (2008); Brandvik et al. (2010c)).

**Table 2.1.** Classification of hydrocarbons by molecular structure (Sørheim and Moldestad, 2008; AMAP, 2010b; Fingas, 2011a)

<i>Classification</i>	<i>Description</i>	<i>Molecular structure characteristics</i>	<i>Example structure<sup>a</sup></i>
Paraffins	Alkanes, known as waxes for $\geq C_{20}$	Straight and branched chains of saturated <sup>b</sup> alkanes ( $C_nH_{2n+2}$ ).	 2-methylpentane
Naphthenes	Cycloalkanes	Saturated cyclic molecules	 Decalin
Aromatics	Cyclic hydrocarbons, known as PAHs for $\geq 3$ conjugated rings	Unsaturated cyclic molecules	 naphthalene
Resins	Polar molecules that can include heteroatoms or trace metals	Mixture of saturated and unsaturated cyclic hydrocarbons, molecular weights of 367-423 Da (Porter et al., 2004)	 Carbazole
Asphaltenes	Large, polycyclic molecules that can include heteroatoms or trace metals	Consisting of 6-20 aromatic rings, molecular weights of 500-1000 Da (Groenzin and Mullins, 2000)	 From Schuler et al. (2015)

<sup>a</sup> The discrepancy between the proposed molecular weights and molecular structures for resins and asphaltenes shows that there are still uncertainties regarding the chemical structures of these components in crude oil.

<sup>b</sup> Saturated components have the maximum number of hydrogen atoms per carbon and contain only single C-C bonds.

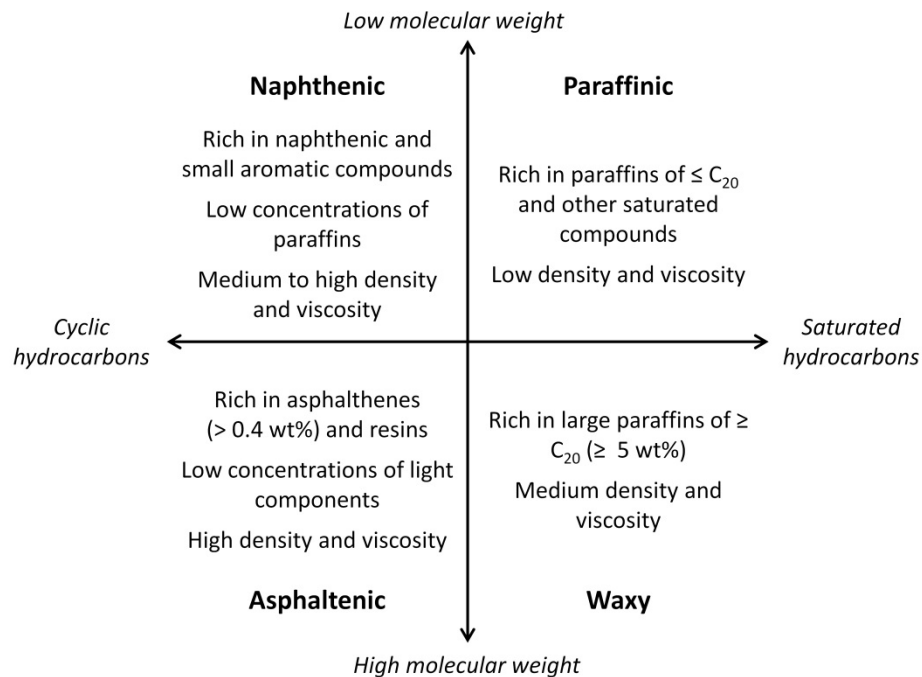


**Figure 2.4.** Crude oil categorization graph based on the abundance of certain classes of chemical components (based on Sørheim and Moldestad (2008); AMAP (2010b)).

Alternatively, crude oils can also be categorized as a function of their density and are then labeled as light, medium or heavy crude oils (see e.g. National Research Council (2014)). The density and other physical properties of a crude oil are determined by the weighted averages of the respective properties of each of the components in the crude oil. Thus, the properties of a crude oil reflect the physical properties of its most defining chemical fractions, which are labeled in a similar fashion. For example, light crude oils are rich in components that have low densities such as paraffinic components of  $\leq C_{20}$  and hence these components are referred to as the light fraction of a crude oil. Similarly, heavy crude oils are rich in components that have high densities such as asphaltenes, which are referred to as the heavy fraction of a crude oil. These oil fractions have been defined by Buist et al. (1997) in terms of boiling point ( $T_b$ ) ranges, namely  $T_b < 204$  °C (light),  $204 \leq T_b < 538$  °C (medium) and  $T_b \geq 538$  °C (heavy).

The density of a hydrocarbon is indirectly related to its other physical properties because all its physical properties depend on the molecular structure of a hydrocarbon. Although there are no exact correlations between the physical properties, similar molecular structures have generally similar physical properties (see

Section 2.2.2). Therefore, the density categories for crude oils can give a general impression of other properties such as the viscosity, flashpoint and volatility (Table 2.2). The presented values should be considered as an estimated range rather than strict boundaries, because varying definitions and values have been reported for these oil categories (Wang et al., 2003; Fingas, 2011a; National Research Council, 2014; ITOPF, 2016).

**Table 2.2.** Oil categorization based on density (AMAP, 2010b; Fingas, 2011a)

<i>Oil category</i>	<i>Density (g/ml)</i> <i>at 15 °C</i>	<i>Viscosity (cP)</i> <i>at 15 °C</i>	<i>Flashpoint (°C)</i>	<i>Volatility</i>
Light crude oil	≤ 0.87	5 – 50	-30 – 30	High
Medium crude oil	0.87-0.90	25 – 100	-30 – 50	Medium
Heavy crude oil	≥ 0.90	100 – 50000	-30 – 100	Low

### 2.2.2 Physical properties of hydrocarbons

The physical properties of a hydrocarbon are a function of the molecular weight and molecular structure group. Within a group, such as *n*-alkanes, cycloalkanes or aromatics, physical properties are a direct function of the molecular weight (i.e. the number of atoms) of the molecules. With increasing molecular weight, the density (Yaws, 2015), boiling point (Egloff et al., 1940), flashpoint (Nolan, 2011), viscosity (Carmichael et al., 1964; Korsten, 2001), heat of combustion (kJ/mol) (Prosen and Rossini, 1945; Seaton and Keith Harrison, 1990) and heat of vaporization (kJ/mol) (Bradford and Thodos, 1967; Vetere, 1979; Růžička and Majer, 1994) increase, whereas the vapor pressure decreases (Piacente et al., 1994; Chickos and Hanshaw, 2004). Independent of structure groups, these properties are not perfect functions of the molecular weight, but the trends remain applicable in general. As such, the light, medium and heavy fractions of a crude oil are mostly related to the sizes of the molecules in these fractions. Combined with the classification descriptions in Table 2.1, the oil categories in Table 2.2 can then be related to those in Fig. 2.4, as light crude oils are similar to paraffinic crude oils, medium crude oils are similar to naphthenic and waxy oils, and heavy crude oils are similar to asphaltenic oils.

For fire dynamics analyzing purposes, the heat of combustion and heat of vaporization should be expressed per unit mass (kJ/kg) rather than per unit mole (kJ/mol) (as in Eqs. (4), (8), (10) and (12)). The properties show a linear increase with increasing molecular weight in the same structure group when expressed in kJ/mol, but

show an asymptotic decrease with increasing molecular weight when expressed in kJ/kg. For pure hydrocarbons, the heat of combustion per unit mass varies approximately between 50-40 MJ/kg (it decreases with increasing molecular weight). Most crude oils therefore have an averaged heat of combustion of 44-45 MJ/kg. The heat of vaporization, however, varies significantly depending on the temperature and cannot simply be expressed as a function of the molecular weight. At the normal boiling point of hydrocarbons, the heat of vaporization decreases with increasing molecular weight (Vetere, 1979), whereas the heat of vaporization is near constant at 298 K with increasing molecular weight (Osborne and Ginnings, 1947; Růžička and Majer, 1994; Chickos and Hanshaw, 2004). This is a relevant difference because it changes the correlation between the mass transfer number ( $B$ ) (Eq. (13)), also known as the Spalding number (Spalding, 1955), and the molecular weight.

$$B = \frac{\Delta H_c}{\Delta H_v + c_p \cdot (T_s - T_\infty)} = \frac{\Delta H_c}{\Delta H_g} = \frac{1}{\chi_s} \quad (13)$$

The  $B$  number shows whether the heat of combustion of a fuel is sufficient to sustain the required evaporation for self-sustaining combustion, i.e. when  $B \geq 1$ . When fuels have low temperatures during combustion (e.g. 298 K), the bulk of the liquid fuel needs to be heated up to the evaporation temperature at the surface, which increases with increasing molecular weight. Therefore, the  $T_s - T_\infty$  term increases in Eq. (13) and because  $\Delta H_v$  remains relatively constant, the  $B$  number decreases with increasing molecular weight (Emmons, 1956). When fuels are at their normal boiling point during combustion, the  $T_s - T_\infty$  term becomes zero and since  $\Delta H_v$  decreases more rapidly than  $\Delta H_c$ , the  $B$  number increases with increasing molecular weight (Emmons, 1956). The development of the temperature gradient in a burning fuel ( $Q_{grad}$ ) is thus an important parameter to the self-sustainability of a fire because it influences the  $B$  number. This can be in particular relevant for multicomponent fuels with components that have a wide range of evaporation temperatures and for fuel bulks that are cooled during combustion. Since both of these descriptions apply to *in-situ* burning of crude oil on water, the temperature gradient in a burning oil slick is expected to be an important parameter that influences the burning efficiency.

### 2.2.3 Chemical analysis of crude oils

The chemical composition of a crude oil is typically analyzed by gas chromatography (GC) (Wang et al., 2006; Fingas, 2011b). In this analysis method a sample of the crude oil is injected at a high temperature into a column and pushed through the column by an inert carrier gas (moving phase) to a detector. The column is coated with material (stationary phase) that interacts with the sample as it is pushed through the column by the moving phase. Depending on the strength of the interaction between each component in the sample and the stationary phase, the time to elute from the column and reach the detector (retention time) varies per component. The interaction strength depends on the molecular structure of a component and as such the retention time is unique for each component. Once a specific component reaches the detector, the signal strength is determined by its concentration in the sample. Gas chromatography is thus a method that can provide both qualitative and quantitative information of the chemical composition of a sample. A more detailed description of gas chromatography is beyond the scope of this thesis and more information can be found in for example Skoog et al. (2007).

By gradually increasing the temperature inside column (up to approximately 300 °C), the lightest components in a crude oil elute first, followed by the medium and then heavy components (e.g. (Malmquist et al., 2007)). Because components with very high boiling points remain in the solid phase inside the column, these components cannot be transported by the carrier gas to the detector. Gas chromatography is therefore limited to the analysis of components of approximately  $\leq C_{35}$ , which means that components such as asphaltenes are not detected by a gas chromatograph. A GC analysis can thus not be used to obtain a complete compositional analysis of a crude oil. Instead, it is used to provide a quick overview of the primary component types and the internal ratios between the light, medium and part of the heavy fraction. These primary component types and internal ratios are for example used to categorize crude oils, analyze the composition of *in-situ* burning residues (Fritt-Rasmussen et al., 2013a) or determine the evaporated fraction from a weathered oil (Sørheim and Moldestad, 2008) (see Section 2.3.1).

In order to increase the resolution to be able to differentiate between components with similar retention times, a gas chromatography can be combined with mass spectrometry (GC-MS) (Skoog et al., 2007). Overlapping components on the GC chromatogram can then be further separated based on molecular weight to improve the qualitative analysis of the sample. In GC-MS, components eluting from the column are broken up in the mass spectrometer into ions, charged fragments of the full molecular structure of a component. Based on the mass-to-charge ( $m/z$ ) ratio of each ion, the time to reach the mass spectrometer detector varies.

As such, components with similar gas chromatography retention times can be differentiated based on the time it takes for their fragmented molecular structure to reach the mass spectrometer detector. An ion chromatogram of an ion with a specific  $m/z$  value, resulting from a GC-MS analysis, consists of all the components that contain this ion in their molecular structure. Because ion  $m/z$  values can correspond to unique chemical structure fragments, the GC-MS analysis method allows for studying specific component structure groups in a crude oil. This is for example used to analyze the compositional changes of certain component groups in weathered oils (Malmquist et al., 2007) or for the chemical fingerprinting of oil (Daling et al., 2002; Wang et al., 2006). The chemical analysis methods discussed in this section were used to analyze the chemical composition of burning residues with respect to the vaporization order of crude oil (Section 4.2).

## 2.3 Weathering of crude oils

The dominant weathering processes that influence *in-situ* burning of oil on water, in addition to spreading of the oil slick, are evaporation of the light components and emulsification with water. Other physical and chemical processes also contribute to the weathering of spilled oil on water (see e.g. AMAP (2010b)), but studying these processes was beyond the scope of this study. These weathering processes firstly affect the ignition of the oil and subsequently the flame spreading, as discussed below. The weathering extent of a spilled oil increases as a function of time, which continuously reduces the ignitability of the oil (Wu et al., 2000; Brandvik et al., 2004; Fritt-Rasmussen et al., 2012). This creates a window-of-opportunity that states the time period after the spill within which the oil can be ignited with the available ignition methods. Outside of the window-of-opportunity, the oil is considered to be non-ignitable and *in-situ* burning can no longer be applied (Nordvik, 1995; Brandvik et al., 2010c; Fritt-Rasmussen et al., 2012). Secondly, it has been shown that the burning efficiency could decrease for weathered oils compared to their fresh counterparts. For example, the burning efficiency of weathered oil was reduced to 50% compared to 90% for fresh oil in wavy conditions (Bech et al., 1993) and reduced to 75% compared to 92% for fresh oil under free spreading conditions (Guénette and Sveum, 1995). This shows that even when spilled oil is within the ignitable window-of-opportunity, weathering of the oil can still reduce the effectiveness of *in-situ* burning.

### 2.3.1 Evaporation

When a crude oil is exposed to the atmosphere, the light components with a high vapor pressure will evaporate from the oil over time (Reijnhart and Rose, 1982). Because these components also have generally low flashpoints (Section 2.2.2) the flashpoint of an oil weathered by evaporation will increase. Relative to the initial state of the oil, the oil slick therefore has to be heated to higher temperatures to reach a combustible amount of gaseous fuel above the oil slick. This requires a stronger ignition source (Wu et al., 2000) and the initial fire should also be large enough to be able to provide the higher heat feedback required to propagate the flame across the fuel surface of a less volatile fuel.

Evaporative weathering of oil starts instantly upon release of the oil on the water surface. The evaporation rate is the highest at the start of the spill, after which it declines over time as the oil gradually loses its volatile components, until approximately after a week all volatile components have evaporated (Mackay et al., 1983). The fraction of the oil that is lost through evaporation, i.e. the evaporative losses, is expressed as a weight percentage relative to the initial weight (wt%) or volume (vol%) of the oil. Depending on the compositional type of the oil, these losses can vary from > 40 vol% for light crude oils to < 15 vol% for some heavy crude oils (e.g. Fritt-Rasmussen et al. (2012)). Although the evaporative loss gives an impression of the weathering extent, it is not an accurate estimation of the ignitability of an evaporated crude oil. For example, crude oils with evaporative losses of > 40 vol% were successfully ignited and burned to high burning efficiencies (80-90%) in a field study by Bech et al. (1993). Because of the wide range of flashpoints for crude oils, weathered light crude oils can still have lower flashpoints than fresh or less weathered heavy crude oils (e.g. Wu et al. (2000)). Evaporation by itself is thus not a limiting weathering process for the application of *in-situ* burning. In combination with emulsification of the oil, however, it can rapidly change the ignitability status of the oil to non-ignitable.

### 2.3.2 Emulsification

Water-in-oil emulsification is caused by the mixing energy from turbulence induced by wind and waves that continuously mixes water into the oil (Lee, 1999). During this process, the water is broken up in droplets that can bind to the more polar components in the oil and thereby form water-in-oil emulsions. Over time, and depending on the composition of the crude oil, the size of water droplets in the oil reduces, which makes the droplets easier to stabilize and inhibit the coalescence of the droplets. The emulsion therefore shifts from an

unstable emulsion to a mesostable or stable emulsion during the weathering process. Whereas unstable emulsions break up into a water and oil layer within a few hours, mesostable and stable emulsions can remain emulsified for a few days to several years, respectively (Fingas et al., 2003).

The final stability of a water-in-oil emulsion mainly depends on the chemical composition of the oil. A large number of studies has shown that water droplets in oil are stabilized by large or polar components in the crude oil, i.e. asphaltenes, resins and waxes (e.g. Bobra (1991); McLean and Kilpatrick (1997); Aske et al. (2002); Fingas and Fieldhouse (2009)). In the form of submicrometer particles, asphaltenes and resins can form a sphere (supported by waxes) around the surface of a water droplet and as such stabilize the droplet within the oil (Mackay (1987) in Lee (1999)). Because these components only stabilize water-in-oil emulsions in the form of precipitated particles, crude oils that contain a relatively high amount of solvents (e.g. small aromatics) do not result in stable emulsions. Light crude oils with low concentrations of mainly dissolved asphaltenes and resins are therefore less likely to form stable emulsions than heavy crude oils with high concentrations of (precipitated) asphaltenes and resins.

The weathering extent of a water-in-oil emulsion is expressed in terms of the water content (in vol%) in the emulsion. On open waters, water is mixed rapidly into the oil and water uptake percentages as high as 80% can be reached in a few hours in the form of an unstable emulsion (Lewis et al., 1995; Daling et al., 2003; Brandvik et al., 2004). Evaporative losses of the light fractions of oil aid the stabilization of the emulsion because the concentration of asphaltenes and resins increases while the light solvent fraction decreases in concentration. As the evaporative losses increase over time, the emulsification of the oil transits from an unstable emulsion formed in the first hours after a spill to a (meso)stable emulsion over the course of multiple days to a month (Mackay et al., 1983; AMAP, 2010b). The weathering extent furthermore shows in the viscosity of the oil, which increases by several orders of magnitude for emulsions (see e.g. Brandvik et al. (2010c); Fritt-Rasmussen et al. (2012)).

Formation of stable emulsions is the main weathering process that determines the window-of-opportunity for *in-situ* burning because stable emulsions have a very limited ignitability (Bech et al., 1993; Buist and Glover, 1995; Guénette et al., 1995; Fritt-Rasmussen et al., 2012). To ignite a water-in-oil emulsion, a water-free layer of oil on top of the emulsion that provides the combustible gases required for ignition has to be formed (Bech et al., 1993; Guénette et al., 1995; Walavalkar and Kulkarni, 2001). This water-free layer can be acquired by evaporating water from the emulsion with heat or by breaking the emulsion with either chemicals (e.g.

Canevari (1982)) or heat, with the heat being applied by the ignition source. Once ignited, the flame then needs to provide sufficient heat feedback to the surface of the emulsion to create a new water-free oil layer and heat the oil to its fire point so that the flame can propagate. Flame propagation on a stable emulsion may require such large ignition sources (> 200 L of fresh oil) (Bech et al., 1993) that such emulsions might have to be considered to be non-ignitable in practice.

Laboratory and field studies have shown that stable emulsions of evaporated crude oils with a water content of  $\geq 25\%$  were non-ignitable for various environmental conditions and ignition sources (Bech et al., 1993; Buist and Glover, 1995; Guénette et al., 1995). In the presence of waves, the ignitable water content limit was further reduced to 12.5% (Bech et al., 1993). Unstable emulsions of fresh crude oils, however, could be ignited with a water content up to 60% (Buist and Glover, 1995), which highlights that the stability of an emulsion is an important parameter to the window-of-opportunity. When stable emulsions were successfully ignited in intermediate scales, the emulsions could be burned with high burning efficiencies (> 80%) (Bech et al., 1993; Buist and Glover, 1995; Guénette et al., 1995; Guénette and Wighus, 1996), although waves and spreading of the burning emulsion reduced the burning efficiency (50-75%) (Bech et al., 1993; Guénette and Sveum, 1995). Fritt-Rasmussen et al. (2012) showed that non-ignitable emulsions with 40-60% water content could form after 1-36 hours of weathering in open water, depending on the composition of the oil. The crude oil that had the highest asphaltenic content, and thus formed the most stable emulsion, formed a non-ignitable emulsion much faster (1 h) than the light (36 h) and waxy (18 h) crude oils, as expected. As such, the emulsification of oil, when stabilized by evaporation, creates a limited window-of-opportunity by rapidly reducing the ignitability of the oil as a function of the weathering time.

### **2.3.3 Weathering in cold climates**

The evaporation and emulsification processes were shown to be considerably slower in ice-infested waters and in cold climates. Evaporative losses in cold ( $< 0\text{ }^{\circ}\text{C}$ ), ice-infested sea water were reduced to 25% compared to 40% for evaporative losses on relatively warm ( $10\text{ }^{\circ}\text{C}$ ), open sea water (Brandvik et al., 2004) and were also lower than in laboratory weathering experiments at  $20\text{ }^{\circ}\text{C}$  (SL Ross and DF Dickins, 1987). The introduction of ice (5/10 and 9/10 coverage) in cold water reduced the evaporative losses by approximately 5% (Brandvik et al., 2010c) These results thus indicate that evaporation of oil is reduced with increasing ice coverage (due to reduced spreading (Brandvik et al., 2004)) and decreasing temperatures.

Water-in-oil emulsification had a strong correlation to the ice coverage. The water uptake was reduced from 70-80% in the first day on warm, open sea water to 20% after seven days on sea in an ice coverage of 9/10 for similar crude oils (Brandvik et al., 2004). No notable emulsification was observed within five hours of an oil spill in a dynamic ice coverage of 6/10-9/10 on sea, despite wavy and windy conditions (SL Ross and DF Dickins, 1987). In cold water conditions, increasing the ice coverage from open water to a 9/10 ice coverage reduced the water uptake by 20-60% for all crude oils with a low asphaltenic content (Brandvik et al., 2010c). After 75 hours of weathering in a high ice coverage, the water content in these crude oils was only 5-20%. The maximum water content of a heavy crude oil with a high asphaltenic content remained 70% in high ice coverages, but the water uptake rate was reduced by a factor seven (from 10 hours to 70 hours for 70% water). As a result of this slowed emulsification process in ice-infested water, the window-of-opportunity for ignition of the weathered oils was extended from 1-36 hours in open water to 9-75+ hours in a 9/10 ice-coverage (Fritt-Rasmussen et al., 2012). This extended window-of-opportunity because of the slowed weathering processes is another important reason why *in-situ* burning is considered to be a suitable oil spill response method in the Arctic environment (see also Section 1.3.2) (Buist et al., 2013).

The suppressing effect of ice on the emulsification process has been attributed to the dampening effect of ice on waves, which reduces the mixing energy at the oil-water interface (SL Ross and DF Dickins, 1987; Brandvik et al., 2010c). The correlation between the wave energy and emulsification rate was clearly shown by Singsaas et al. (1994) in a flume experiment in which the wave frequency was increased during the weathering process. After 12 hours the wave frequency was increased from low (non-breaking waves) to high (breaking waves) which resulted in a rapid increase of the water uptake rate. In the first 12 hours the water content in the oil increased from 0% to 10%, whereas it increased from 10% to 45% in the same time period after the wave frequency was increased.

## **2.4 Multicomponent fuel combustion models**

The model most commonly associated with the vaporization order of burning crude oil is the *Equilibrium Flash Vaporization* (EFV) model, as described in a recent comprehensive review on *in-situ* burning (Buist et al., 2013). This model was earlier proposed by Petty (1983) and describes the vaporization of a multicomponent fuel as being of “essentially constant composition” with a constant vaporization rate. Thus, all components evaporate

simultaneously, here defined as a uniform vaporization order, and each individual component contributes to the vaporization rate relative to its concentration in the oil. Characteristics of this model are that the crude oil burns with constant surface temperature at a constant rate, has a temperature gradient in the oil slick and lighter components are present in the residue (Petty, 1983; Buist et al., 2013).

An alternative to the EFV model was proposed by Buist et al. (1997), based on their studies on crude oil residues. Their results showed that crude oil residues had an increased concentration of heavy hydrocarbon fractions ( $T_b > 538$  °C) and complete removal of the light hydrocarbon fractions ( $T_b < 204$  °C). This trend was also found in previous studies on crude oil residue compositions (Buist et al., 1997; Garrett et al., 2000; Fritt-Rasmussen et al., 2013a). Buist et al. (1997) suggested that the burning proceeded according to an *Imperfect EFV* model in which lighter oil fractions are favored over heavier oil fractions during the burning. Thus, for this model the relative vaporization rate of lighter components is higher than their relative concentrations. Apart from this difference, the model follows the EFV model and as such features a constant vaporization rate and uniform vaporization order.

Also, three models have been developed for the vaporization of multicomponent fuels based on the Peclet number for mass diffusion ( $Pe_m$ ) (Eq. (14)) (Law, 2006). The value of  $Pe_m$  of a fuel determines which of these three models is the most appropriate to describe the vaporization (Makino and Law, 1988). Although these models were not developed specifically for the burning of crude oils, they describe the general vaporization process of multicomponent fuels in great detail.

$$Pe_m = \frac{K}{D_l} = \frac{\text{vaporization rate}}{\text{mass diffusion rate}} \quad (14)$$

For fuels where  $Pe_m$  approaches infinity, usually due to a negligible mass diffusion such as in solids, the composition of the fuel is fixed and no internal changes occur during the combustion. This means that the fuel is burned layer by layer and hence this model is known as the *Onion Skin* model. The vaporization order depends on the internal distribution of the components, e.g. uniformly or by density, and will be fuel dependent.

For fuels where  $Pe_m$  approaches zero, the fuel can be considered to have a uniform distribution of its components due to its relatively high mass diffusion rate. As a result, the vaporization order depends only on the relative volatility differences of the components. This model is known as the *Batch Distillation* model and

describes the fuel as being burned component by component with decreasing volatility (Law, 1976). Because the volatility is in general inversely proportional to the molecular weight for hydrocarbons, the vaporization order of this model is effectively in order of increasing molecular weight.

For fuels with a low, non-zero  $Pe_m$  value the vaporization is controlled by the concentration boundary layers (Law, 1978; Wang et al., 1984; Law, 2006). At the start of the combustion, the most volatile component at the surface will determine the vaporization rate by its volatility, like the batch distillation model. However, when its surface concentration becomes too low to support this vaporization rate, the vaporization becomes controlled by the mass diffusion rate of this component. Because the mass diffusion is much slower, the less volatile components at the surface will now also be able to contribute significantly to the vaporization rate. Thus, components do not evaporate one at a time, but rather a small amount of components with similar volatility evaporate simultaneously. The vaporization order is the same as for the Batch Distillation model, i.e. from the most volatile to the least volatile component. In this study, we will refer to this model as the *diffusion-limited vaporization* (DLV) model.

Because of the substantial amount of light hydrocarbons present in crude oil, it is unlikely that the onion skin model correctly describes the vaporization order. The onion skin model has only been associated with water-in-oil emulsions, as there is no mass diffusion between the water and oil components (Law, 1977, 2006). For heavily weathered crude oils (emulsified and evaporation of the lighter fractions) solid-like behavior has also been observed during flame spread experiments (Wu et al., 2000). The onion skin model may therefore be a suitable model for highly viscous and weathered oils. However, this study focuses on fresh crude oil and as such the onion skin model is not considered relevant herein.

The vaporization orders of the four remaining models are classified in two order types (uniform and volatility-controlled) and two sub-orders per vaporization order type, as summarized in Table 2.3. Each model has a unique combination of burning parameters that distinguishes between the vaporization orders and sub-orders so that these can be used to identify the correct model for a certain fuel. The modeling of these burning parameters is discussed in detail in Section 4.2.1.

**Table 2.3.** Vaporization order and burning features of four multicomponent fuel combustion models

<i>Model</i>	<i>Vaporization</i>		<i>Vaporization order</i>	<i>Vaporization sub-order</i>
	<i>Order</i>	<i>Sub-order</i>	<i>burning parameters</i>	<i>burning parameters</i>
EFV	Constant rate and uniform order	Vapor composition equal to fuel	<b>Constant</b> surface temperature	<b>Unchanged</b> residue composition
Imperfect EFV		Relatively more light components	<b>Constant</b> burning rate & flame height	Residue <b>depleted of light</b> components
Batch Distillation	In order of decreasing volatility	One component at a time	<b>Increasing</b> surface temperature	<b>Abrupt transition</b> from burned to unburned components in residue
DLV		Several components at a time	<b>Decreasing</b> burning rate & flame height	<b>Concentration gradient</b> from burned to unburned components in residue

## 2.5 Chemical herders

Herders, like many surfactants, consist of molecules with both polar (hydrophilic) and nonpolar (hydrophobic) properties and are poorly soluble in water. In order to minimize the energy in a water-herder system, the herder tends to form a monolayer of molecules at the water surface with the polar part in the water layer and the nonpolar part in the air (Kontogeorgis and Kiil, 2016a). This monolayer reduces the surface tension of the water, which makes it harder for other liquids (such as oil) to spread on the water surface.

When two liquids are competing to spread on water, the liquid that results in the lowest surface tension on the water is dominant over the other liquid. The tendency of a liquid to spread on water is more commonly expressed in terms of its spreading pressure. The spreading pressure of a liquid ( $\pi$ ) is defined as the difference between the original surface tension of the water ( $\gamma_w$ ) and the surface tension of the new water-liquid system ( $\gamma_N$ ) (Eq. (15)) (Garrett, 1969). The surface tension of the new water-liquid system is the sum of the surface tension of the liquid ( $\gamma_l$ ) and the surface tension of the water-liquid interface ( $\gamma_{wl}$ ) (Kontogeorgis and Kiil, 2016b).

$$\pi = \gamma_w - \gamma_N = \gamma_w - (\gamma_l + \gamma_{wl}) \quad (15)$$

The liquid with the highest spreading pressure is energetically favored to spread over water and thus will force liquids with lower spreading pressures to contract and prevent them from spreading on the water. Water typically has a surface tension of 70-75 mN/m, crude oils have spreading pressures of 10-30 mN/m (Winoto et al., 2014) and herders therefore need to have spreading pressures of > 40 mN/m to be effective at thickening oils on water (Garrett and Barger, 1970). This process is illustrated in Fig. 2.5 for the herding of a spread oil slick.

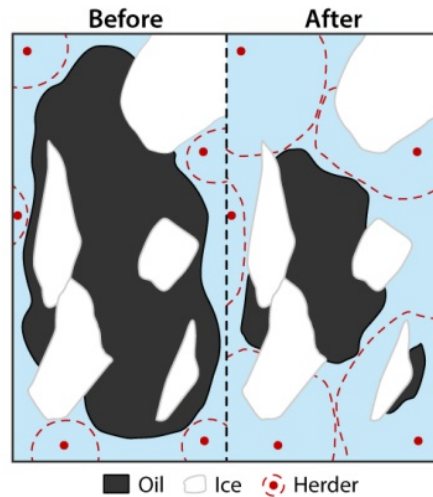


**Figure 2.5.** Schematic of the herding process of a spread oil slick. The herder (red dots) is applied around the oil slick and starts to spread out over the water surface (red dashed lines). As the herder comes into contact with the oil, it will replace the oil on the water surface because it has a higher spreading pressure, resulting in the contracting of the oil slick.

Initial herder research in the 1970s has shown that the monolayer of the tested surfactants was easily disrupted in wavy and windy conditions, which allowed the oil to spread out again (e.g. Garrett and Barger (1970)). These herders have therefore not been actively used in oil spill response operations (Buist et al., 2011). Recent research with (new) herders (Buist et al., 2010a), however, showed promising results for herding oil in a variety of environmental conditions. Crude oil has been successfully herded under swell wave conditions (SL

Ross, 2012), on open sea (Buist et al., 2011) and in cold temperatures (-21 to 0 °C) (SL Ross, 2007). *In-situ* burning was also successfully applied on several herded oil slicks, with burning efficiencies up to 94% as a result (SL Ross, 2007; Buist et al., 2011). Based on these results, herders are currently considered as a promising measure to counter oil spreading, among others to facilitate *in-situ* burning in Arctic waters (EPPR, 2015).

### 3 Materials and methods

This chapter presents the experimental setups and corresponding materials and methodologies that were used during this study. Section 3.1 presents the setup that was used for studying the vaporization order of crude oils and the influence of the initial slick thickness, of which the main results are presented in Section 4.2 and 4.3, respectively. Section 3.2 presents the setup that was used for studying the herding of crude oil in ice-infested waters, of which the results are presented in Section 4.4. Further, Section 3.3 presents the setup that was used to study the ignitability of fresh and weathered oils, of which the results are presented in Section 4.5. Then, Section 3.4 presents the setups and methodologies that were used for additional studies on the burning efficiency, of which the results are presented in Section 4.6. Finally, Section 3.5 presents the newly developed experimental setup for the simultaneous study of the composition of the byproducts from burning crude oil on water, of which the initial results are presented in Section 4.8. The experimental setups presented in Sections 3.1, 3.4 and 3.5 were all used to study the influence of the water layer and the boilover phenomenon, of which the results are presented in Section 4.7.

#### 3.1 Crude Oil Flammability Apparatus

The majority of the operational parameters were studied in the Crude Oil Flammability Apparatus (COFA) (Fig. 3.1) (Brogaard et al., 2014). The experimental setup consists of a 1.0 x 1.0 x 0.50 m<sup>3</sup> water basin featuring a Pyrex glass cylinder ( $D = 0.16$  m), standing on an open foot, that contains the oil sample. The open foot allows water to move freely at the bottom of the cylinder and therefore the level of a burning oil surface is maintained constant for a longer period of time. An adjustable thermocouple array hangs above the Pyrex glass cylinder that measures the temperature of the oil at its surface and at 2, 3, 5, 10, 20, 30, 40, and 50 mm below the surface. The COFA was specifically designed to have a large body of water to create an oil-water ratio comparable to on sea operations. This design choice was made to mitigate the complications with heat transfer issues that could be seen in laboratory studies with less or no surrounding water (Petty, 1983; Koseki and Mulholland, 1991; Garo et al., 1994; Walavalkar and Kulkarni, 2001). While heat transfer models have been used to accommodate for oil-water interface interactions (e.g. (Garo et al., 1999b; Hristov et al., 2004)), the uncertainties remained significant. The COFA setup has been verified against data on the ignitability of fresh and weathered crude oils from Fritt-Rasmussen and Brandvik (2011).

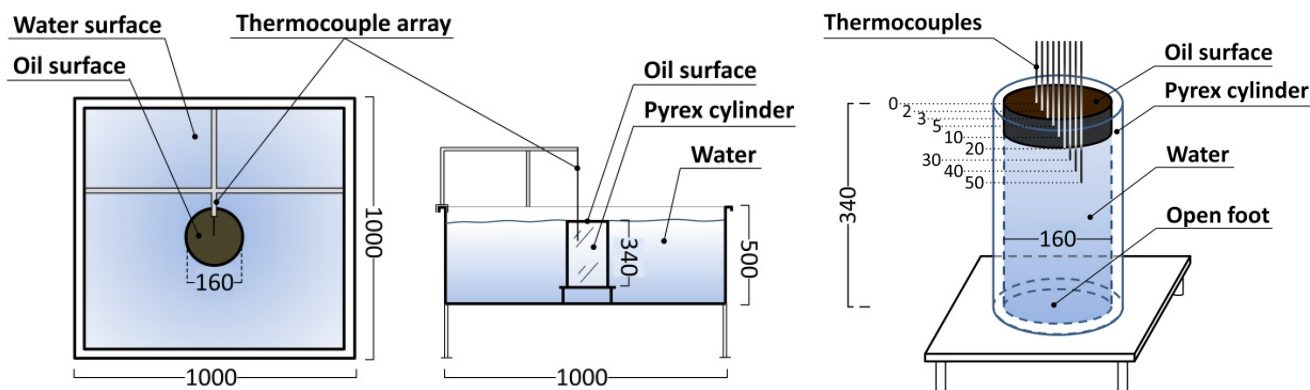


**Figure 3.1.** Schematics of the COFA setup from a top view (left) and cross sectional view (middle) and a close-up of the Pyrex glass cylinder on its open foot featuring the thermocouple distribution in the oil layer (right). All measurements are in mm.

In a standard experiment in the COFA, the COFA was filled with fresh water (5-25 °C) until it reached to about 1-5 cm from the top of the Pyrex glass cylinder. A known amount of oil, corresponding to an initial thickness of 2-40 mm, was then poured carefully on the water surface inside the cylinder. The oil volume corresponding to an oil layer with the thickness of interest was measured using a scale, based on the density of the oil. Additional water was added to the basin to raise the level of the oil surface to 1 mm below the edge of the Pyrex glass cylinder. The position of the thermocouple array was then adjusted so that the top thermocouple would touch the surface of the oil. All oils were ignited with a butane hand torch. After the fire extinguished, the residue was collected with 3M hydrophobic absorption pads and weighed to determine the burning efficiency with Eq. (16). Overnight drying of absorption pads with residue in an oven at 50 °C had shown that only trace amounts of water are absorbed by the hydrophobic pads and the pads are therefore considered to only collect oil residue. In general, the reproducibility of the experiments was good, unless specified otherwise. Experiments in the COFA setup were typically performed two to three times and showed results within a 10% variation of the reported data.

$$\text{Burning efficiency} = \frac{\text{mass}_{\text{initial}} - \text{mass}_{\text{residue}}}{\text{mass}_{\text{initial}}} \cdot 100\% \quad (16)$$

In order to analyze the flame height, all experiments conducted in the COFA were recorded on a black, non-reflecting background by a camera that faced the flame in a horizontal fashion. Videos of the flames were converted with a Matlab script to a series of binary pictures with an interval of 0.5 – 10 seconds, resulting in 300 – 600 flame images per experiment. The script then determined the flame height in pixels for each image. A still reference picture with a ruler at the center of the Pyrex glass cylinder in the same resolution as the video was used to convert the pixel flame height to a height in millimeters. To reduce scatter in the data caused by flame puffing, the average of every 10 data points was taken to represent the value of the flame height as a function of time with 30-60 data points per experiment.

### 3.1.1 Burning rate setup

The burning rate of oils tested in the COFA was measured in a separate experimental setup that allowed for the use of a load scale, but was otherwise similar to the COFA setup (Fig. 3.2). The Pyrex glass cylinder was placed on its open foot in a 0.30 x 0.30 x 0.40 m<sup>3</sup> metal bucket filled with fresh water (5-25 °C). The bucket stood on a load scale with a reading interval of 1 g and a two second data acquisition interval that was covered by an aluminum tray (0.9 x 0.9 m) to protect the scale from ejected oil droplets during boilover. In order to prevent re-radiation from the metal bucket edges to the oil surface, the top of the Pyrex glass cylinder was set at approximately the same height as the bucket edge. The flame height, temperatures from the thermocouple array and the burning efficiency were also recorded during burning rate experiments to be able to correlate the burning rate results with results from the COFA setup.

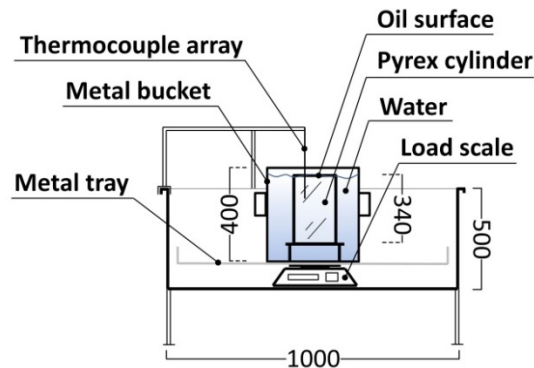


**Figure 3.2.** Schematic of the burning rate setup. All measurements are in mm.

### 3.1.2 Crude oils, refined oils and reference oils

Several crude oils, refined oils and reference fuels (alkanes) were used to study the operational parameters identified in Section 1.5. Depending on the parameter studied, different crude oils, refined oils and reference oils were used, as specified in each of the experimental methodologies described in this chapter. The crude oils used in this study were Danish Underground Consortium (DUC, from the North Sea), Russian Export Blend Crude Oil (REBCO, from the North Sea), Alaska North Slope (ANS, from the Chukchi and Beaufort Sea) and Grane (from the North Sea). The used refined fuels consisted of Intermediate Fuel Oil (IFO) 180, a heavy refined oil, gasoline and diesel and the used reference fuels were three pure *n*-alkanes. An overview of the tested oils and their characteristics that were most relevant for the purposes of this study is shown in Table 3.1.

**Table 3.1.** Physical and chemical characteristics of the used (crude) oils

<i>Oil</i>	<i>Density</i> (g/ml) <sup>a</sup>	<i>Boiling</i> point (°C)	<i>Flashpoint</i> (°C) <sup>b</sup>	<i>Viscosity</i> (cP) <sup>a</sup>	<i>Wax content</i> (wt%)	<i>Asphaltenic</i> content (wt%)
n-Octane (C <sub>8</sub> H <sub>18</sub> )	0.699	125-126	13	0.386	-	-
Dodecane (C <sub>12</sub> H <sub>26</sub> )	0.745	215-217	71	1.294	-	-
Hexadecane (C <sub>16</sub> H <sub>34</sub> )	0.770	287	135	3.036	-	-
Gasoline <sup>c</sup>	0.74-0.78	30-260	< -40	NA	-	-
Diesel	0.823	150-385 <sup>d</sup>	65-66	3.350	-	-
DUC	0.853	230+	7	6.750	4.2 <sup>e</sup>	< 0.05 <sup>e</sup>
REBCO	0.863	300+	23	12.40	4.9 <sup>f</sup>	1.0 <sup>f</sup>
ANS	0.871	NA	21	10.85	3.0 <sup>h</sup>	1.8 <sup>h</sup>
Grane	0.934	380+	20-21	268.7	7.0 <sup>g</sup>	0.9 <sup>g</sup>
IFO 180	0.968	330+	90	969.3	NA	NA

<sup>a</sup> Measured at 25 °C using an Anton Paar SVM 3000 viscometer.

<sup>b</sup> Measured using a Pensky-Martens Flash Point Tester: PM 4 (closed cup).

<sup>c</sup> Shell (2011); <sup>d</sup> BP (2011); <sup>e</sup> Maersk Oil (2005); <sup>f</sup> DG environment (2009); <sup>h</sup> BP (2015); <sup>g</sup> Statoil (2017), different values have been reported in Fritt-Rasmussen et al. (2012).

### 3.1.3 Water

In all experiments, fresh water was used for the water body on which the burning experiments with the above mentioned oils were conducted. The thermal properties of fresh water and sea water are very similar (see e.g. (Bromley et al., 1970); Caldwell (1974)) and therefore no significant differences were expected for the heat transfer mechanics for these water during *in-situ* burning of oil on water. Fresh water was thus considered to be representative of the water body associated with *in-situ* burning of oil operations. Due to the lower density of freshwater compared to salt water, the use of fresh water was also more conservative in terms of sinking of the residue.

### 3.1.4 Vaporization order of crude oil

For the study on the vaporization order of crude oil, the surface temperature, burning rate, flame height, burning efficiency and residue composition were measured for three alkanes (*n*-octane, dodecane and hexadecane), a mixture of these alkanes (1:1:1 volumetric ratio) and two crude oils (DUC and REBCO) (Table 3.1). The alkanes were studied to provide a benchmark for the model predictions and a reference for the crude oil experiments. Pure fuels have by definition a uniform vaporization order and thus can be used to test the model predictions for the EFV type models. The alkane mixture was studied to test if such a simplified, but more well-defined multicomponent fuel, could be used to represent the complex multicomponent character of the crude oils.

Experiments were conducted with different initial slick thicknesses (Table 3.2) because the measurement accuracy depended on the initial slick thickness differently for the tested burning parameter. A thin initial slick thickness ( $\leq 15$  mm) has relatively little height difference in the oil surface level, so therefore it was easier to measure the surface temperature for thin slicks. Thicker slicks (20-40 mm), however, provided better results for the burning rate and flame height due to their longer burning duration. Hexadecane could not be ignited at an initial slick thickness of 10 mm and hence was only tested for an initial slick thickness of 20 mm. The ignition occurred instantly for the crude oils and *n*-octane, whereas the ignition time was a few seconds for the alkane mixture, 15-60 seconds for dodecane (depending on the water temperature) and over two minutes for hexadecane. Residue samples of the alkane mixture, DUC and REBCO were taken for gas chromatography analysis of the chemical composition.

**Table 3.2.** Experimental matrix of vaporization order of crude oil

<i>Oil type</i>	<i>Thickness (mm)</i>	<i>Parameter(s) tested</i>
<i>n</i> -Octane/Dodecane	10	$T_s$
<i>n</i> -Octane/Dodecane	40	$\dot{m}, L_f$
Hexadecane	20	$T_s, \dot{m}, L_f$
Alkane mixture	15	$T_s$
Alkane mixture	30	$\dot{m}, L_f$
DUC/REBCO	10	$T_s$
DUC/REBCO	40	$\dot{m}, L_f$

The chemical composition of burning residues and fresh crude oils was analyzed on an Agilent 6890 Gas Chromatograph with a flame ionization detector, equipped with a 7683 autosampler and a 30 m ZB5 column (0.25 mm internal diameter and 0.25  $\mu\text{m}$  film thickness). Samples were dissolved in dichloromethane (2.0 g/L) for injection. The inlet temperature was 310 °C and 1  $\mu\text{L}$  was injected in split mode (5:1) and held for 2 min. Hydrogen was used as carrier gas with a flow rate of 2.0 mL/min and the detector setup had a temperature of 300 °C, hydrogen flow rate of 35 mL/min, air flow of 350 mL/min and nitrogen makeup flow of 40 mL/min. The initial oven temperature (40 °C) was held for 2 min, then increased to 310 °C at a rate of 15 °C/min and held for 10 min, resulting in a total analysis time of 30 min.

### 3.1.5 Residue composition as a function of the burning efficiency

To support the study on the vaporization order for crude oils, the residue composition was studied as a function of the burning efficiency for DUC (Table 3.1). Three burning experiments were conducted with an initial slick thickness of 5 mm, of which two were manually extinguished after a specific burning time that corresponded to a burning efficiency of 15% and 30%. The final burning experiment was burned until the fire extinguished naturally, which was expected to be 40% burning efficiency based on previous experiments in the COFA. The correlation between the burning efficiency and burning time was based on the mass loss curve for DUC with a 5 mm initial slick thickness obtained in the burning rate setup (Section 3.1.1). After each experiment, samples of the residue were taken for density and viscosity measurements and chemical analysis

of the residue section. The residue was then collected with 3M hydrophobic absorption pads and weighed to determine the actual burning efficiency.

The residue samples and a fresh DUC sample were analyzed for the *n*-alkane composition and selected PAHs by GC-MS on an Agilent 5975C inert XL MSD with electron ionization operating in selected ion monitoring mode. Oil samples were dissolved in dichloromethane (2.0 g/L) for injection. The gas chromatograph was equipped with a 60 m HP-5 capillary column with 0.25 mm inner diameter and 0.25  $\mu\text{m}$  film thickness. Helium was used as carrier gas with a flow rate of 1.1 ml/min. Samples of 1  $\mu\text{l}$  sample were injected in splitless mode (inlet at 300 °C). The initial oven temperature (40 °C) was held for 2 minutes, ramped with 25 °C/min to 100 °C, followed by 5 °C/min to 315 °C and held for 13.4 minutes, resulting in a total analysis time of 60.8 minutes. The temperature for the transfer line was 315 °C, for the ion source 230 °C and for the quadrupole 150 °C. A total of 55 *m/z* values divided into 12 groups were monitored for 13 *m/z* ions each, with a dwell time of 25 ms for each ion, according to Gallotta and Christensen (2012). Peaks were quantified using Chemstation V2.0 (Agilent technologies, Inc.). Monitored *m/z* ion chromatograms were analyzed using a Principal Component Analysis (PCA) to identify significant differences in the chemical composition between fresh DUC and the residue samples. A full description of the principles of the PCA method is beyond the scope of this thesis and more information can be found in (Christensen et al., 2005; Christensen and Tomasi, 2007; Malmquist et al., 2007).

### **3.1.6 Influence of initial slick thickness**

The influence of the initial slick thickness on the regression rate, burning rate, flame height and burning efficiency was studied for two alkanes (*n*-octane and dodecane) and one crude oil (REBCO) (Table 3.1). Experimental data on the regression rate, flame height and burning efficiency as a function of the initial thickness of Grane crude oil (Brogaard et al., 2014) was also included in the analysis of the results. Slick thicknesses of 2, 5, 10, 20 and 40 mm were used for the crude oil and slick thicknesses of 3 (due to ignitability issues of dodecane), 5, 10, 20 and 40 mm for the alkanes. The boilover tendency during these experiments was also monitored as a function of the slick thickness and the temperatures near the oil-water interface.

### 3.2 Crude oil herding setup

The experimental herder application procedure was designed to create semi-realistic testing conditions. Experiments were conducted in a small scale laboratory setup (1.0 m<sup>2</sup> x 0.5 m (water depth) square water basin) and in an outdoor intermediate scale setup (19 m<sup>2</sup> x 1.0 m (water depth) octagonal water basin) (Fig. 3.3). The water basins were filled with fresh water and artificially made brash ice (ice fragments < 2 m in length (WMO, 2014)) was used to create ice coverages of 3/10, 5/10 and 7/10. In these basins, the herder (Section 3.2.1) was applied in only a single corner to simulate the herding of oil at the edge of a spill towards its center (Fig. 3.4). The boundaries of the water basins should as such be considered as large ice floes, between which the oil could spread. The amount of oil used (200 g/m<sup>2</sup> of open water surface) was inversely proportional to the ice coverage in order to maintain the same open water surface area-to-oil ratio and achieve a similar spread thickness in each experiment.

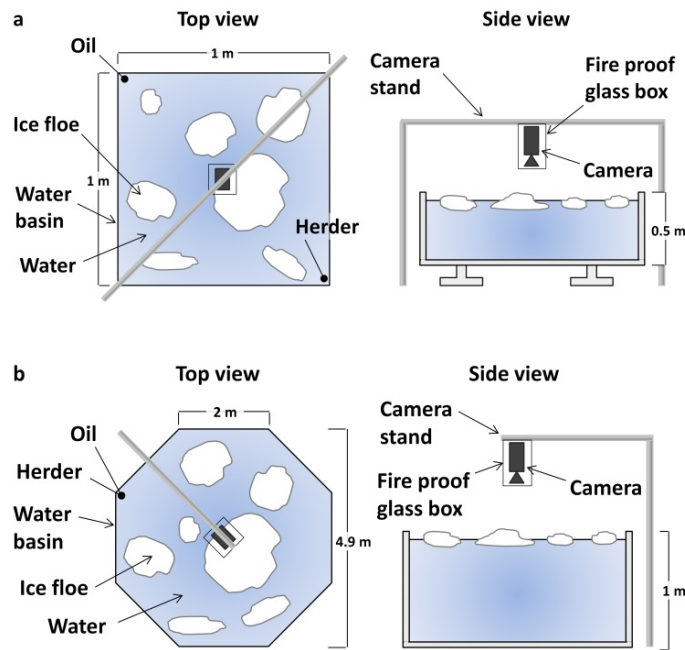


**Figure 3.3.** Experimental setup for the small scale (a) and intermediate scale (b) experiments. Small scale experiments were conducted indoor and intermediate scale experiments were conducted outdoor. The “oil” and “herder” labels indicate the location in the basin where these products were applied on the water surface.

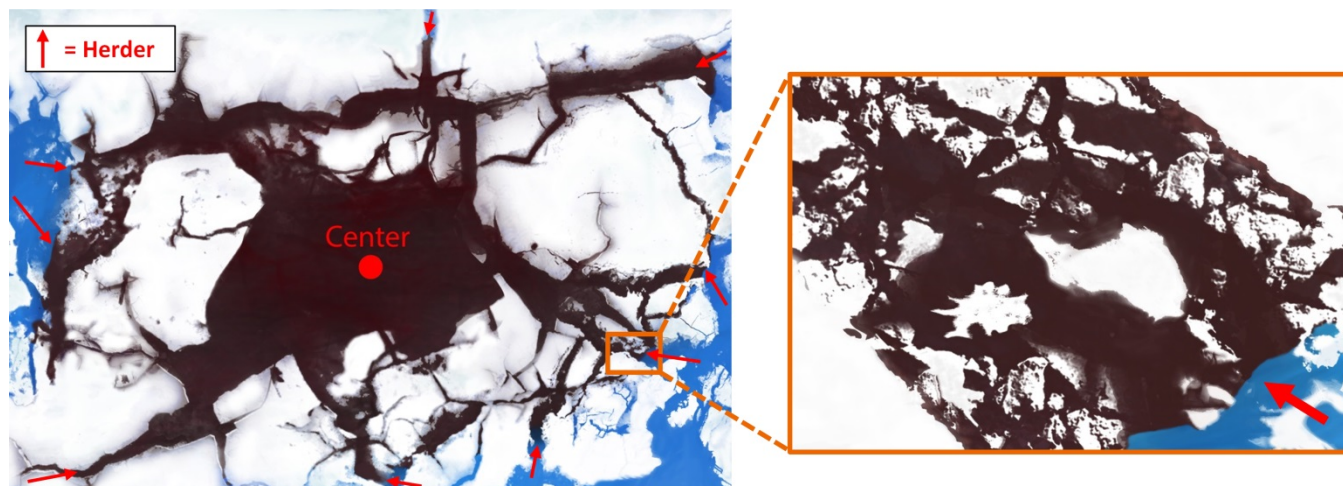


**Figure 3.4.** Sketches of a full scale oil spill scenario (left) and close-up of the edge of the oil slick (right), annotated by the orange rectangle and simulated in the experiments.

In a typical experiment, DUC crude oil (Table 3.1) was poured slowly on the water surface from a corner of the basin and was allowed to spread for 30 min. The herder was then applied in a corner of the basin and after 30 min the herded oil was ignited one slick at a time and allowed to burn until extinction. The burn residues were collected with 3M hydrophobic absorption pads, were then dried overnight in an oven at 50 °C and weighed afterwards to determine the burning efficiency. A digital camera was used to monitor the experiment from above. Images were taken every 10 seconds to measure the surface area and surface distribution of the crude oil.

The experimental conditions of the small scale and intermediate scale experiments are summarized in Table 3.3 and their procedural details are described below. For the small scale experiments (indoors), the artificial brash ice was 3-5 cm thick and made from fresh water. The herder (50  $\mu\text{L}/\text{m}^2$  water) was applied in the corner opposite of the original spreading location of the oil (see Fig. 3.3a) and ignition of the oil slicks was attempted with a butane hand torch. The basin was thoroughly cleaned with a hot water solution of Alconox detergent powder (10 g/L), before and after each experiment, to remove the herder from the steel walls. Surface tension measurements of the water prior to applying the ice and oil were in the expected range (68-71 mN/m) and confirmed that the herder had been removed successfully. Each of the small scale experiments was conducted twice.

For the intermediate scale experiments (outdoors) the oil was applied in an upwind corner to ensure the oil would spread over the water surface. The wind had a significant influence on the spreading and herding behavior of the oil, which caused some repeatability issues and hence the experiments are shown individually in Table 3.3. Nevertheless, these issues were, after thorough analysis, not seen to alter the main outcome of the study. The recommended operational herder dose of  $150 \mu\text{L}/(\text{m}^2 \text{ water surface})$  was used to overcome the effects of the wind (Buist et al., 2016). The herder was applied in the same upwind corner as the oil so that the wind would not inhibit the herding process (see Fig. 3.3b). Local wind speeds were measured on site using a wind speed meter (see Table 3.3). The brash ice in these experiments was made in  $80 \times 50 \times 30 \text{ cm}^3$  casts in a  $-20 \text{ }^\circ\text{C}$  freezer. Initial ice coverages of 3/10 were prepared, but due to melting of the ice during the preparation of the experiments with ice the actual ice coverages tested were 2/10 and 2.5/10. Ignition of the oil slicks was attempted with either a weed burner or a burner and 3-50 ml ignition gel (8:2:0.1 mixture of diesel, gasoline and G-760 gelling agent) that was poured and ignited on a central location of an oil slick. Surface tension measurements of the water ( $70\text{-}71 \text{ mN/m}$ ) prior to applying the ice and oil showed that there was no significant herder residue left in the basin in between experiments.

The ignition of a larger volume of free-floating herded oil (15 L) was also tested in the intermediate scale setup. During this experiment, the herder was applied in six doses of  $473 \mu\text{L}$  of herder around the oil slick. After thirty minutes of herding, the oil slicks were adjacent to the basin boundaries and an additional  $2100 \mu\text{L}$  was applied around the oil slicks to force the oil slicks onto the open water surface prior to ignition. The oil slicks were each ignited with approximately 50 ml of ignition gel and a weed burner.

The camera images were analyzed in Photoshop CC 2015 using color sensitive selection tools to select the pre- and post-herding oil slicks on the water surface. These tools were chosen over manual selection of the oil slicks to eliminate subjective bias. Pixel measurements of the oil slicks indicated the number of individual areas and were compared to the pixel area of the water basin to calculate the slick areas in  $\text{m}^2$ . Based on the initial oil volume (the weight of the oil divided by the density of the oil) and assuming a uniform thickness distribution, the average slick thickness of the oil could then be calculated (SL Ross, 2007).

**Table 3.3.** Experimental matrix of herding crude oil

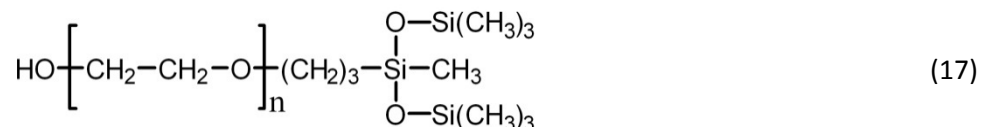
Experimental scale	Water surface area (m <sup>2</sup> )	Ice coverage	Oil amount (g)	Herder amount (μL)	Ice fragment diameter (cm)	Water temperature (°C)	Wind speed (m/s) <sup>b</sup>
Small	1	No ice	200	50	-	5.4	-
Small	1	3/10	140	50	10-30	8.2	-
Small	1	5/10	100	50	10-30	8.1	-
Small	1	7/10	60	50	10-30	3.3	-
Intermediate	19	No ice	3780	2835	-	7.4	3-4
Intermediate	19	No ice	3780	2835	-	8.8	3-4
Intermediate	19	2.5/10 <sup>a</sup>	2646	2835	40-75	6.1	< 2
Intermediate	19	2/10 <sup>a</sup>	2646	2835	40-75	7.2	3-6
15 L experiment	19	No ice	12795	4935	-	14.3	< 2

<sup>a</sup>The initial ice coverage was 3/10 but due to melting of the ice the actual tested ice coverage was lower.

<sup>b</sup>Measured on site.

### 3.2.1 Chemical herder

The chemical herder that was used in this study is Siltech OP-40 (previously known as Silsurf A004-UP (Lane et al., 2012)), a silicon based herder that consists for > 80 wt% of a trisiloxane polymer surfactant (Eq. (17)) (Siltech, 2012). This herder has been shown to sufficiently thicken crude oils in fresh and salt water for *in-situ* burning purposes (≥ 2 mm) (SL Ross, 2012). Because the herder performed better in salt water, but was still effective in fresh water, the use of fresh water was considered to be the more conservative option.



## 3.3 Cone setup for ignition studies

The ignition time, surface temperature upon ignition, heat release rate and peak of the heat release rate were studied with a cone calorimeter (see Babrauskas (2016a) for more information) for two crude oils (DUC and

Grane) and one heavy refined oil (IFO 180) (Table 3.1). In addition, the boilover tendency and burning efficiency as a function of the incident heat flux were studied in relation to the discussed theories on boilovers (Section 1.5.5) and heat transfer mechanics (Section 2.1.4). Experiments were conducted in a custom-made stainless steel circular sample holder, featuring a hollow bottom for water cooling of the fuel sample, which was placed under a standard radiative conical heater (Fig. 3.5). Initial tests used a solid metal sample holder without heat sinks, leading to a hot surrounding of the burning oil, which resulted in unrepresentative results compared to experimental data obtained in the COFA setup. The oil samples were therefore continuously cooled by water (12 °C) with a flow of 7 L/h to create a heat sink that simulates the heat losses observed during *in-situ* burning of oil on water (Brzustowski and Twardus, 1982; Buist et al., 1999). The temperature and flow of the water were calibrated so that the burning rate and burning efficiency of DUC would match between the cone setup and the modified COFA setup (Fig. 3.7).

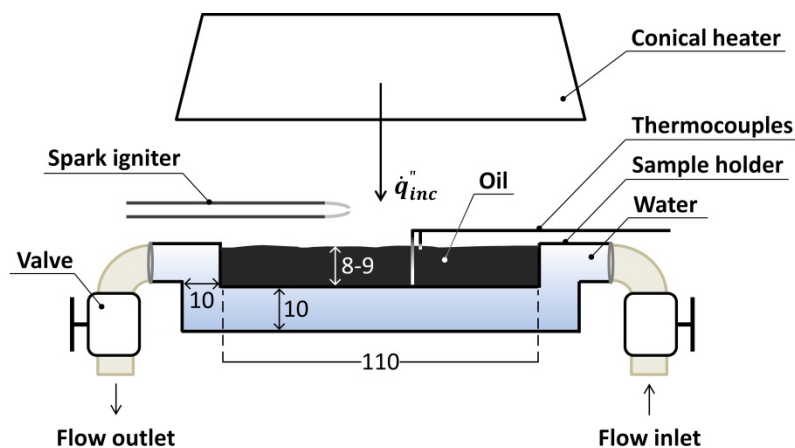


**Figure 3.5.** Cross section of the custom-made cone calorimeter setup. All measurements are in mm. See Babrauskas (2016a) for more information about the general cone calorimeter setup.

In a typical experiment, an 8-9 mm oil sample (76-86 ml) in the sample holder was subjected to an incident heat flux of 5, 8, 10, 20, 30, 40 or 50 kW/m<sup>2</sup> and ignited by a spark igniter. Reference experiments without an incident heat flux and experiments that were non-ignitable ( $t_{ig} > 10$  min for a given incident heat flux) were ignited with a butane hand torch. Two thermocouples were used to measure the surface temperature and the temperature of the steel below the oil. Heat release rates were obtained by measuring the oxygen, carbon

dioxide and carbon monoxide concentrations in the exhaust gases (i.e., the oxygen consumption method (Babrauskas, 2016b)). The water inlet and water outlet could be closed by valves, so that the sample holder could be weighed with and without residue to determine the burning efficiency.

The experiments were conducted with three fresh oils (DUC, Grane and IFO 180), weathered DUC with 30 and 40 wt% evaporative losses and weathered DUC with 40% evaporated losses emulsified with a 40 vol% water content (Table 3.4). DUC was evaporated by bubbling air through 4 L samples in open containers for three days (30 wt% losses) and one week (40 wt% losses). The evaporative losses were monitored based on the weight of the oil sample. DUC samples (300-600 ml) with evaporative losses of 40% were mixed with 200-400 ml of fresh water to create the water-in-oil emulsions. Water-oil mixtures were shaken by hand initially (1-2 min) and were then placed on a rotary shaking table (Laboshake 500) for 20 hours at 175 rounds per minute. The resulting emulsions were tested shortly after the 20 hour shaking period and in between experiments shaking of the emulsion was resumed to minimize the separation of water from the emulsion.

**Table 3.4.** Physical properties of weathered DUC crude oil

<i>Oil</i>	<i>Evaporated losses (wt%)</i>	<i>Water content (vol%)</i>	<i>Density (g/ml)<sup>a</sup></i>	<i>Viscosity (cP)<sup>a</sup></i>	<i>Flashpoint (°C)<sup>b</sup></i>
DUC 30/0	30	0	0.897	44.93	80
DUC 40/0	40	0	0.900	60.91	102
DUC 40/40	40	40	0.924	93.20	NA

<sup>a</sup> Measured at 25 °C using an Anton Paar SVM 3000 viscometer.

<sup>b</sup> Measured using a Pensky-Martens Flash Point Tester: PM 4 (closed cup).

## 3.4 Burning efficiency studies

### 3.4.1 Burning efficiency as a function of the oil composition

Experiments with three refined oils (gasoline, diesel and IFO 180) and a heavy crude oil (Grane) (Table 3.1) were conducted in the COFA setup (Fig. 3.1) and burning rate setup (Fig. 3.2) to study the burning efficiency as a function of the oil composition. These experiments complemented the results of the alkanes, alkane mixture and light crude oils (Sections 3.1.4 and 3.1.6) to result in a broad range of crude and refined oil types tested in

the same experimental setups. The burning efficiency of gasoline and diesel was tested for an initial slick thickness of 10 mm in the COFA setup. Burning efficiency of IFO 180 and Grane were tested for an initial slick thickness of 5 mm in the COFA setup and burning rate setup, and samples of the residues were taken for viscosity and density measurements. The experimental procedures for these experiments conducted in the COFA setup and burning rate setup are described in Section 3.1 and in Section 3.1.1, respectively.

### **3.4.2 Burning efficiency as a function of the pool diameter**

The burning efficiency was studied as a function of the pool diameter of crude oil in ice cavities to test the size dependency of the burning efficiency for alternative *in-situ* burning conditions. ANS crude oil (Table 3.1), with an initial slick thickness of 10 mm, was burned in ice cavities with diameters of 0.1, 0.25 and 1.1 m (small, medium and large cavity sizes, respectively) (Fig. 3.6). The influence of the ice cavity conditions (ullage height, initial slick thickness and an initial water layer) on the burning efficiency was studied in the small ice cavities for *n*-octane (reference fuel) and ANS. The small ice cavities were made by drilling a hole with a 0.1 m diameter in a conical shaped ice block with an upper diameter of 26 cm and a height of 13.5-21.5 cm. The medium ice cavities were made by cutting a hole with a 0.25 m diameter and a depth of 0.1 m into ice blocks of 0.25 x 0.50 x 0.50 m<sup>3</sup>. The large ice cavities were made by fusing six ice blocks of 0.25 x 0.50 x 1.0 m<sup>3</sup> together with a combination of water, snow and dry ice to form a 1.0 x 1.0 m<sup>2</sup> ice cavity. A water layer of 3 cm was added inside the ice cavity to prevent oil from spreading underneath the ice blocks. The experimental conditions for the three different experimental cavity sizes are summarized in Table 3.5.

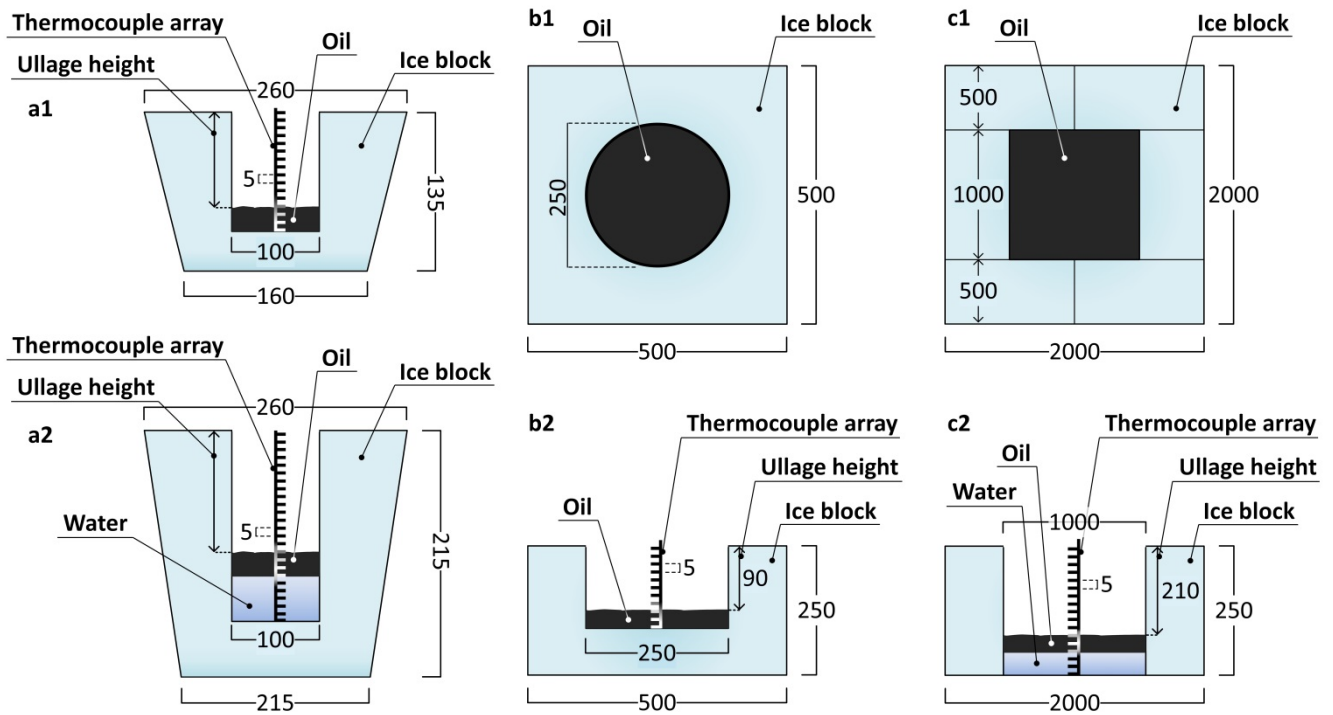


**Figure 3.6.** Schematics of the small (a), medium (b) and large (c) ice cavity setups. Higher ice blocks (a2) were used in the small ice cavity experiments to test deep ullages (100 mm) and initial water layers. Schematics of the medium and large ice cavities show a top view (b1 and c1) and cross sectional view (b2 and c2). All measurements are in mm.

**Table 3.5.** Experimental matrix of burning oil in ice cavities

<i>Fuel</i>	<i>Cavity diameter (m)</i>	<i>Initial slick thickness (mm)</i>	<i>Oil amount (g)</i>	<i>Ullage height (mm)</i>	<i>Water layer thickness (mm)</i>
<i>n</i> -Octane	0.1	5-20	25-100	15-60	0
ANS	0.1	5	30.5	12.5-100	0
ANS	0.1	10	61	25-100	0-7
ANS	0.1	20	122	50-75	0
ANS	0.25	10	423	90	0
ANS	1.1	10	9800	210	3

All experiments followed a similar procedure. After the oil was poured into the ice cavity, the oil was ignited with a small hand torch ( $D = 0.1$  m) or a weed burner ( $D = 0.25$  m and  $D = 1.1$  m) and burned until the fire naturally extinguished. A thermocouple array in the centerline of the oil slick was used to monitor the temperatures inside the oil slick and the vertical position of the oil layer. The vertical oil layer position was influenced by a combination of water from the melting ice flowing below the oil and regression of the oil surface. The ice blocks with a cavity of  $D = 0.1$  m were positioned on a load scale during the experiment to determine the burning efficiency. For the experiments with cavity sizes of  $D = 0.25$  m and  $D = 1.1$  m, the residue was collected with 3M hydrophobic absorption pads and weighed to determine the burning efficiency. An analysis of the influence of the burning oil on the (lateral) ice cavity was beyond the scope of this study and is therefore not included in this thesis. For more information on this topic and additional experimental data see Farmahini Farahani et al. (2015a), Farmahini Farahani et al. (2015b) and Shi et al. (2016).

### **3.5 Chemical composition of in-situ burning byproducts**

For the study on the compositional changes of the smoke plume, the residue and the oil fraction in the water as a function of time, the COFA was modified to better represent the conditions of large scale operations at sea. At the time of writing this thesis, it had not yet been possible to conduct experimental work in the full modified COFA setup. Because the design of the setup was finished and is used for discussions in this thesis, the setup is still described here in detail. The current design of the experimental setup was based on experimental results from the vaporization order study (Section 4.2), the cone setup study (Section 4.7.3) and initial experiments with a first prototype of the setup (Section 4.8.1). The methodologies for the initial experiments conducted in this prototype used to provide input for and to evaluate the new experimental setup are described in Sections 3.5.1 and 3.5.2.

In the modified COFA setup (Fig. 3.7), the oil is contained in a relatively low Pyrex glass cylinder (height of 50 mm,  $D = 164$  mm). This low cylinder allows for the water under the oil to be continuously refreshed by a mild water current in the basin. The water current was created with a small propeller in order to avoid boilover occurrence. The thermocouple array consisted of three thermocouples all placed at the surface to increase the accuracy of the surface temperature measurements. In order to increase the burning efficiency in these small scale experiments, four short wave infrared (IR) heaters (1.9 kW) that could provide an external heat flux of 5-

50 kW/m<sup>2</sup> to the oil surface were placed around the Pyrex glass cylinder. This additional heat flux simulated the relatively higher heat feedback to the fuel surface in large scale experiments, caused by the higher burning rate per unit area (Fig. 2.1), compared to small scale experiments. An increase in the maximum burning efficiency allows for studying the vaporization order and byproduct compositions of a larger fraction of the oil and thus yield more representative results compared to large scale operations. The influence of an increased heat flux to the oil surface on the burning efficiency was confirmed in the ignition experiments in the cone setup (Section 3.3) and the results (Section 4.7.3) were used to evaluate the modified COFA setup.

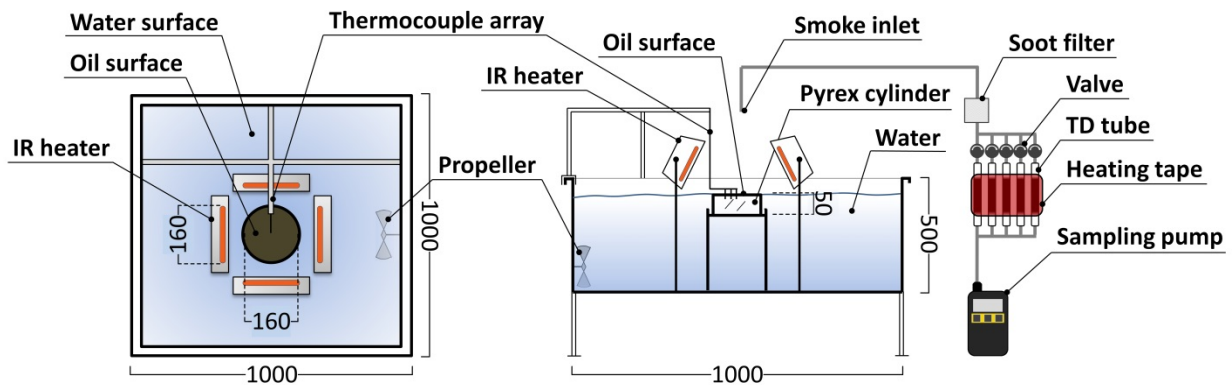


**Figure 3.7.** Schematics of the modified COFA setup featuring a low Pyrex glass cylinder of 50 mm, a propeller to create a current in the water layer below the oil, infrared heaters to provide an external heat flux to the oil surface and a gas trapping system to sample the combustion gases. All measurements are in mm.

A gas trapping system was installed to sample the soot and combustion gases in the smoke plume. An air sampling pump (AirCheck 2000) pumped soot and combustion gases that entered the smoke inlet with 50 ml/min through a soot filter and thermal desorption (TD) tubes packed with a sorbent material. The thermal desorption tubes (prepacked and conditioned by Gerstel) were packed with a weak (Carbopack C, 5 mm), medium (Carbopack B, 5 mm) and strong (Carbosieve S-III, 5 mm) sorbent to be able to trap a wide range of components from the combustion gases (Woolfenden, 2010). Valves placed in front of the TD tubes were used to regulate the sampling moment and duration of each tube. The TD tubes were heated with an electrical heating tape to 70 °C to minimize the adsorption of water on the sorbent materials. Soot samples were collected from the filter and analyzed by gas chromatography. The analytes on the TD tubes were thermally

extracted and transferred onto a GC column for analysis by GC-MS. After the analyte extraction, the sorbent materials in the TD tubes were conditioned for 30 minutes at 300 °C prior to reuse in subsequent experiments.

### **3.5.1 Smoke composition test**

To test the sampling of combustion gases from the smoke plume, a burning experiment was conducted with DUC (5 mm initial slick thickness) (Table 3.1) in a prototype of the modified COFA setup. This prototype did not contain the infrared heaters or the heating tape around the thermal desorption tubes but was otherwise identical to the setup as described above. In addition to analysis of the smoke composition, the experiment was also used to assess the boilover tendency of oil burning on water with a subsurface current compared to oil burning on still water. The thermal desorption tubes were opened one at a time for 30 s after burning times of 1) 0:30 min (flow of 50 ml/min), 2) 1:20 min (flow of 76 ml/min), 3) 2:00 min (flow of 25 ml/min), 4) 3:30 min (flow of 50 ml/min) and 5) 4:15 (flow of 78 ml/min). After the fire extinguished naturally (7:59 min), the residue was collected with 3M hydrophobic absorption pads and weighed to determine the burning efficiency following the common procedure described in Section 3.1.

The components adsorbed on the thermal desorption tubes were analyzed by GC-MS on an Agilent 5975C inert XL MSD with a Gerstel Thermal Desorption Unit. The thermal desorption tubes were heated to 70 °C and held for 3 min, ramped with 720 °C/min to 300 °C and held for 1 min to inject desorbed sample into the cold trap (50:10 split). The cold trap was heated from -150 °C at a rate of 12 °C/s to 300 °C and held for 5 min to load the sample onto the gas chromatograph column (15:10 split). The gas chromatograph was equipped with a 60 m HP-5 capillary column with 0.25 mm inner diameter and 0.25 µm film thickness. Helium was used as carrier gas with a flow rate of 1.1 ml/min. The initial oven temperature (30 °C) was held for 2 minutes, ramped with 15 °C/min to 320 °C and held for 10 min, resulting in a total analysis time of 31.3 minutes. The temperature for the transfer line was 315 °C, for the ion source 230 °C and for the quadrupole 150 °C. Ions were scanned in the total ionization mode (range of 10-330  $m/z$ ).

### **3.5.2 Residue and water fraction composition tests**

To test the water sampling and residue composition compared to experiments in the COFA as a function of the burning efficiency, a series of burning experiments with DUC (Table 3.1) was conducted in the prototype of the

modified COFA setup as described in Section 3.5.1. Five burning experiments with DUC (5 mm initial slick thickness) were manually extinguished at time intervals that corresponded to 10% burning efficiency intervals (so at 10%, 20%, 30%, 40% and 50% burning efficiency). The correlation between the burning efficiency and burning time was based on the mass loss curve for DUC with a 5 mm initial slick thickness obtained in the burning rate setup (Section 3.1.1). After each experiment, two samples of the residue were taken for density and viscosity measurements and analysis by gas chromatography. A 5 ml water sample was also collected near the water surface for analysis by gas chromatography. This sampling location was chosen deliberately to test whether the current in the water properly mixes the water body in the experimental setup because no oil concentration was expected at this location from diffusion alone. The residue was then collected with 3M hydrophobic absorption pads and weighed to determine the actual burning efficiency. The water body was refreshed between the experiments.

Samples of the residues, fresh DUC and the water fractions were prepared for gas chromatography by extraction of 0.1 g oil or 5 ml water using 20 ml *n*-hexane with 0.4 g MgSO<sub>4</sub>·7 H<sub>2</sub>O (anhydrous) for 2 hours. The *n*-hexane contained 2 mg/l *n*-tetracontane (C<sub>40</sub>H<sub>82</sub>) and 1 mg/l *n*-decane (C<sub>10</sub>H<sub>22</sub>) as GC retention time markers. Anhydrous Na<sub>2</sub>SO<sub>4</sub> was added to the extract prior to solid phase extraction clean-up. For this, 12 ml, 2 g Florisil cartridges (LC-Florisil, Supelco), with 2 g Na<sub>2</sub>SO<sub>4</sub> on top of the Florisil, were equilibrated using 10 ml *n*-hexane before passing the extract through. The flow-through was collected and evaporated under a gentle stream of nitrogen until approximately 1 ml was left and the exact volume was then determined gravimetrically. The extracts were analyzed using an Agilent 6980 gas chromatograph with flame ionization detector. The gas chromatograph was equipped with a 30 m DB-1HT capillary column with 0.25 mm inner diameter and 0.1 μm film thickness. Helium was used as carrier gas with a flow rate of 1 ml/min. Samples of 1 μl sample were injected in splitless mode (inlet at 280 °C). The initial oven temperature (35 °C) was held for 3 minutes, ramped with 20 °C/min to 350 °C and held for 5 minutes, resulting in a total analysis time of 23.8 minutes.



## 4 Results and Discussion

Section 4.1 presents some observational results of a typical experiment in the COFA setup and a visual impression of these experiments to aid with the interpretation of the results presented in subsequent sections. The next three sections, Sections 4.2 (vaporization order), 4.3 (initial slick thickness) and 4.4 (crude oil herding in ice-infested water), are largely based on the published papers number 3, 1 and 4, respectively (listed on page iii). The results presented in Section 4.5 (ignition) have not yet been developed into a full paper and some of the data analyses may need further experimental work to completely close the discussion of the results. Sections 4.6 (boilover) and 4.7 (burning efficiency) present a compilation of results obtained from the three published papers on these topics and additional experimental results to support the discussions. Finally, Section 4.8 presents the initial results that were used to evaluate the potential of the newly designed experimental setup for the study of the chemical composition of the *in-situ* burning byproducts.

### 4.1 Observational results

Figure 4.1 shows a visual overview of a typical experiment in the COFA setup featuring DUC crude oil with an initial slick thickness of 10 mm. Due to the density difference between the tested oils and water, the oil surface level in the Pyrex glass cylinder was a few millimeters higher than the water surface level outside the cylinder. The light crude oils, *n*-octane and gasoline contained a high amount of volatiles and were easily ignited with a lighter or butane hand torch. The heavy crude and refined oils, dodecane, hexadecane and diesel could only be ignited by the butane hand torch, after heating up the oil for 1-2 min before eventually resulting in a self-sustaining fire.

Once ignited, all oils followed the same burning phases. The fire would first propagate over the full oil surface, during which pulsating flames close to the fuel surface were observed (Fig. 4.1c), which indicated that the fire was in a growing phase. The fire then reached its fully developed stage and bright yellow-orange flames were established (Fig. 4.1d). Depending on the fuel type and initial slick thickness (see Sections 4.3 and 4.6), the fire would extinguish either after the flames had become small and intermittent or after occurrence of a boilover. The boilovers would start with single explosions that increased the flame diameter and ejected oil droplets outside of the Pyrex glass cylinder (Fig. 4.1e). The frequency and intensity of these explosions would increase until a full boilover phase was reached of several seconds of continuous violent burning, which then abruptly

ended and extinguished the fire (Fig. 4.1f). The remaining residue, independent of boilover occurrence, was always observed to be more viscous than the starting oil (Fig. 4.1g). Sinking of the residues was not observed during any of the experiments conducted during this study, so the residues could therefore easily be collected from the water surface with a 3M absorption pad (Fig. 4.1h). As such, all the burning efficiencies reported in this thesis are considered to be accurate measurements of the true burning efficiency.

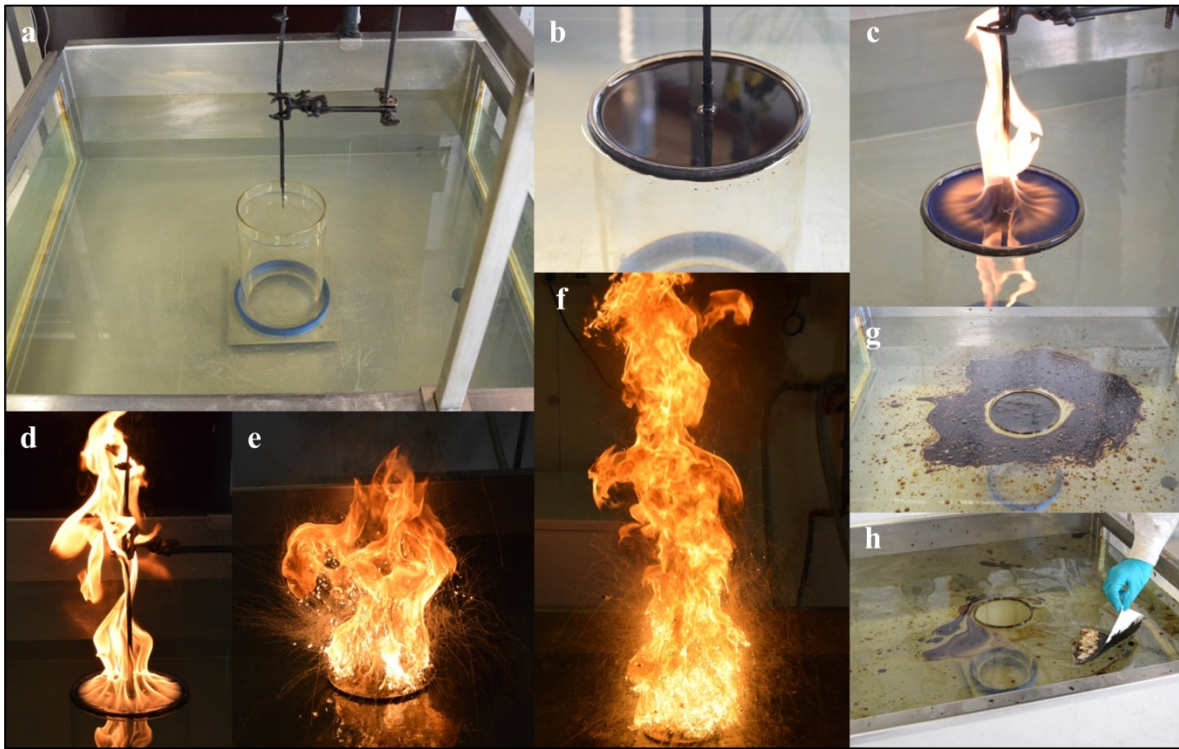


**Figure 4.1.** Snapshots of a typical experiment in the COFA setup featuring DUC with an initial slick thickness of 10 mm. Overview of the Pyrex glass cylinder in the water basin (a), the thermocouple is adjusted to match the oil surface level (b), growing fire after ignition (c), fully developed fire (d), initiating of boilover (e), full boilover explosion (f), residue after *in-situ* burning (g) and collection of the residue with a 3M absorption pad (h).

## 4.2 Vaporization order

The results presented in this section were obtained with the COFA setup (Section 3.1) and the burning rate setup (Section 3.1.1), according to the methodologies described in Section 3.1.4 and 3.1.5.

### 4.2.1 Modeling of burning parameters

Model predictions of the burning parameters for crude oil were carried out by combining the vaporization order of the multicomponent fuel combustion models (Section 2.4) with the general properties of hydrocarbons (Section 2.2) and fire dynamics of pool fires (Section 2.1). Because the models provide a clear description of the molecular composition of the evaporating gases from the fuel, Eq. (4) and (5) can be used to predict the surface temperature, burning rate and flame height of a fresh crude oil burning on water. Although some of the models lack the numerical details that would allow for quantitative modeling, the qualitative descriptions are sufficient to draft up trends, as visualized in Fig. 4.2. Combining these trends with the measured residue composition provides sufficient detail to distinguish between the four models for a given fuel, as discussed below and shown in Table 2.3. The data presented in Fig. 4.2 do not represent actual values but only show the relative differences among the four models. The data were normalized for the model with the highest expected values for the surface temperature, burning rate and flame height (y-axis) and the burning time from ignition to extinction of the flame (x-axis).

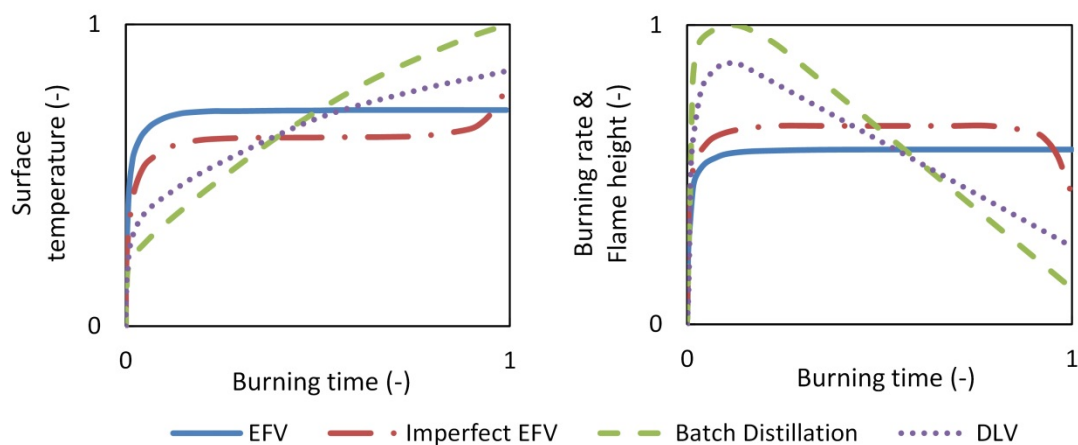


**Figure 4.2.** Crude oil combustion model predictions of the surface temperature (left) and the burning rate and the flame height (right). Due to the similarities between the trends for the burning rate and the flame height predicted by the models, these parameters are both represented by the same plot.

In the EFV and Imperfect EFV models the vaporization has a constant rate and composition and thus the crude oil essentially burns as if it consists of only a single component. This behavior results in constant values for the

surface temperature, burning rate and flame height after the initial growing phase of the fire (Fig. 4.2). These constant values of the burning parameters represent the average of the respective values of all the evaporating components. For the EFV model, this average lies in the range of the middle hydrocarbon fraction ( $T_b$  of 204-538 °C (Buist et al., 1997)), whereas the average for the Imperfect EFV model should lie closer to the light hydrocarbon fraction ( $T_b \leq 204$  °C (Buist et al., 1997)). As a result, the surface temperature will be lower and the burning rate and flame height will be higher for the Imperfect EFV model compared to the EFV model, as seen in Fig. 4.2. Once the lighter components have been burned off the fuel in the Imperfect EFV model, the fire will either extinguish or the combustion will shift to the heavier fractions (depicted in Fig. 4.2).

The vaporization order of decreasing volatility for the Batch Distillation and DLV models implies that the combustible gases evaporating from the fuel have an increasing molecular weight as a function of time. Thus, these models feature an increasing surface temperature and decreasing burning rate and flame height (Fig. 4.2). Combustion in the Batch Distillation model starts with the single most volatile component and the evaporating gases shift abruptly from one component to the other. In the DLV model, the combustion gases start with a mixture of volatile components and the composition changes gradually as components are removed and introduced to the mixture one at a time. Thus, the initial surface temperature is lower and the initial burning rate and flame height are higher in the Batch Distillation model than in the DLV model (Fig. 4.2) and the Batch Distillation model features a steeper slope for these parameters. Still, the most important aspect of these models is that they in principal do not reach a steady state burning phase because the gases in the combustion zone constantly change composition. This feature is the main distinction between the volatility order models and the EFV type models.

In order to distinguish between the two EFV type models or between the two volatility order models, the residue composition can be used. The residue composition can be predicted by expressing it as a function of the vaporization order and the burning time. For a uniform vaporization order (EFV model) the chemical composition of the crude oil does not change during the burning. Thus, the residue composition is independent of time and is the same as the starting composition. For a near-uniform vaporization order (Imperfect EFV model) the components with a relative vaporization rate higher than their relative concentration will have a reduced concentration in the residue compared to the fresh crude oil. The burning time determines the concentration of these components in the residue, up to the point when they are completely removed. Thus, an unchanged or reduced concentration of the lighter components in the residue can be used as the characterizing distinction between the EFV model and the Imperfect EFV model.

For a vaporization order of decreasing volatility (Batch Distillation and DLV model), the burning time determines up to which point in the volatility order the individual components participate in the burning. Because lighter components are generally more volatile, the unburned components mainly consist of heavier hydrocarbons. The components are removed one at a time from the burning oil for the Batch Distillation model and as such the residue composition features an abrupt change between removed and present components. The removal of components from the burning oil goes more gradually for the DLV model, resulting in a concentration gradient for the partially burned components between the fully removed and unburned components in the residue. Depending on the burning time, the abrupt switch and gradient move more towards the heavier components. The difference between an abrupt concentration change and a concentration gradient in the burning residue is the characterizing distinction between the Batch Distillation model and the DLV model.

#### **4.2.2 Experimental results**

The experimental results for surface temperature for the alkanes, alkane mixture and crude oils are shown in Fig. 4.3. The data are up to the point where the surface thermocouple was no longer attached to the surface due to thinning of the slick as the burning progressed. Disconnection of a thermocouple from the fuel surface was clearly visible in the temperature data from a sudden spike in the measured temperature, indicating a transition from measuring liquid to gas temperatures. Overall, the surface temperature measurements showed good repeatability (error bars < 10% from the average temperature) for both the pure and multicomponent fuels (Fig. 4.3).

For the alkanes the surface temperatures are close to their respective boiling points, which provide a measure of validity to the method used to collect the surface temperature data. Hexadecane proved difficult to ignite as it suffered from significant heat losses to the water, which is reflected in the scattered surface temperature data and high starting temperature. The surface temperature clearly increased over time for the crude oils. This result indicates that these multicomponent fuels followed a volatility controlled vaporization order. In addition, the increasing surface temperatures of these fuels are in clear contrast with the constant trends of the alkanes, which provided a representation of an EFV type vaporization order. For the alkane mixture, the surface temperature shows an initial increase up to the point where it reaches the boiling point of hexadecane. After this point, at about 190 s ( $t = 0.55$  in Fig. 4.3), the burning seemed to reach an equilibrium state dominated by

hexadecane. Because the total burning duration for the 15 mm alkane mixture was about 1130 seconds, it is unlikely that the mixture was depleted of *n*-octane and dodecane after 190 s. Thus, the vaporization of the alkane mixture is closer to an EFV type model than to a volatility controlled model.

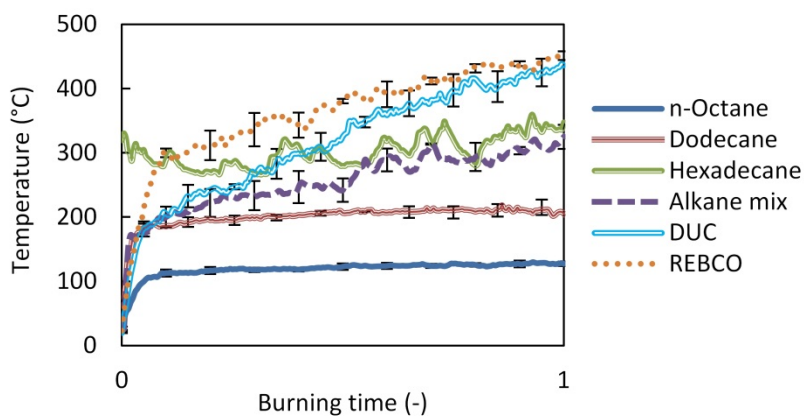


**Figure 4.3.** Experimental data of the surface temperature for the alkanes, alkane mixture and crude oils.

Experimental results for the burning rate and the flame height of the alkanes, alkane mixture and crude oils are shown in Fig. 4.4. The burning rate data was corrected to only show the oil burning rate by deducing the water loss rate from the total burning rate, assuming a constant rate for the water evaporation. The mass balance between the residue weight and total weight lost showed that between 60-250 g of water evaporated, depending on the burning time and thus the fuel layer thickness. The hexadecane (20 mm) burned for 27 minutes, the alkane mixture (30 mm) and *n*-alkane (40 mm) for about 35 minutes and the dodecane (40 mm), DUC (40 mm) and REBCO (40 mm) burned for 50-60 minutes. Data points represent an averaged value over approximately 2% (30-60 seconds) and 3% (45-90 seconds) of the burning time for the flame height and the burning rate, respectively. A visual impression of the experimental flame height data of a 40 mm REBCO experiment is shown in Fig. 4.5.

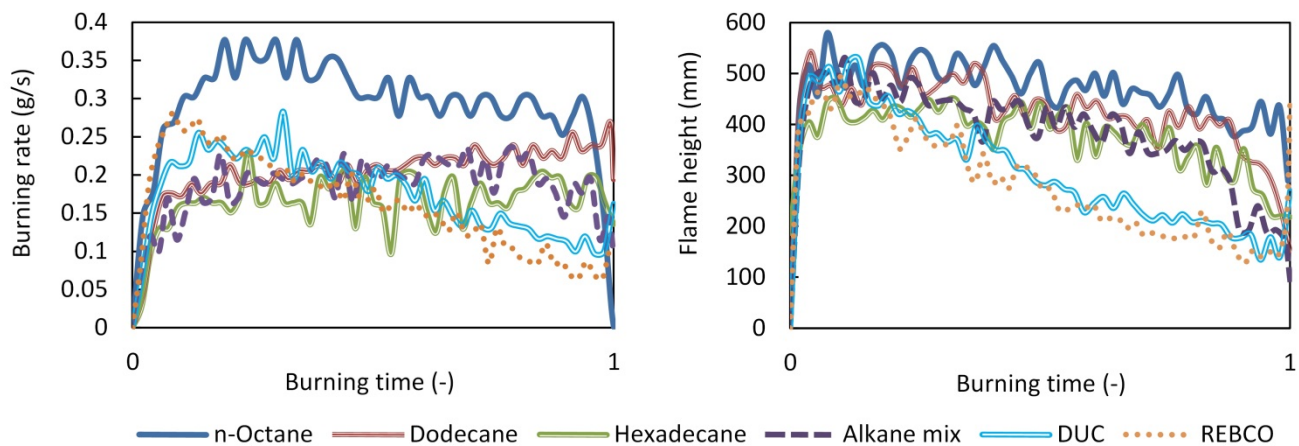


**Figure 4.4.** Experimental data of the burning rate and flame height for the alkanes, alkane mixture and crude oils. Data points are presented as lines for clarity reasons.

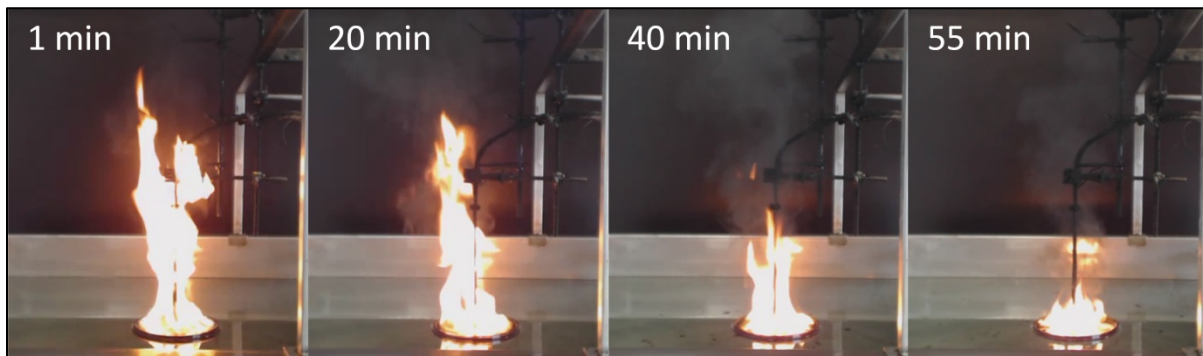


**Figure 4.5.** Video snapshots of the flame height recordings of 40 mm REBCO in the COFA at different times during the burning. The total burning time was 59:20 min. Each frame is 59 cm wide and 68 cm high.

For each fuel, the same trends are observed between its burning rate and flame height in Fig. 4.4, as expected. Again, the alkane results provide a reasonable representation of an EFV type vaporization. Near-constant values were observed for the alkanes with some minor declines after approximately half of the burning duration. This decrease in burning rate and flame height is likely caused by increasing heat losses to the water as the oil layer thickness decreases during the burning. For dodecane, however, a minor increase in the burning rate was observed. Because its flame height shows the same declining trend as *n*-octane and hexadecane, this increasing burning rate was contributed to an increasing evaporation rate of the surrounding water as the

burning progressed. While this implies that a constant water loss rate is incorrect, no better alternative was found to correct the oil burning rate. Because it was found that the exact function of the water loss rate did not significantly alter the burning rate results (see Section 4.3.2), this phenomenon was not further investigated. The alkane data also clearly shows that hydrocarbons with a higher molecular weight resulted in a lower burning rate and flame height, thus verifying some of the theories used for the model predictions in Section 4.2.1.

The crude oil data differed significantly from the alkane data. The crude oils initially show similar values for the burning rate and the flame height as *n*-octane, after which they rapidly decreased to values below those of hexadecane. These decreasing trends match well with the volatility order model predictions and combined with the surface temperature data clearly indicate that the crude oils had a vaporization order of decreasing volatility.

The alkane mixture again showed values close to dodecane and hexadecane, indicating that the evaporating gases consisted of a mixture of all the components. As the combustion became dominated by hexadecane after approximately 70% of the burning time, it seems that the lightest components, *n*-octane, had been mostly depleted at this time. This suggests that the mixture followed a near-uniform vaporization order. Although the flame height shows a decreasing trend, this could be explained by heat losses to the water layer and depletion of *n*-octane rather than a volatility controlled vaporization order.

GC chromatograms of fresh REBCO crude oil, a typical REBCO residue and a typical alkane mixture residue are shown in Fig. 4.6. The shown crude oil chromatograms are representative for both fresh crude oils and their burn residues. Estimates of the residue thicknesses and obtained burning efficiencies are shown in Table 4.1. The crude oil data clearly shows that fresh REBCO consisted of a large amount of light and medium weight hydrocarbons that were almost completely absent in the residue. This type of residue composition matches well with what would be expected of a volatility controlled vaporization order. The components in the range between  $C_{14}$ - $C_{31}$  in the residue were only partially removed. These components were still present in the residue but their concentration ratios to the  $C_{31}$  concentration had decreased compared to the fresh crude oil. The resulting concentration gradient clearly indicates that, of the two volatility controlled vaporization models, the *diffusion-limited vaporization* model best matches the pool burning of a crude oil. The alkane mixture residue consisted mainly of hexadecane (99.6%) with only a trace amount of dodecane (0.4%) and contained no *n*-octane. Both *n*-octane and dodecane were clearly evaporated preferentially over hexadecane, yet were

present up to at least half of the burning duration, as suggested by the other results (Fig. 4.3 and Fig. 4.4). These results indicate that the alkane mixture had a near-uniform vaporization order and that the *Imperfect EFV* model best matches the pool burning of an alkane mixture.

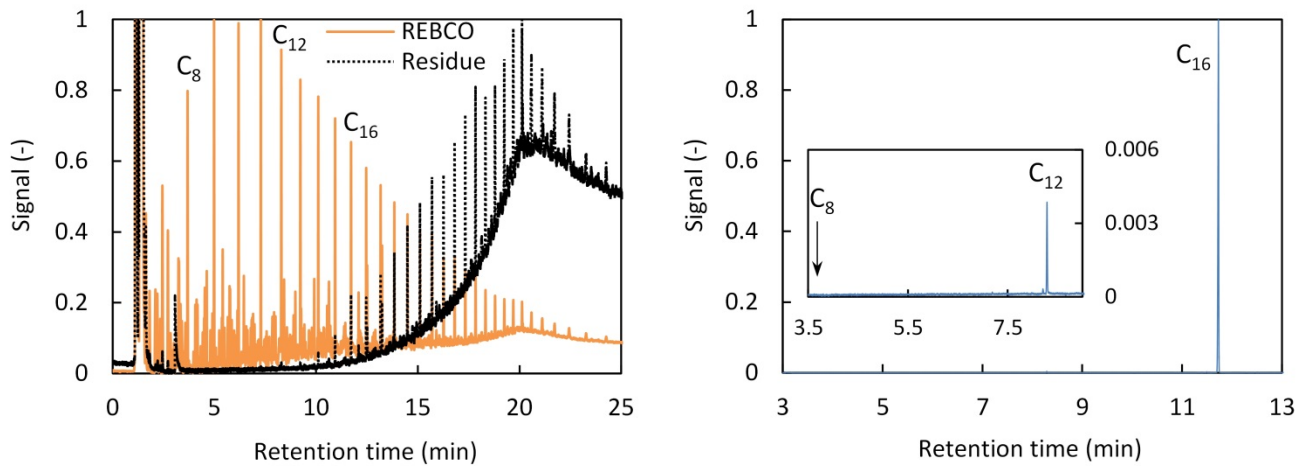


**Figure 4.6.** Gas chromatograms of Fresh REBCO and a typical REBCO residue (left) and a typical alkane mixture residue (right).

**Table 4.1.** Burning efficiencies for the tested oils

<i>Oil type</i>	<i>Thickness (mm)</i>		<i>Burning Efficiency (%)</i>
	<i>Initial</i>	<i>Final<sup>a</sup></i>	
<i>n</i> -Octane	10/40	0.1/0.05	99/99
Dodecane	10/40	0.2/0.9	94/97
Hexadecane	20	0.4	87
Alkane mixture	15/30	2.1/1.0	77/92
DUC	10/40	1.5/5.7	60/79
REBCO	10/40	1.6/7.9	52/75

<sup>a</sup> Based on the residue mass inside the cylinder and the initial density.

However, experimental work on multicomponent and crude oil droplet combustion has shown somewhat different results for the vaporization controlling mechanisms. Ikegami et al. (2003) showed that the combustion of crude oil droplets followed a distillation-like vaporization mechanism, even though the theoretical Peclet number indicated that the vaporization was diffusion-limited. This discrepancy was contributed to the “violent inter-circulation of fuel” caused by droplet swellings and contractions and gas generation and nucleation inside the droplet. Such processes are not expected to have a significant effect on the circulation within pool fires, so that the Peclet number would be determining the vaporization mechanism. Therefore, the vaporization mechanism for crude oil pool fires on water would indeed be diffusion-limited, as indicated by the data.

According to experiments on multicomponent droplets of two and three components, these types of fuels have a mixture of a distillation-like and diffusion-limited vaporization mechanism (Wang et al., 1984; Randolph et al., 1988). In these experiments, the droplets went through several steady state burning phases, each during which a new component was added to the vaporization. Although the lightest component evaporated preferentially at the start of the burning, it was still present at the last stages of the burning. When comparing these results to the performed pool fire experiments that have much longer burning times, it is not surprising that such a vaporization mechanism can be approximated with a near-uniform vaporization order. The narrow range of components in the alkane mixture would quickly lead to a steady state in which all components evaporate simultaneously. Such a steady state would remain until the lightest component(s) are depleted from the fuel near the end of the combustion. Thus, even though the alkane mixture might have a volatility controlled vaporization order, a near-uniform vaporization order is a representative approximation for pool fires, as shown by the experimental results. This approximate near-uniform vaporization order may also apply to other fuels with a narrow range of hydrocarbons such as refined fuels (gasoline or diesel). However, multicomponent fuels with a very wide range of components were shown to have significantly different behavior during the burning. The crude oils had a much more prominent volatility controlled vaporization order and can therefore not be represented by multicomponent fuels with only a narrow range of components.

#### **4.2.3 Residue composition as a function of the burning time**

The DUC residues from the experiments that were extinguished at fixed burning times had burning efficiencies of 15% (after 1:24 min), 32% (after 3:46 min) and 39% (naturally extinguished after 5:41 min). The chemical

analysis of the *n*-alkane composition in these residue samples and fresh DUC was based on the 85 *m/z* ( $C_6H_{13}$  fragment) ion chromatogram. This ion is observed in all *n*-alkanes with  $n \geq 6$  in  $C_nH_{2n+2}$  and the *n*-alkanes are very abundant in this ion chromatogram, as shown in the 85 *m/z* ion chromatogram for fresh DUC (Fig. 4.7). Almost all of the major peaks in this ion chromatogram correspond to the *n*-alkanes ranging from  $C_8$  to  $C_{31}$ , of which some are annotated in the chromatogram. The 85 *m/z* ion is therefore a very suitable ion to follow the compositional changes in crude oil as a function of the burning efficiency.

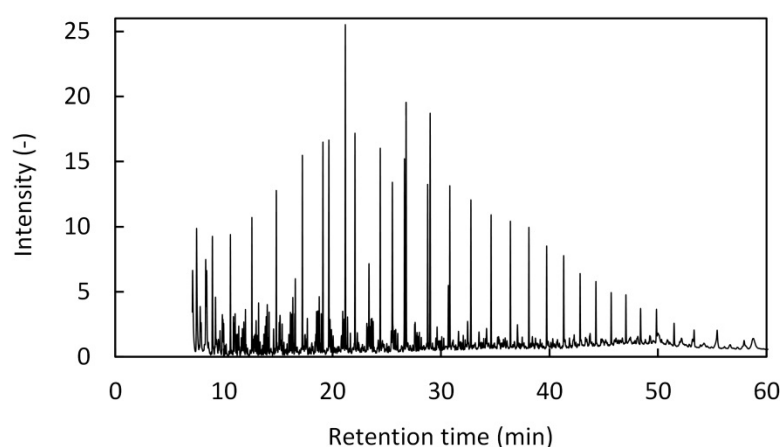


**Figure 4.7.** Ion chromatogram for 85 *m/z* of fresh DUC. The majority of the major peaks represent the *n*-alkanes, of which several are annotated.

The principal component analysis of the 85 *m/z* ion for fresh DUC and the burned DUC residues is shown in Fig. 4.8. Figure 4.8a is the loading plot, which shows the average relative concentration of hydrocarbons among all four samples and the loadings of the principal component (i.e. the alkane composition) relative to the average. The intensity of the loadings of the principal component indicates to what degree the individual samples differed from the shown average. A high intensity of the principal component loading for a specific hydrocarbon means that there was a large variation in the concentration of this hydrocarbon among the samples (e.g.  $C_{12}H_{26}$ ). A low intensity of the principal component loading for a specific hydrocarbon means that the relative concentration of this hydrocarbon was similar to the shown average in all samples.

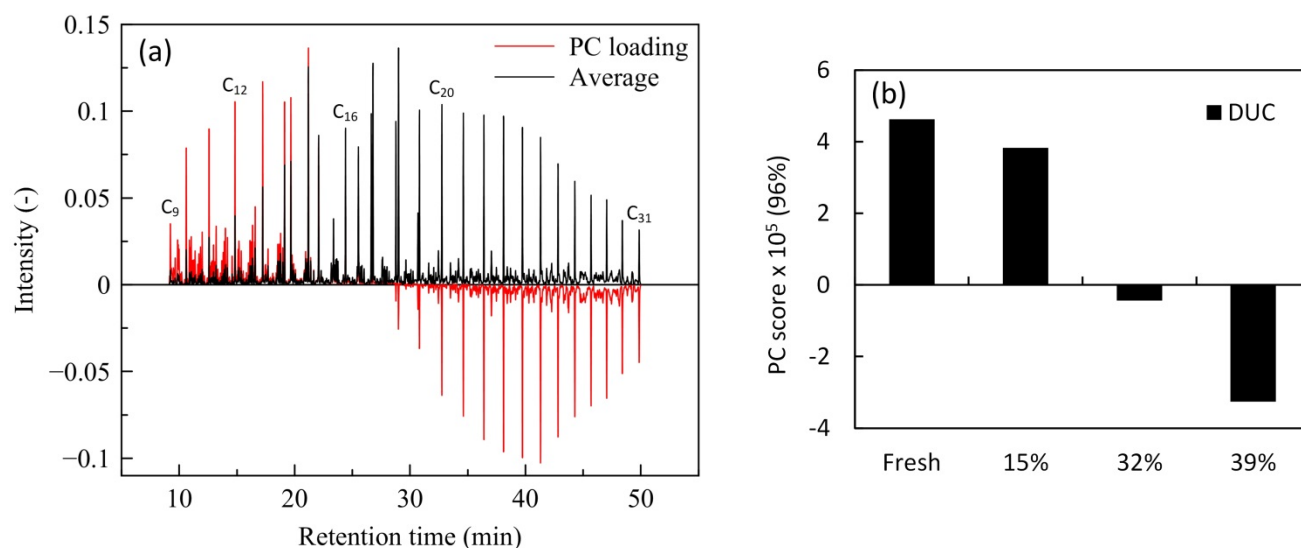


**Figure 4.8.** Principal component analysis of 85  $m/z$  ion in fresh DUC and burned DUC residues. The loading plot (a) shows the average ion chromatogram of all samples and the loadings of the principal component (alkane composition). The score plot (b) shows the score of the each sample for the principal component loadings. Positive scores indicate changes relative to the average according to the principal component loadings. Negative scores indicate changes relative to the average opposite of the principal component loadings. The higher the score (from zero), the larger the difference of the chemical composition was from the average. The percentage on the y-axis shows that 96% of the variance in the chemical composition between the samples was explained by the shown principal component loadings.

Figure 4.8b is the score plot, which shows the loadings score of the principal component for each sample. A high positive score indicates a large change of the chemical composition of the sample, in the direction of the shown principal component loadings, compared to the average. A negative score indicates that the chemical composition of the sample changed in the opposite direction of the shown principal component loadings compared to the average. Low scores (i.e. close to zero) indicate that the alkane concentrations only changed little in the (opposite) direction of the principal component loadings compared to the average. For example, fresh DUC has a high positive score, so it contained relatively more of the hydrocarbons between C<sub>9</sub>-C<sub>17</sub> and relatively less of the hydrocarbons between C<sub>18</sub>-C<sub>31</sub>, compared to the average chromatogram. This difference can be visually confirmed by comparing the ion chromatogram for 85  $m/z$  of fresh DUC in Fig. 4.7 to the average chromatogram in Fig. 4.8.

The principal component analysis in Fig. 4.8 clearly shows that the relative concentrations of the light hydrocarbons decrease and of the heavy hydrocarbons increase with increasing burning efficiency. These results confirm that the components in crude oil are burned in order of decreasing volatility and thus provide quantitative proof that the proposed vaporization order for crude oils is correct. The chemical composition of the oil changed most between a burning efficiency of 15% and 32%, which is also reflected in the viscosity increase between these samples (Table 4.2). A detailed chemical analysis of the components that were the main contributors to these changes was beyond the scope of this thesis.

**Table 4.2.** Density and viscosity of burned DUC residues

<i>Burning efficiency (%)</i>	<i>Burning time (min)</i>	<i>Density (g/ml)<sup>a</sup></i>	<i>Viscosity (cP)<sup>a</sup></i>
Fresh	0:00	0.853	6.750
15	1:24	0.884	22.06
32	3:46	0.915	202.7
39	5:41	0.935	716.7

<sup>a</sup> Measured at 25 °C using an Anton Paar SVM 3000 viscometer.

The principal component analysis of a selection of ion chromatograms with different  $m/z$  values for fresh DUC and burned DUC residues is shown in Fig. 4.9. The selected ion chromatograms contain several PAHs that are commonly used as biomarkers for crude oils (Christensen et al., 2010; Gallotta and Christensen, 2012). These PAHs consist of methylated pyrenes ( $m/z$  of 216), benzo(a)anthracene, triphenylene and chrysene ( $m/z$  of 228), methylated chrysenes ( $m/z$  of 242,) 5-ringed PAHs ( $m/z$  of 252) and indeno[1,2,3-c,d]pyrene and benzo[g,h,i]perylene ( $m/z$  276). Of these PAHs, the ones that contain  $m/z$  ions 228, 252 and 276, are pyrogenic components, which means that these PAHs are formed during combustion. The PAHs that contain  $m/z$  ions 216 and 242 are petrogenic components, which means that these PAHs are typically found in fresh crude oils (Gallotta and Christensen, 2012). In theory, these PAH biomarkers should thus be able to be used to follow the burning efficiency of the DUC samples.

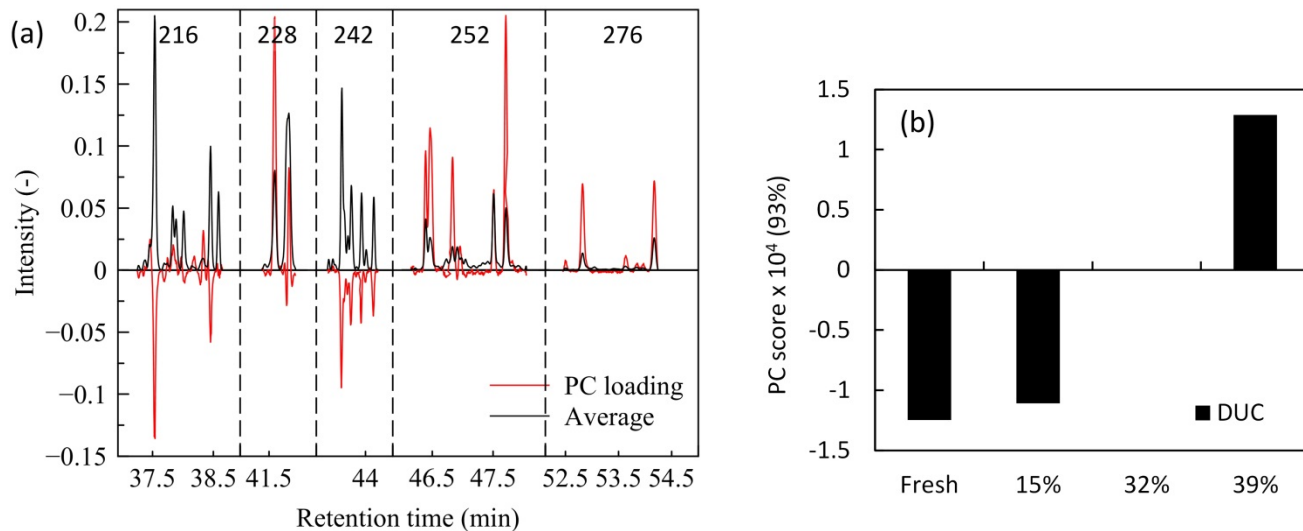


**Figure 4.9.** Principal component analysis of five ion chromatograms for fresh DUC and burned DUC residues. The ion chromatograms are separated in the loading plot (a) by the dashed lines and the corresponding  $m/z$  value of each ion is annotated in the plot. The loading plot (a) shows the average ion chromatograms of all samples and the loadings of the principal component (PAH composition). The score plot (b) shows the score of the each sample for the principal component loadings. Positive scores indicate changes relative to the average according to the principal component loadings. Negative scores indicate changes relative to the average opposite of the principal component loadings. The higher the score (from zero), the larger the difference of the chemical composition was from the average. The percentage on the y-axis shows that 93% of the variance in the chemical composition between the samples was explained by the shown principal component loadings.

The results of the principal component analysis in Fig. 4.9 indeed show that the pyrogenic PAHs increase in relative concentration with increasing burning efficiency. The petrogenic PAHs present in the fresh crude oil react on the other hand are removed with increasing burning efficiency. These results give a measure of the accuracy with which the byproducts of *in-situ* burning of crude oils on water can be analyzed as a function of the burning time and burning efficiency. In addition, these results validate the results from the 85  $m/z$  ion principal component analysis because the burning efficiencies of the residue samples are correctly reflected in their respective chemical compositions. As such, the results of the principal component analyses provide strong, quantitative evidence that the vaporization order of crude oil is volatility controlled.

#### 4.2.4 Influence on heat transfer mechanics and burning efficiency

With the best vaporization model established for crude oil, the significance of this vaporization order for the burning efficiency was assessed by analyzing its influence on the heat transfer mechanics (Section 2.1.4). The main equations that were specifically derived for pool fires on water and that are relevant to the current discussion are repeated here for convenience purposes (Eq. (7) and (12)):

$$\dot{Q}_{evap} = \dot{Q}_{net} - \dot{Q}_{grad} - \dot{Q}_{loss} \quad (6)$$

$$\chi_s = \frac{\dot{Q}_{net}}{\dot{Q}} = \frac{\dot{m} \cdot \Delta H_g + \dot{Q}_{loss}}{\dot{m} \cdot \Delta H_c} = \frac{\Delta H_g}{\Delta H_c} + \frac{\dot{Q}_{loss}}{\dot{m} \cdot \Delta H_c} = \frac{\Delta H_g}{\Delta H_c} + \frac{\dot{Q}_{loss}''}{\dot{m}'' \cdot \Delta H_c} \quad (11)$$

For the alkane fuels, the experimental results (Section 4.2.2) show that a semi-steady state is reached shortly after ignition. For such a state,  $\dot{Q}_{net}$  can be assumed to be constant because the burning rate is constant (Eq. (4)). Over time the temperature gradient in the fuel layer, and therefore  $\dot{Q}_{grad}$ , also typically remained constant for a long duration of the burning (Fig. 4.10). Only  $\dot{Q}_{loss}$ , which is a function of the temperature difference between the fuel layer and water layer, will increase over time as the slick thickness is reduced and the hot fuel surface starts to approach the water layer. As  $\dot{Q}_{loss}$  increases,  $\dot{Q}_{evap}$  decreases up to the point where it becomes too low to maintain an evaporation rate that can sustain the fire. At this 'critical point' the fire is extinguished and a residue is left on the water. Because larger hydrocarbons generally show lower flame heights and higher surface temperatures (Fig. 4.3 and Fig. 4.4), it is likely that their  $\dot{Q}_{net}$  is lower and  $\dot{Q}_{grad}$  and  $\dot{Q}_{loss}$  are higher. The critical point can therefore be expected to be reached relatively faster, which is reflected in the lower burning efficiencies and higher residue thicknesses in Table 4.1 for dodecane and hexadecane. For thicker slicks, it takes longer for the hot surface to approach the water layer and the increase in  $\dot{Q}_{loss}$  is slower. Thus, relatively more fuel can be burned before the critical point is reached and therefore the burning efficiencies are higher for the thicker initial slicks.

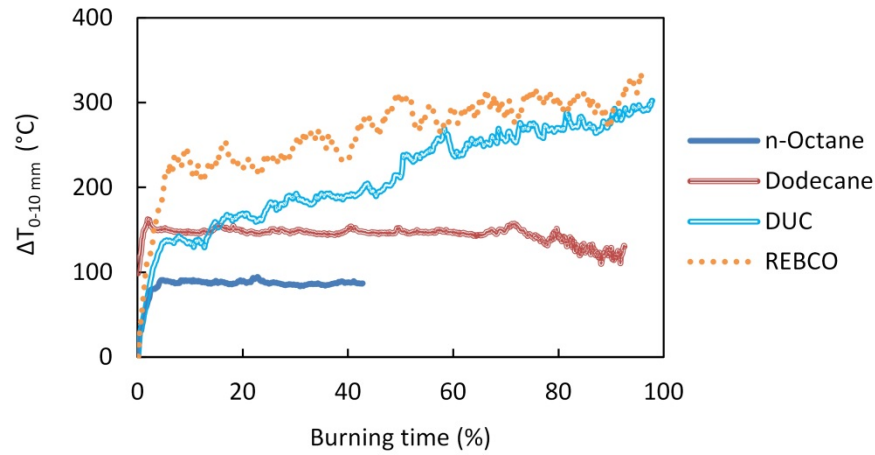


**Figure 4.10.** Temperature difference between the fuel surface and the temperature 10 mm below the fuel surface (initial oil-water interface) for fuels with an initial slick thickness of 10 mm as a function of the burning time. The data shown is up to the moment when the thermocouple placed at the fuel surface no longer measured the surface temperature. The temperature gradients were representative for the temperature gradients in the fuels between all measured locations below the fuel surface (2, 3, 5 and 10 mm).

Whereas the critical point for the alkane fuels is mostly determined by the balance between  $\dot{Q}_{evap}$  and  $\dot{Q}_{loss}$ , the heat transfer mechanics are more complicated for the crude oils. Because the crude oils were shown to have a volatility controlled vaporization order,  $\dot{Q}_{net}$  and  $\dot{Q}_{grad}$  cannot be assumed to be constant. Over the course of the burning, the flame height for the crude oils was reduced by 70% (Fig. 4.4), which would result in a reduction of  $\dot{Q}_{net}$  over time. As shown in Fig. 4.10, the temperature gradient inside the crude oils increased over time, causing  $\dot{Q}_{grad}$  to increase, which was also observed in an earlier study (Vali et al., 2015). Furthermore, the crude oils reached higher temperatures than the alkane fuels, both at the surface (Fig. 4.3) and the oil-water interface (Fig. 4.3 and Fig. 4.10), so  $\dot{Q}_{loss}$  also was more significant. These heat transfer mechanics lead to  $\dot{Q}_{evap}$  being reduced in an increasingly faster rate over time. The critical point can therefore be reached well before the crude oil has been fully burned, which explains the low burning efficiencies (Table 4.1). Thus, in order to reach high burning efficiencies for crude oils, the accumulative effect of a decreasing flame height (and thus  $\dot{Q}_{net}$ ) and increasing heat losses ( $\dot{Q}_{grad}$  and  $\dot{Q}_{loss}$ ) needs to be overcome.

The above discussions show that in terms of Eq. (12), the  $\dot{Q}_{loss}$  term has a more limiting effect on  $\dot{Q}_{evap}$  for crude oils, due to their volatility controlled vaporization order, than for pure oils. This in turn increases the effect that the burning rate per unit area has on  $\dot{Q}_{evap}$  in Eq. (12), which decreases as a function of time for

crude oils (Fig. 4.4) but increases with increasing diameter (Section 2.1.3). As such, this equation provides a possible explanation to the size dependency of the burning efficiency of crude oil. When the increasing burning rate per unit area with increasing diameter balances out against the increasing heat losses for crude oil burning on water, the limiting effect of  $\dot{Q}_{loss}$  on  $\dot{Q}_{evap}$  is mitigated. The critical point would not be reached until the final stages of the burning when the slick becomes very thin and  $\dot{Q}_{loss}$  starts to dominate the heat transfer mechanics, such as for the pure fuels. The burning efficiency of a fuel burning on water, when its  $\dot{Q}_{evap}$  is limited by  $\dot{Q}_{loss}$ , will therefore be a function of the pool diameter.

The current results indicate that fuels with low volatilities are more limited by  $\dot{Q}_{loss}$  than high volatility fuels, because more energy is required to evaporate the fuel and thus  $\dot{Q}_{evap}$  needs to be larger. This suggests that *in-situ* burning of weathered crude oils, which have lower volatilities than fresh crude oils, is also limited by  $\dot{Q}_{loss}$ . Burning efficiencies for weathered oils have indeed been shown to be size dependent (see e.g. Fritt-Rasmussen et al. (2012) and Brandvik et al. (2010a)). The principles of this heat transfer model and Eq. (12) can therefore likely be applied to the *in-situ* burning of crude oil on water in general, independent of the state (weathered or fresh) of the oil.

#### 4.2.5 Sub-conclusion

The comparison between model predictions and experimental results for the surface temperature, burning rate, and flame height of crude oil pool fires on water showed that the crude oil had a volatility controlled vaporization order. Crude oil residue compositions showed that this order was furthermore diffusion-limited, meaning that several components evaporate simultaneously from the fuel as the evaporating components shift from most volatile to least volatile. Principal component analyses of the alkanes and a select group of PAHs in fresh DUC and burned DUC residues provided clear evidence for this proposed vaporization order for crude oils. Alkanes were progressively removed in order of volatility from the crude oil as a function of the burning efficiency. As the burning efficiency increased, the concentration of pyrogenic PAHs in the residues also increased, whereas the concentration of petrogenic PAHs was reduced. This indicates that the higher burning efficiency residue samples were clearly more burned samples. It can therefore be stated that the vaporization order of crude oils during *in-situ* burning on water is volatility controlled.

The alkane mixture, studied as an alternative, simplified substitute for crude oil with a more narrow range and limited number of components, showed significantly different results from the crude oil. Whereas the crude oil did not reach a steady state burning, the alkane mixture results were similar to the steady-state behavior of the pure alkane fuels. The alkane mixture was better described by a near-uniform vaporization order, where all components in the fuel evaporate simultaneously but with a relatively higher vaporization rate for the lighter components. This shows that simplified fuels with a narrow range of hydrocarbons do not accurately represent crude oils, because the burning behavior of a multicomponent fuel depends on the (volatility) range of its components. Great caution should thus be taken when making statements about oil burning based on simplified experiments.

The established vaporization model for crude oils was analyzed in terms of the heat transfer mechanics (Section 2.1.4) to give an explanation for the size dependency of the burning efficiency for crude oils. Due to volatility controlled vaporization order, the fuel surface temperature increases and flame height decreases as a function of the burning time. This causes the heat losses to the water to increase, while less energy is supplied to the fuel through heat feedback from the flame. These heat transfer mechanics reduce the energy available for the evaporation of the fuel, until the fire is no longer self-sustaining, causing it to extinguish prematurely, as compared with predictions based on adiabatic models. Because the burning rate per unit area increases with increasing diameter, large scale experiments have more energy available to overcome the increasing heat losses. As a consequence, more heat remains available for evaporating the crude oil and, as a result, large scale experiments would result in higher burning efficiencies than small scale experiments.

### **4.3 Initial slick thickness**

The results presented in this section were obtained with the COFA setup (Section 3.1) and the burning rate setup (Section 3.1.1), according to the methodology described in Section 3.1.6.

#### **4.3.1 Regression rate**

The regression rate as a function of the initial oil slick thickness for both pure and crude oils is shown in Fig. 4.11. Modelled predictions of the regression rates for *n*-octane, dodecane and crude oil are also shown, using

the model developed by Garo et al. (1999b) and Torero et al. (2003) (Eq. (18)). The average experimental regression rate was calculated by multiplying the burning efficiency with the initial slick thickness and dividing this number by the burning time (from ignition to flame extinction). This method neglects any density changes in the crude oils that might affect the actual thickness of the residue. The experimental regression rate data for the crude oils thus only show an approximate regressions rate and the trends emerging from the data are the main results.

$$r = \frac{1}{\Delta H_v \cdot \rho_F} \left[ \chi_s \cdot \left( \frac{(4 \cdot \rho_\infty \cdot c_p \cdot (T_\infty \cdot g \cdot (T_f - T_\infty))^{1/2})}{\pi} \right) \cdot D^{1/2} - \frac{a_F \cdot k \cdot (T_b - T_\infty)}{y_{S,i} \cdot (\sqrt{\alpha_F} + \sqrt{\alpha_W})^2} \right] \quad (18)$$

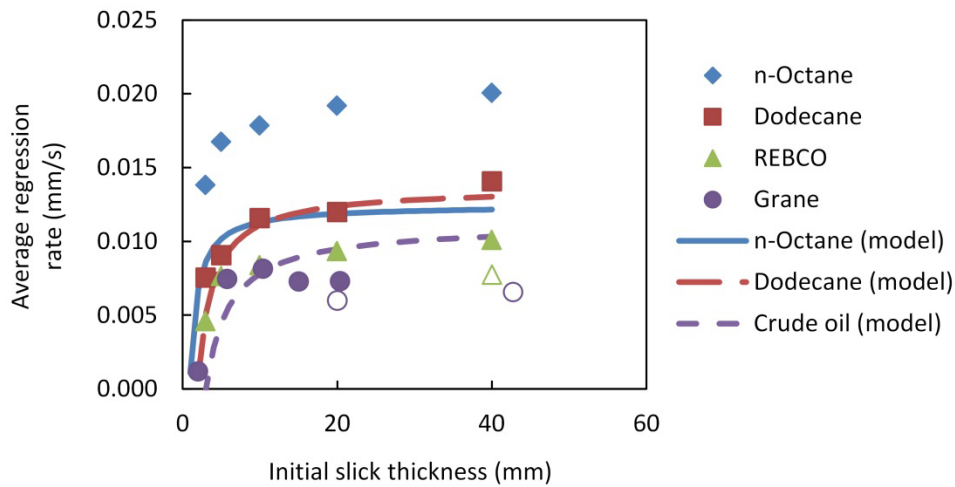


**Figure 4.11.** Average regression rates as a function of initial oil slick thickness for the alkanes and two crude oils (REBCO and Grane). The open symbols represent crude oil experiments without boilover. The Grane data was adapted from Brogaard et al. (2014).

Equation (18) describes the regression rate as a function of the heat feedback from the flame to the fuel surface (first term in the brackets) and heat losses to the water layer based on the thermal properties of the fuel and water (second term in the brackets). Here,  $r$  is the regression rate of the fuel,  $\rho_F$  is the density of the fuel,  $\rho_\infty$  is the density of air at ambient conditions,  $T_f$  is the temperature of the flame (in this study taken as 1100 K, based on results in Torero et al. (2003)),  $g$  the gravitational acceleration ( $9.81 \text{ m/s}^2$ ),  $\alpha$  the thermal

diffusivity of the fuel ( $\alpha_F$ ) and water ( $\alpha_W$ ), and  $y_{s,i}$  is the initial slick thickness. The heat feedback fraction ( $\chi_s$ ) was taken as a constant value of  $2.9 \times 10^{-3}$  (as defined by Torero et al. (2003)). Model input parameters are listed in Table 4.3 and were obtained from Tanaka et al. (1988) and Torero et al. (2003). The crude oil parameters from Torero et al. (2003) used to represent both REBCO and Grane were updated with the boiling point and density of Grane (Table 3.1) for improved representation of the tested crude oils.

**Table 4.3.** Regression rate model parameters (Tanaka et al., 1988; Torero et al., 2003)

<i>Fuel</i>	$T_b$ (K)	$\Delta H_v$ (kJ/kg)	$k$ (at 20 °C) (W/m K)	$\rho_F$ (at 20 °C) (kg/m <sup>3</sup> )	$c_p$ (at 20 °C) (kJ/kg K)	$\alpha$ ( $\times 10^{-7}$ ) (at 20 °C) (m <sup>2</sup> /s)
<i>n</i> -Octane	399	300	0.128	703	2.2	0.82
Dodecane	489	256	0.137	750	2.2	0.83
Crude oil (Grane)	653	250	0.132	941	2.3	0.68
Air	-	-	0.026	1.16	1	225
Water	373	2257	0.59	998	4.18	1.414

Model calculations showed the same trend for all three oils, i.e. an increasing regression rate with increasing slick thickness that approaches a maximum value, as expected. Altering the flame temperature between 900 and 1300 K did not significantly change the model output qualitatively. Due to the uncertainties concerning the model, changing the flame temperature only for quantitative purposes seemed unwarranted. The fact that *n*-octane was predicted to have a lower maximum regression rate than dodecane and experimental data was contributed to inaccuracies in the model combined with similar model parameters for *n*-octane and dodecane. The main purpose of showing the modeled predictions is to provide a qualitative reference to which the experimental data can be compared. As the predicted trend for *n*-octane was similar to the other model predictions as expected, it was deemed sufficiently accurate.

The general trend in the data shows that for all oils the regression rate increases with increasing slick thickness and then approaches a fairly constant value. The initial slick thickness at which the constant value is approached varies for each individual oil (10-20 mm for *n*-octane, 10-20 mm for dodecane, 20-40 mm for REBCO and 20-40 mm for Grane), but it is always equal to or larger than 10 mm. This is in accordance with

previous reported studies and the trend in model predictions (Garo et al., 1994; Garo et al., 1999b; Torero et al., 2003; Buist et al., 2013). The low regression rates for slick thicknesses below 10 mm can be explained by heat losses to the underlying water layer (Brzustowski and Twardus, 1982; Buist et al., 1999). As the oil functions as an insulating layer between the burning surface and the water surface, a thicker initial slick decreases the heat losses to the water, which in turn causes the regression rate to increase. Increasing the initial slick thickness will therefore minimize the heat losses up to the point where the regression rate reaches a maximum constant value. The obtained maximum values lie within the same order of magnitude as the model predictions and regression rates for pool fires of similar *n*-alkanes reported in literature (Burgess et al., 1961; Mudan, 1984). The maximum regression rate that an oil can reach is determined by its intrinsic parameters (mainly the mass transfer number (Spalding, 1955, 1962)) and the pool diameter (Koseki and Mulholland, 1991; Garo et al., 1994; Garo et al., 1999b; Torero et al., 2003).

While the experimental data mainly follow the expected trends, a few deviations can be seen. The regression rate for Grane seems to peak around 10 mm after which it reaches a constant value around an initial slick thickness of 20-40 mm. The elevated regression rates for initial thicknesses of 5-15 mm were most likely caused by a boilover just before the flames extinguished. (The regression rate data in Fig. 4.11 includes boilovers, contrary to the regression rate data from Garo et al. (1994) and Garo et al. (1999b).) During boilover, the regression rate increases significantly and can easily be twice as high as the pre-boilover regression rate (Evans et al., 1988; Evans et al., 1992). For Grane, boilover was only observed for an initial slick thickness between 5 and 20 mm and occurred only during half of the 20 mm experiments (see Section 4.5.4 for further discussion of the boilover results). Thus, boilovers likely explain the increased regression rates for initial slick thickness of 5-15 mm compared to 20-40 mm. It is expected that the pre-boilover regression rate as a function of initial slick thickness for Grane followed the same trend as found for the other oils and shown in previous studies (Garo et al., 1994; Garo et al., 1999b; Torero et al., 2003).

### **4.3.2 Burning rate**

The burning rate data of *n*-octane and dodecane clearly showed that water evaporated during the burning of the oil because the total mass lost was higher than the initial oil mass (Fig. 4.12). Evaporation of water occurred during all burning rate experiments and water losses increased with increasing slick thickness (Fig. 4.13). The water mass lost in each experiment was derived from the difference between the total measured mass lost at

the end of the experiment and the weight of the collected oil residue. Temperatures of the flames\* and in the oil slick were independent of the initial slick thickness for a specific oil and the total water mass lost was therefore assessed to be only a function of the burning time. Because the water requires time to heat up in order to significantly contribute to the total mass loss rate, it will have a larger effect on experiments with a longer burning time. The boilover phenomenon was also clearly identifiable in the burning rate data as the burning rate rapidly increased during this period, as annotated in Fig. 4.12. Such a sudden loss of a relatively high amount of mass results in an increased average regression rate and these results thus confirm that the boilover occurrence increased the average regression rate (Fig. 4.11).

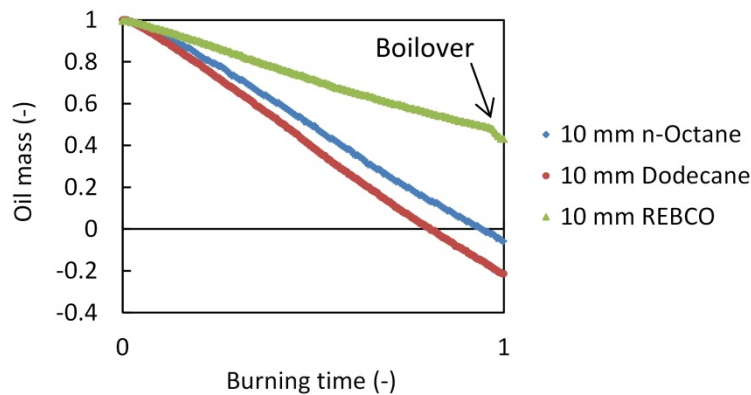


**Figure 4.12.** Normalized mass loss curves from ignition to extinction of the flames for the alkanes and REBCO. The relative mass is based on the initial amount of oil used in each experiment. The negative mass balances for *n*-octane and dodecane are caused by evaporation of water.

Figure 4.13 shows an overview of the average mass loss rate including and excluding water mass losses as a function of the slick thickness. The average mass loss rates were calculated from the mass lost between 10% and 90% of the burning time, to avoid the inclusion of the growing phase, the extinction phase where the burning can become intermittent and the boilover occurrence. The results clearly show that the mass loss rate increases with increasing slick thickness, but that the water mass losses distort the average mass loss trend from the trend that was observed for the regression rate (Fig. 4.11). The average mass loss data suggests that

\* Several burning rate experiments featured an extended thermocouple array with three thermocouples placed 0.25, 0.40 and 1.0 m above the fuel surface to monitor the flame temperature with respect to the water mass losses.

there is either no maximum mass loss rate, or that the maximum rate is not yet reached. However, considering that the mass loss rate and the regression rate represent similar aspects of the burning process (assuming a constant oil density), the same trend was expected. When excluding the water mass loss, assuming a constant water mass loss rate (explained below), the data show a good correlation with the regression rate data. Thus, mass loss rate data should be corrected for any water mass losses to properly represent the burning rate of the oil.

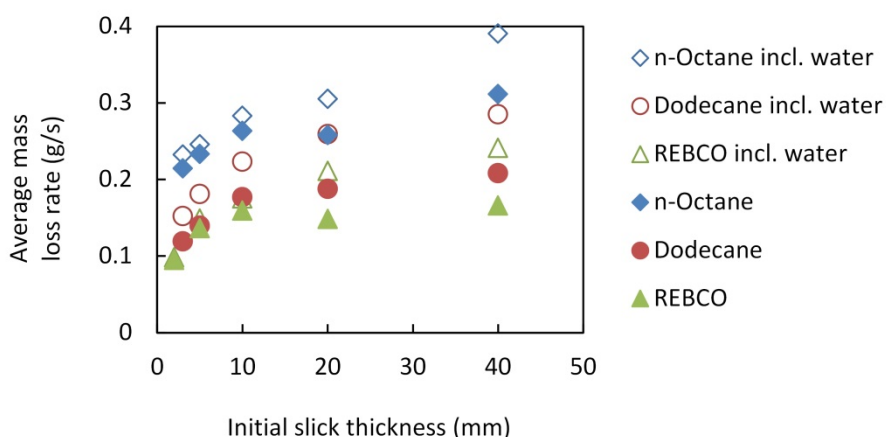


**Figure 4.13.** Average mass loss rates of oil and oil including water mass losses as a function of the initial oil slick thickness for the alkanes and REBCO.

In order to correct for the water mass losses, it was assumed that the water mass loss rate only depended on the burning time and the oil type. The average water mass loss rates for each tested thickness of a specific oil type could then be combined to provide five water mass loss rate data points as a function of the burning time. Based on these data points, a linear, logarithmic and polynomial trendline were plotted to determine the best fitting function of the water mass loss rate as a function of time (Fig. 4.14a). From these trendlines, the water mass loss rates were calculated and then subtracted from the total mass loss rates to acquire the mass loss rates excluding water losses (i.e. the burning rate) of each experiment. The burning rates of the experiments were also calculated for a constant water mass loss rate, equal to the average water mass loss rate. The resulting burning rates as a function of time were then compared, as shown as example for dodecane in Fig. 4.14b, to determine the best fitting water mass loss rate function.

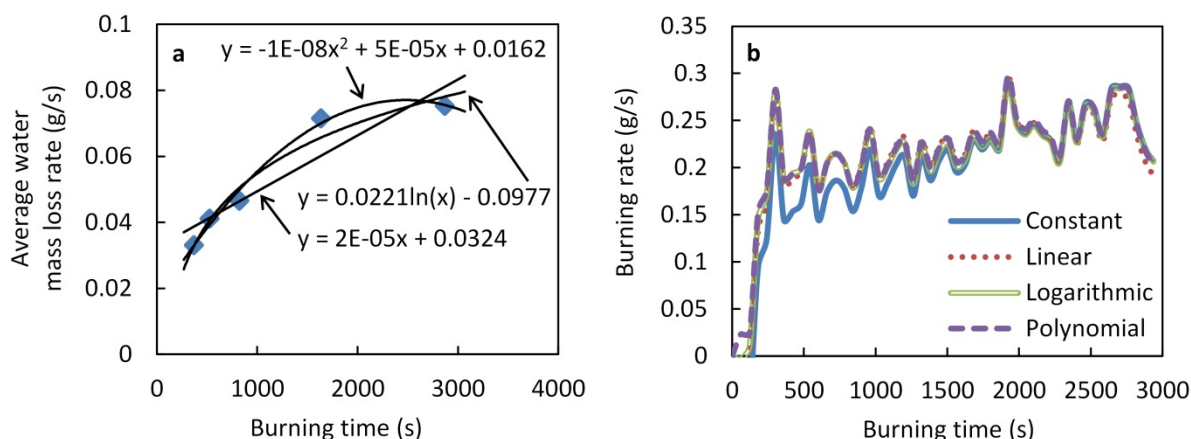


**Figure 4.14.** Average water mass loss rates of dodecane (a) and burning rates excluding water losses of 40 mm dodecane (b) as a function of the burning time. Burning rate data points are shown as lines for clarity reasons. The legend in (b) denotes the corresponding function in (a) for the water mass loss rate that was used to calculate the burning rate of the fuel. The differences between the calculation methods in (b) were representative for all tested oil types and thicknesses.

The calculated burning rates in Fig. 4.14b, show that none of the tested water mass loss rate functions results in a significantly different burning rate compared to the other methods. As such, a constant water mass loss rate was used in this study, as this correction does not depend on other data sets of the same oil with different initial slick thicknesses. This allowed for correcting the burning rate consistently among all burning rate experiments (e.g. hexadecane in Fig. 4.4), without the need to conduct a multitude of experiments only to derive the water mass loss rate function. A test experiment with 40 mm dodecane was conducted that featured a metal lit over the water to shield it from radiation of the flame and therefore minimize the water losses. Although the water losses decreased, the water losses were not fully prevented and the total mass loss rate still increased as a function of the burning time. Because of the limited influence of the water mass loss function on the burning rates of *n*-octane, dodecane and REBCO (Fig. 4.14), the precise water loss mechanisms were not investigated further.

### 4.3.3 Burning efficiency

The burning efficiency as a function of initial slick thickness is shown in Fig. 4.15. As expected, the observed trend compares with that for the average regression rate (Fig. 4.11) and average mass loss rate (Fig. 4.13). For

both alkanes, the burning efficiency reached up to 99%, leaving only a very thin colored oil sheen behind. The slightly lower burning efficiencies (93-98%) for thinner alkane slicks (3-10 mm) were attributed to heat losses to the underlying water layer. For the crude oils, the burning efficiency increased with increasing initial slick thickness from 23% to 75% for REBCO and from 6% to 63% for Grane. The very low burning efficiencies for thin crude oil slicks (2-5 mm) are most likely caused by the fast boilover occurrence after ignition, which extinguished the fire after a short period of intense burning (see also section 4.5.4). This early boilover occurrence can be explained by a combination of fast superheating of the water due to heat losses and a thin slick that allows for the early penetration of water vapor after the water was superheated. Thus, while boilover occurrence increases the regression rate and burning rate and may increase the burning efficiency (e.g. 40 mm REBCO), it likely has a negative impact on the burning efficiency for thin oil slicks.

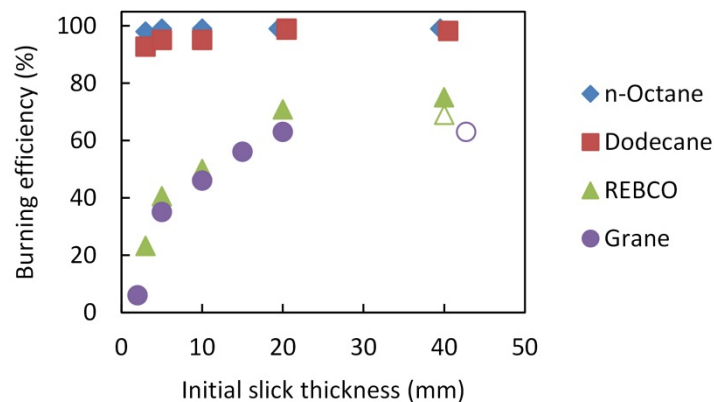


**Figure 4.15.** Burning efficiency as a function of initial slick thickness. The open symbols represent crude oil experiments without boilover. The Grane data was adapted from Brogaard et al. (2014).

The difference between burning efficiency for thin and thick slicks was in particular observed for the 10 and 20 mm REBCO results (respectively a BE of 50% and 71%). Usually, the burning time doubled when doubling the slick thickness. However, the typical 10 mm REBCO experiment took between 550-600 seconds, whereas the 20 mm REBCO experiments took over 1500 seconds. As discussed in Section 4.6.1, this difference was most likely caused by the insulating properties of the oil slick that prevented the superheated water from penetrating the oil slick. Boilover was therefore significantly postponed at an initial slick thickness of 20 mm, which allowed for

the burning to continue longer and thus more oil was burned before flame extinction as a result of the boilover. Considering the small difference in burning efficiency between 20 and 40 mm for the crude oils, an initial slick thickness of 20 mm was optimal in terms of the burning efficiency.

Figure 4.15 clearly shows that the crude oils do not reach a burning efficiency of near 99%. In fact, a minimum residue formation of about 30 wt% was observed for the 20 and 40 mm REBCO experiments. Considering that the obtained residues never sank and thus have a density  $< 1.00$  g/ml, the residues were estimated to have a thickness of 3.5 mm and 6.5 mm, respectively. Previous studies have described a “rule of thumb” regarding residue formation that states that for an initial slick thickness of  $\leq 40$  mm, a residue thickness of about 1 mm is formed (Buist et al., 1999; Buist et al., 2013). Based on this theory, a logarithmic increase would be expected for the burning efficiency as a function of the initial slick thickness with an asymptote close to a 100%. However, the data clearly show much lower burning efficiencies. While a burning efficiency of 90% would be expected for a 10 mm slick based on this rule of thumb, the observed burning efficiencies did not reach over 50%. The clear asymptotic function of the initial slick thickness in Fig. 4.15 shows that the burning efficiency is not expected to reach above 80%, even for much higher slick thicknesses. These results thus provide another clear example of the limited burning efficiencies for crude oils on water in small scale experiments. As such, the initial slick thickness only has a limited influence on the maximum achievable burning efficiency, which is also controlled by the pool diameter.

As discussed above, the logarithmic trend observed in Fig. 4.15 (and in Fig. 4.11 and Fig. 4.13) is likely caused by heat losses to the underlying water layer. For thin slicks, too much of the heat fed back to the fuel surface from the flame is lost to the water to sustain the fire, due to a lack of insulation. Considering that such heat losses play a role during large scale fires, the same logarithmic relation between the burning efficiency and the initial slick thickness is expected for large scale fires. Because the relative heat feedback to the fuel surface is larger for large scale fires than for small scale fires (Section 2.1.4), less insulation from the thickness of the slick will be required to sustain the fire. It is therefore reasonable to expect that the maximum burning efficiency for large scale fires can be obtained for initial slick thicknesses lower than the optimal thickness of 20 mm found in this study. Above this optimal initial slick thickness, which can be as low as the ignitability limit (1-2 mm), the

burning efficiency will be independent of the initial slick thickness. The optimal initial slick thickness would thus be a function of the pool diameter. Because the optimal initial slick thickness is expected to decrease with increasing pool diameter, the effect of the initial slick thickness on the burning efficiency for operational scale fires may become near negligible.

#### 4.3.4 Flame height

The average flame height, defined as the height up to which 50% of the time flames were present, is shown in Fig. 4.16 as a function of the initial slick thickness. For each oil type, the flame height profiles as a function of the burning time were similar to the 40 mm data presented in Fig. 4.4, independent of the slick thickness. The average flame height results for the alkanes were similar to the results for the burning rate (Fig. 4.13), as expected from Eq. (5). The general asymptotic trend was followed as the average flame height reached a maximum constant value at initial slick thicknesses of  $\geq 10$  mm. For the thinner slicks, the flame height was influenced by heat losses to the water layer that reduced the burning rate (Fig. 4.13).

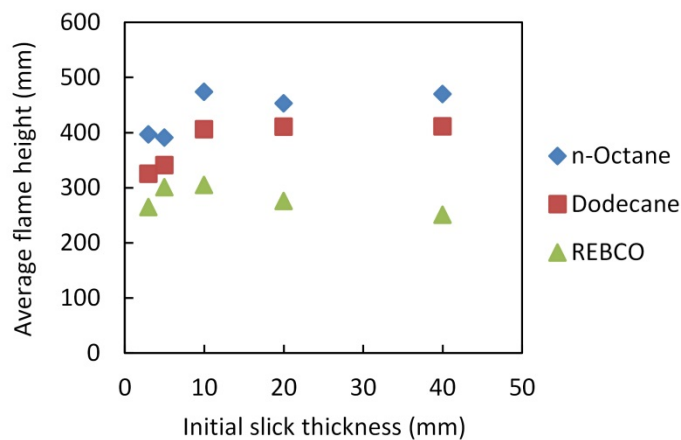
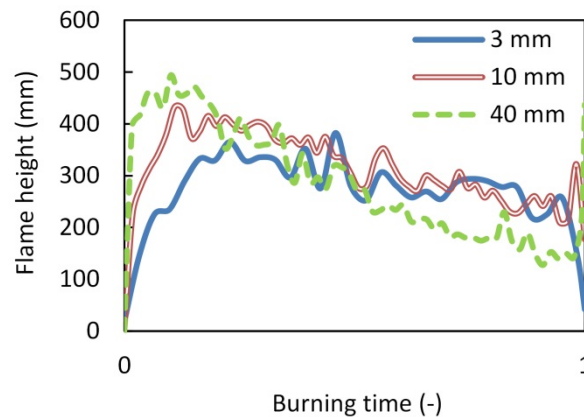


Figure 4.16. Average flame height as a function of the initial slick thickness for the alkanes and REBCO.

The crude oil, however, showed a decreasing average flame height after an initial slick thickness of 10 mm. This decrease was caused by a combination of higher burning efficiencies for thicker initial oil slicks and a

decreasing flame height for crude oils as a function of the burning time (Fig. 4.4). Because of the volatility controlled vaporization order (4.2), the higher the burning efficiencies of a crude oil, the higher the fraction of heavy components that contributes to the combustion relative to the burning time. Since the flame height decreases with increasing molecular weight (Fig. 4.4), the average flame height must decrease with increasing burning efficiency.

This effect is clearly shown in Fig. 4.17, which shows the flame height as a function of the normalized burning time of REBCO with initial slick thicknesses of 3, 10 and 40 mm. The flame height for an initial slick thickness of 40 mm has the steepest slope and reaches the lowest flame height because its burning efficiency is the highest of the three thicknesses shown. Even though an initial slick thickness of 40 mm is affected least by heat losses to the water layer and showed the highest maximum flame height, the steep slope resulted in a lower average flame height than for a 10 mm initial slick thickness. At an initial slick thickness of 3 mm, the flame height is limited by heat losses to the water layer, resulting in a low overall flame height. The average flame height is therefore highest for an initial slick thickness of 10 mm, because it has the optimal balance between insulation from the slick thickness and a relatively high fraction of light components contributing to the combustion.



**Figure 4.17.** Flame height as a function of the normalized burning time for REBCO with different initial slick thicknesses. The sudden increase of the flame height at the end of the burning in the 10 mm and 40 mm experiments was caused by boilover.

#### **4.3.5 Sub-conclusion**

The results on the influence of the initial slick thickness showed a clear relationship between the initial slick thickness and the regression rate, mass loss rate, burning efficiency and flame height. Initially, increasing the initial slick thickness resulted in an asymptotic increase of these burning parameters, up to a maximum asymptote value after which they remained constant. At this point an optimal initial slick thickness is reached and increasing the slick thickness will not further improve the burning effectiveness. Only for crude oil (REBCO), the average flame height decreased for slick thickness higher than the optimal initial slick thickness, which was caused by the volatility controlled vaporization order.

For the studied scale (160 mm diameter pool), the optimal initial slick thickness was reached at an initial slick thickness of 20 mm, with a maximum burning efficiency of 65-75% for the used crude oils. Burning efficiencies of up to 99% could not be obtained by further increasing the initial slick thickness, suggesting that the initial slick thickness only has a limited influence on the burning efficiency. The principle of a maximum asymptote value is probably independent of the diameter and it is anticipated that for larger scales the optimal initial slick thickness can decrease to a minimum of 1-2 mm. As such, the effect of the initial slick thickness on the burning efficiency would decrease as a function of the pool diameter. The pool diameter might thus have a more dominating influence on the burning efficiency, considering that the highest burning efficiencies of  $\geq 90\%$  have only been obtained for large scale experiments. Therefore, from an operational point of view, it may be sufficient to focus on the initial slick thickness only in terms of ignitability rather than as a means to increase the burning efficiency.

### **4.4 Crude oil herding in ice-infested water**

The results presented in this section were obtained with the small and intermediate scale crude oil herding setups and the methodology described in Section 3.2.

#### **4.4.1 Slick thickness**

The average slick thicknesses after 30 minutes of spreading of the oil spill, here referred to as the spread thickness, and subsequently 30 minutes of herding are shown in Fig. 4.18 as a function of the ice coverage. The

data show that the spread oil slicks were in general not ignitable, as the majority of the spread thicknesses in all ice coverages was well below the theoretical ignitability limit of 1-2 mm (Buist et al., 1999). Although two of the intermediate scale experiments showed thicker spread thicknesses (1-2 mm), the causes were not related to the presence of ice. The spread thickness of the 15 L experiment was about 3-4 times larger (1 mm) than the other experiments without ice, which was expected as its oil-to-water surface ratio was 3.4 times larger. The high spread thickness of 2 mm for the experiment with a 2/10 ice coverage was caused by strong wind gusts from a single direction that pushed the oil and ice to the opposite side of the basin. As a result, the oil and ice were contained in a small area of the basin for most of the 30 min spreading period. The results thus show that none of the tested ice coverages significantly inhibited the spreading of the oil, which corresponds with previous work (SL Ross and DF Dickins, 1987; Brandvik et al., 2006), and thickening of the oil prior to *in-situ* burning was indeed required.

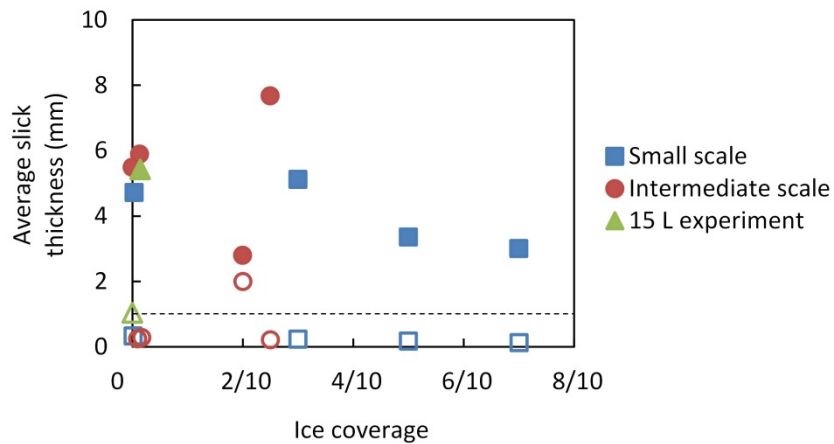


**Figure 4.18.** Average slick thickness after 30 minutes of spreading (open symbols) and 30 minutes of herding (closed symbols) as a function of the ice coverage. Data points of experiments with no ice coverage (0 on the x-axis) are jittered for clarity reasons. The dashed line indicates the theoretical minimal thickness required for ignition (1 mm).

In all experiments, applying herder to the water surface increased the oil slick thickness to a thickness of 3-8 mm (Fig. 4.18). The herded slick thicknesses were all theoretically ignitable, independent of the ice coverage, and were thus sufficiently thickened to apply *in-situ* burning. These results match well with earlier results on herded oil thicknesses in ice-infested water (SL Ross, 2007).

Increasing the ice coverage resulted in a maximum herded slick thickness around an ice coverage of 3/10, after which the herded slick thickness decreased for higher ice coverages. The low herded slick thickness of the 2/10 ice coverage experiment compared to the other intermediate scale experiments was attributed to the slick already being pre-herded by the wind into a small area. As a consequence, most of the oil was effectively shielded from the thickening effect of the herder by a barrier of ice and pre-thickened oil. The maximum herded slick thickness for a 3/10 ice coverage was also observed in previous experiments on herding oil in ice-covered water (Buist et al., 2011). This correlation suggests that the ice has two competing effects on the herding process. A possible explanation is that a 3/10 ice coverage provides additional boundaries against which the oil can be herded, while the ice concentration is not yet so high that it physically obstructs the herder. For the purposes of this study, however, the thickness reducing effect of high ice coverages (5/10-7/10) was not considered relevant because all herded thickness were theoretically ignitable. Overall, the slick thickness results corresponded well with results from literature (SL Ross, 2007; Buist et al., 2011), both in absolute values and as a function of the ice coverage. The experiments provided therefore suitable circumstances to study how the theoretical ignitable thickness would translate to the actual ignitability of these herded slicks in ice-infested water.

#### **4.4.2 Herded oil slick distribution**

Although the final herded slick thickness was not significantly affected by the presence of ice, the ice had a clear influence on the herding process. An impression of the oil-ice-herder interactions during the herding process is given in Fig. 4.19 and Fig. 4.20 for the small and intermediate scale experiments, respectively. The herder spread considerably slower over the water surface in experiments with a high ice coverage. Ice blocks physically blocked the herder and this caused the herder front to spread asymmetrically over the water surface. Any oil that was hindered in its movement as it was stuck on, between or adjacent to ice fragments was unable to follow the herder front and became separated from the rest of the oil. Once a fraction of the oil slick was fully surrounded by herder, it would not easily merge with other oil fragments and alternatively form a new slick or droplet. This interaction between the asymmetrically advancing herder front and slowed or trapped oil caused the oil to fracture into tens to hundreds of such separate oil slicks and droplets.

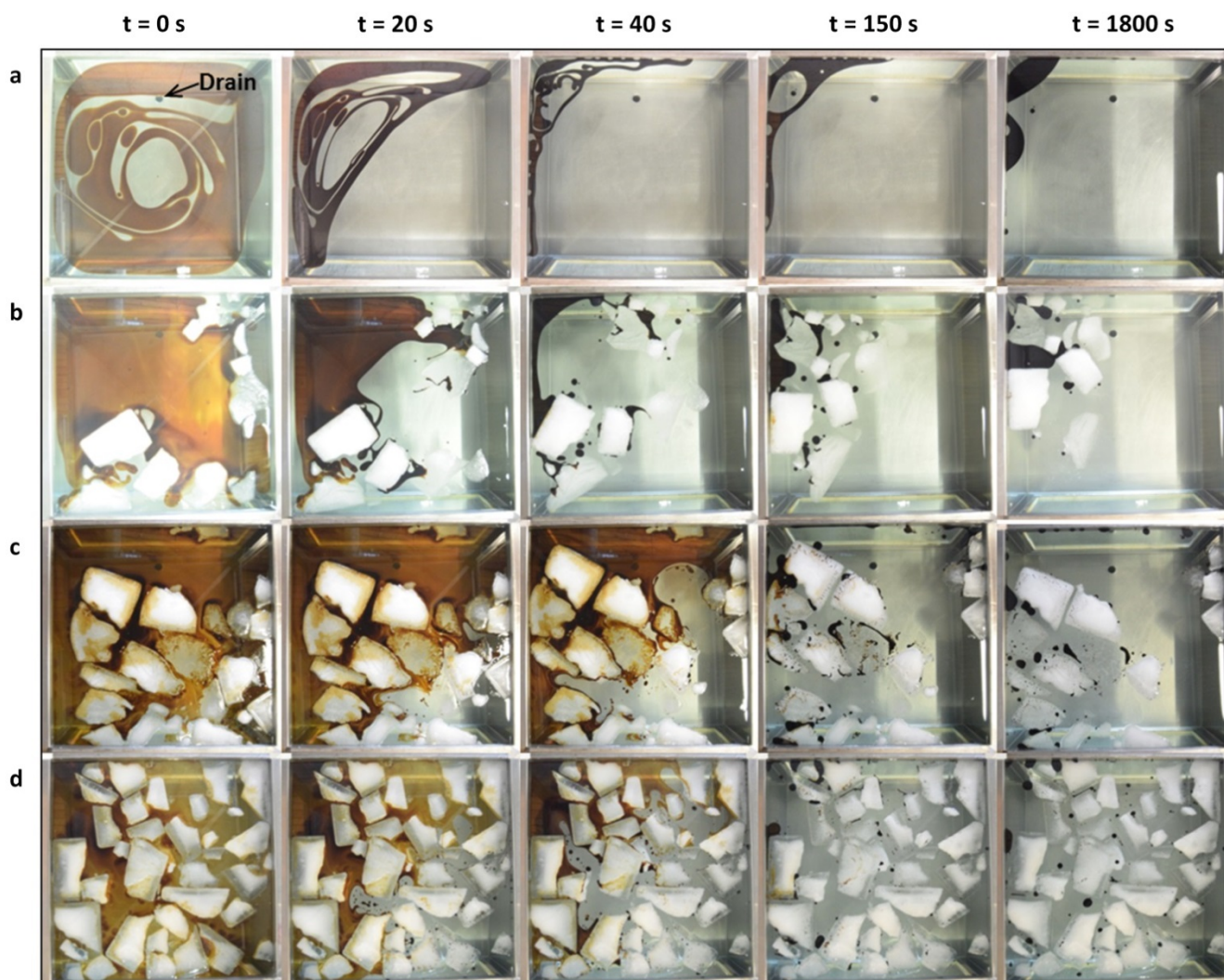


**Figure 4.19.** Snapshots of the herding process of crude oil in a small scale experiment without ice (a) and an ice coverage of 3/10 (b), 5/10 (c) and 7/10 (d). The first picture in each row shows the oil slick right before the herder was applied. The herder front can be observed from the border between the retracting oil surface and the water surface.

In the small scale experiments without ice, the spreading of the crude oil showed a non-uniform distribution over the water surface, which was not observed in experiments with ice (compare e.g. Fig. 4.19a and Fig. 4.19b at  $t = 0$  s). It was speculated that this non-uniform distribution was caused by herder residues on the COFA, despite the measured surface tensions of the water being in the expected range (68-71 mN/m). If the herder would have a preferred affinity for ice over water, the ice could possibly remove such residues and thus facilitate uniform spreading of the oil. Test experiments, however, showed that this theory was incorrect.

Spreading experiments, where ice was added and then removed from the water to remove any hypothetical herder residues prior to applying the oil, showed similar non-uniform oil distributions. It was noticed during these experiments that the water body had a circular motion after filling the basin, which could have caused the circular pattern in the spreading distribution. Ice experiments took longer to prepare, which would reduce this motion, and the ice could also have additional dampening effect on such motions, and therefore allowing the oil to spread uniformly. Because the spreading pattern of crude oil in experiments without ice did not seem to influence the final spread thickness or the herding process, this phenomenon was not investigated further.

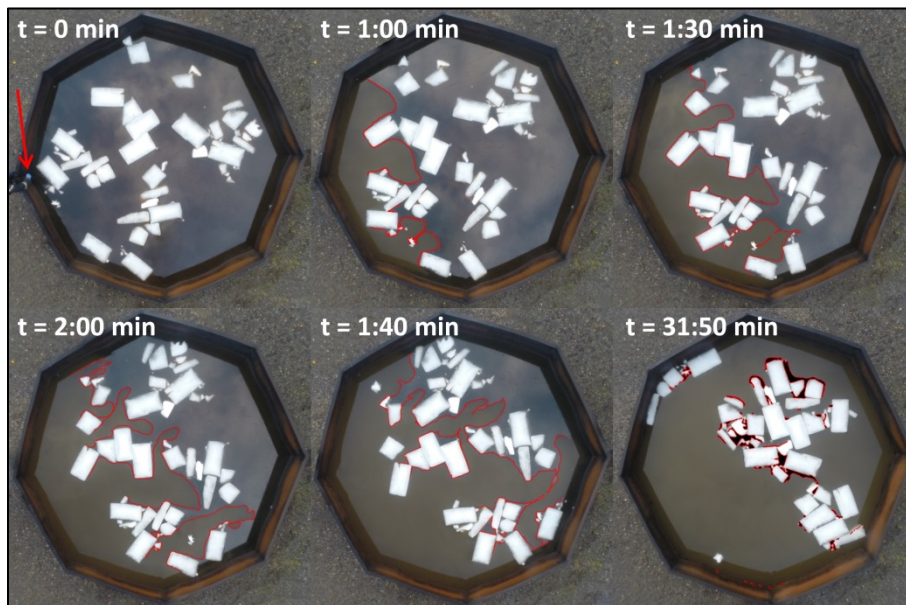


**Figure 4.20.** Snapshots of the herding process of crude oil in an intermediate scale experiment with a 2.5/10 ice coverage. The red arrow indicates the location where the herder was applied. The herder front can be observed from the border (marked in red) between the retracting oil surface and the water surface.

The surface distribution of the herded oil slicks after 30 min of herding is shown in Fig. 4.21. Because the surface distribution of the oil was unique for each experiment, the data sets are shown individually. The total number of oil slicks and droplets and the relative size of the largest oil slick are also summarized in Table 4.4. Each data point in Fig. 4.21 resembles an individual oil slick and the data points are in order of increasing slick size. In this study an individual oil slick or droplet was defined as any amount of oil surrounded completely by

water, ice or the boundaries of the water basin. The relative size of a specific oil slick or droplet can be derived from the difference between its value on the y-axis and the value of the point below it. For example, the second 3/10 ice data set consists of 9 slicks, with the largest slick occupying 37% of the total surface area. Thin oil sheens that had spread on the ice typically formed several hundred oil droplets during the herding process that greatly increased the total number of slicks and droplets, but occupied only a very small area. Including all these droplets in the surface distribution analysis would misrepresent the extent of the fracturing of the oil slick in terms of *in-situ* burning purposes. Therefore, the smallest oil droplets accounting for a cumulative 5% of the total area were omitted from Fig. 4.21 and Table 4.4.

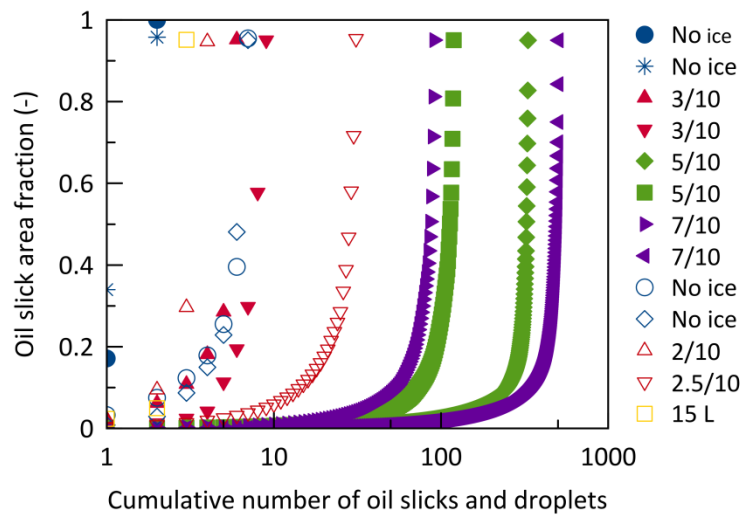


**Figure 4.21.** Surface distribution of the herded oil slicks after 30 min of herding in small scale experiments (closed symbols) and intermediate scale experiments (open symbols).

The oil slick distribution data show a clear increase in the extent of the fracturing of the herded oil slick as a function of the ice coverage (Fig. 4.21). A higher ice coverage increased the number of oil slicks and droplets and reduced the (relative) size of the largest oil slick post-herding in both experimental scales. While the precise distribution and size of the oil slicks could not simply be derived from the ice coverage alone, it was clear from the results that the ice prevented the oil from being herded into a single slick. These results correspond with previous herding experiments of crude oil in ice-infested water (SL Ross, 2007).

**Table 4.4.** Summary of herded oil slick distribution

<i>Scale</i>	<i>Ice coverage</i>	<i>Slicks (#)</i>	<i>Largest slick (oil area %)</i>
Small	No ice	2	83
Small	No ice	2	96
Small	3/10	6	67
Small	3/10	9	37
Small	5/10	331	12
Small	5/10	119	14
Small	7/10	91	14
Small	7/10	506	11
Intermediate	No ice	7	56
Intermediate	No ice	7	47
Intermediate	2.5/10	31	24
Intermediate	2/10	4 <sup>a</sup>	65
15 L experiment	No ice	3	90

<sup>a</sup> Increased coherency due to wind, see also Section 4.4.1.

Fracturing of the oil slick has also been observed in a large scale experiment featuring the herding of 630 L of crude oil on open sea, which resulted in three oil slicks prior to ignition (Buist et al., 2010b). This shows that large oil slicks are also susceptible to fracturing, of which the extent would further increase in the presence of ice. Oil slicks were larger in size and more fractured in the intermediate scale than in the small scale experiments for similar ice coverages. The results also show that the more the oil comes into contact with ice, the higher the extent of the fracturing of the oil becomes. Extrapolating these results to operational scales suggests that herding a large oil slick in ice-infested water would result in a large amount of big oil slicks scattered all over the area occupied by the ice (such as in Fig. 4.19). The implications of such a large, fractured oil slick are discussed in the next section.

#### 4.4.3 Ignition of herded oil

Ignition of the herded oil was attempted on several slicks per experiment and resulted in the successful ignition of and flame spread on at least one slick in each experiment. This confirms that all average herded slick thicknesses (Fig. 4.18) were thick enough for *in-situ* burning and shows that the herder is capable of facilitating this response method in ice-infested waters. Fracturing of oil slicks, as described above, however, considerably complicated and inhibited the ignition procedure. The slick thickness alone was thus not a sufficient measurement to determine the full extent of the ignitability of the herded oil.

Monitoring which oil slicks had been burned and which remained unburned was challenging because slicks were in motion during the burning and occasionally burning slicks would merge with other slicks. Igniting slicks separately was also more labor intensive and combined with the large area that could be occupied by large herded slicks, fracturing of an oil slick in operational scales could create a dilemma. Either the logistics become more complex when trying to ignite all oil slicks, whereas simple logistics is normally a selling point for *in-situ* burning (Buist et al., 1999), or some (small) slicks are neglected but this reduces the burning efficiency. This dilemma would in particular be present when herding oil in ice-infested waters and thorough preparations should be in place for *in-situ* burning operations to be effective in such scenarios.

Successful ignition of an oil slick mainly depended on the size of an oil slick and its immediate surroundings. For the small scale experiments, all slicks with a diameter  $\geq 5$  cm could be ignited. Smaller slicks probably lost too much heat to the surrounding water to sustain a fire. Ignition was much harder for the intermediate scale experiments, partially due to the influence of the wind. Typically, oil slicks that were not adjacent to either ice blocks or the boundaries of the basin could not be ignited for the experiments with 200 g oil/m<sup>2</sup> of water. Ignition attempts with a weed burner and ignition gel (5-10 ml) failed to ignite free-floating slicks with areas of  $\leq 0.45$  m<sup>2</sup> and  $\leq 0.20$  m<sup>2</sup>, respectively. The small ignition sources were not strong enough to overcome the blowout effects of the wind. Adding larger amounts of ignition gel (up to 50 ml) did not aid the ignition of these free-floating slicks as the ignited gel displaced the oil slick rather than spreading on top of the oil to spread the flames. Observations during the experiments gave the impression that the oil slicks were too small to maintain their coherency under the spreading pressure of such higher amounts of ignition gel. This theory was successfully tested during the experiment with 15 L of oil in which a free-floating slick of 1.9 m<sup>2</sup> was burned, starting from an ignition gel ( $\pm 50$  ml) fire of 0.2 m<sup>2</sup>.

Herded slicks adjacent to ice blocks or basin boundaries were more shielded from the wind and not as easily displaced and were therefore easier to ignite. Contrary to free-floating slicks, such confined slicks could be ignited with just the weed burner or small amounts of gel (5-10 ml), although ignition was not always successful either. Larger amounts of ignition gel were also tested for confined slicks that otherwise failed to ignite, but because of their small slick size ( $< 0.25 \text{ m}^2$ ) the ignition gel would only displace the slicks and not spread the flames on the oil. This shows again that small slicks, their small size a consequence of the fracturing of the oil slick, were very difficult or failed to ignite. As a consequence, the success rate of the ignition attempts for the intermediate scale experiments was low ( $< 50\%$ ) and only in the 15 L experiment 96% of the oil was set on fire, compared to 11-57% for the other experiments. Because any unburned oil is treated as residue during cleanup after *in-situ* burning, failure to ignite a fraction of the oil reduces the burning efficiency. Fracturing of a herded oil slick can therefore reduce the burning efficiency by forming (small) oil slicks that are no longer ignitable due to their reduced size.

The ice blocks used in the experiments are representative for the smaller pieces of brash ice and pancake ice that can be observed on sea in ice conditions such as open ice and around larger ice floes (WMO, 2014). Formation of small, non-ignitable slicks in these types of ice-infested water for operational scales should therefore be considered as a possibility. The herded oil slick distribution in the intermediate scale experiments (Fig. 4.21) showed that the formation of very small droplets ( $< 5 \text{ cm}$  in diameter) is negligible in scales larger than the small scale experiments. On sea, smaller pieces of brash ice are thus more probable to form slicks with an area of about  $0.1\text{-}0.5 \text{ m}^2$  that contain a notable amount of oil but are still difficult to ignite, similar to the intermediate scale results.

#### **4.4.4 Burning efficiency**

The burning efficiency of the herded oil slicks is shown in Fig. 4.22 as a function of the ice coverage. Correlating the burning efficiency to the herded slick thickness showed that the burning efficiency was independent of the thickness of the burned slicks. The herded slick thickness (Fig. 4.18) was therefore only relevant for the ignitability of the oil, which corresponds to the results of the burning efficiency as a function of the initial slick thickness (Section 4.3.3). All trends observed in the burning efficiency data could be explained by the scale of the experiment, the presence of ice and the surface distribution of the oil, as discussed below.

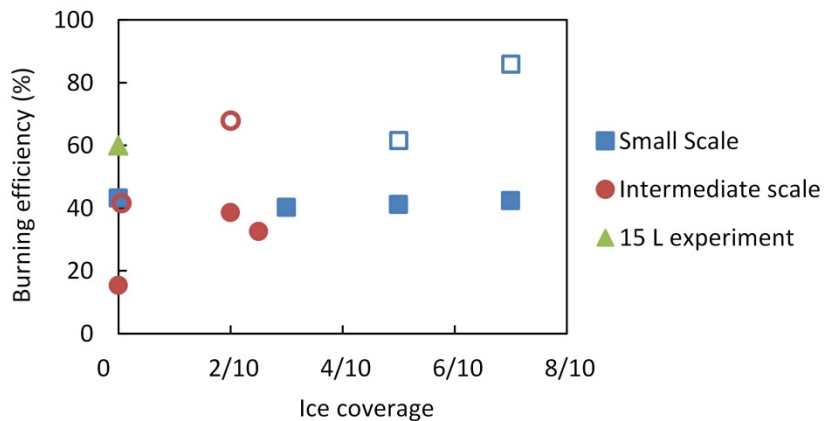


**Figure 4.22.** Burning efficiency of herded oil slicks as a function of the ice coverage. Closed symbols show the absolute burning efficiency, which is based on the initial oil weight and the total weight of the residue (burned and unburned). Open symbols show the effective burning efficiency, which is the absolute burning efficiency relative to the oil area fraction that was set on fire (i.e. burned residue).

For the small scale experiments, the obtained burning efficiencies were independent of the ice coverage. However, due to the fracturing of the oil, 31-56% of the total oil surface area could not be ignited during the experiments with a 5/10 and 7/10 ice coverage. By dividing the burning efficiency with the area fraction of the oil that was set on fire, the burning efficiency of only the burned oil fraction was obtained, i.e. the effective burning efficiency. The effective burning efficiency should be used as an estimate of the potential burning efficiency if all oil could have been ignited and set on fire, rather than as an exact result. For example, the effective burning efficiency was very high for the 7/10 ice coverage experiments (86%) and based on the amount of residue observed in these experiments was likely overestimated. It does, however, give a clear indication that the burning efficiency would increase with increasing ice coverage in the small scale experiments if ignition of small oil slicks would not be an issue.

For the intermediate scale experiments the burning efficiencies were relatively low (15-39%, see Fig. 4.22), which was mainly caused by ignition issues. Hardly any oil slicks could be ignited in the experiments without ice and only 11-37% of the oil area was set on fire, resulting even in a negligible burning efficiency for the first of these experiments. The higher burning efficiencies for the 2/10 and 2.5/10 ice coverage experiments were achieved because a higher area fraction could be set on fire, although this fraction was still below 60%. In comparison, 96% of the oil was set on fire in the 15 L experiment, resulting in a burning efficiency of 60%.

Similar ignition issues have also been observed to decrease the burning efficiency in a study on the burning of herded oil slicks in cold ( $< 0\text{ }^{\circ}\text{C}$ ) weather conditions (SL Ross, 2007). In such experiments dominated by the ignition process, the effective burning efficiency gives a better estimate of the burning results (Fig. 4.22) and was used for further discussion. No top view photos were made of the ignition and burning of oil in the 2.5/10 ice coverage experiment out of safety concerns and hence the effective burning efficiency could not be calculated for this experiment.

The effective burning efficiency of the intermediate scale experiment without ice was relatively low compared to the small scale experiments, as larger oil slicks typically have higher burning efficiencies (Fig. 4.23). The burning efficiency was probably affected by the outdoor conditions such as wind and a light drizzle. Increasing the ice coverage also resulted in an increasing burning efficiency in the intermediate scale (even compared to the 15 L experiment), which matched the results of the small scale experiments. This increase in burning efficiency with increasing ice coverage could be caused by the ice working as a confinement around the oil, inhibiting the spreading of the oil during the burning. Free-floating herded oil slicks expanded upon ignition so their thickness was reduced faster than herded slicks that could not expand. Heat losses to the water affect expanding slicks sooner, leading to earlier extinction of the flame and could therefore lower burning efficiencies. Thus, when fracturing of herded oil in ice-infested waters does not inhibit ignition, the presence of the ice could in fact aid *in-situ* burning of the oil.

Plotting the burning efficiencies as a function of the oil mass and comparing the data to burning efficiencies of similar experiments from literature shows that the results are within the expected range for the tested scales (Fig. 4.23). Apart from the ignition issues, the *in-situ* burning of the herded oil, in both water with and without ice, performed appropriately relative to the experimental scales. These results show that the tested herder can be an effective tool to facilitate *in-situ* burning in ice-infested waters. The main issue that should be solved to optimize its effectiveness is to ensure ignition of all the oil slicks that result from fracturing of an oil slick during the herding process. This can be achieved either by limiting the fracturing of the oil slick and avoiding the formation of many small and difficult to ignite slicks, or by a strong ignition source that can easily be applied on multiple locations in a large area. Research on an operational scale will be required to determine which of these options is the most realistically achievable.

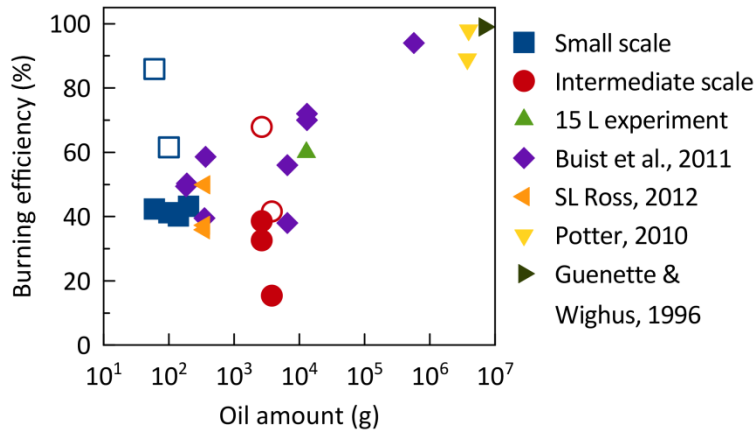


**Figure 4.23.** Burning efficiency as a function of the oil amount. Open symbols show the effective burning efficiency, which is relative to the oil area that was set on fire. Literature data was taken from Buist et al. (2011), SL Ross (2012), Potter (2010b) and Guénette and Wighus (1996).

#### 4.4.5 Sub-conclusion

In small and intermediate scale experiments, spread oil slicks were successfully herded in ice-infested waters from spread thicknesses of 0.1-2 mm to herded thicknesses of 3-7 mm, depending on the ice coverage. These herded slick thicknesses were all theoretically ignitable and indeed at least one oil slick per experiment was successfully ignited. Fracturing of the oil during the herding process, however, complicated the ignition process and many of the smaller slicks and droplets formed were non-ignitable, negatively affecting the burning efficiency. This would cause a dilemma on an operational scale as either more complex logistics are required to ignite all the oil, or some fraction of the oil remains unburned which reduces the burning efficiency.

Of the ignited oil slicks, the effective burning efficiency was within the expected range for the small and intermediate scale experiments (42-86% and 42-68%, respectively). The herder thus successfully facilitated *in-situ* burning of oil in ice-infested water because it herded spread oil to an ignitable thickness and ignited oil resulted in expected burning efficiencies. Ignitability issues of oil slicks, both logistically and the actual ignition, due to fracturing of the oil in ice-infested water should be addressed in order for the herder to become a fully effective tool for the *in-situ* burning of oil.

## 4.5 Ignition

The results presented in this section were obtained with the cone setup (Section 3.3), the COFA setup (Section 3.1) and the crude oil herding setups (Section 3.2), according to the methodologies described in Sections 3.3, 3.1.4 and 3.1.6, and 3.2, respectively.

### 4.5.1 Ignition time

The ignition times of the weathered oils, Grane and IFO 180 are shown in Fig. 4.24 as a function of the incident heat flux. Fresh DUC is not included in Fig. 4.24 because its flashpoint is below the ambient temperature (15-20 °C) and therefore this oil ignited instantly with the spark igniter, independent of the incident heat flux. Of the oils that required an incident heat flux to be ignited by the spark igniter, only Grane could be ignited for a heat flux of 5 kW/m<sup>2</sup>. DUC 40/0, DUC 40/40 and IFO 180 ignited only at an incident heat fluxes  $\geq 10$  kW/m<sup>2</sup>, which indicates that the critical heat flux for these fuels was between 5-10 kW/m<sup>2</sup>. The lowest external heat flux tested for DUC 30/0 was 8 kW/m<sup>2</sup>, for which the time to ignition was similar to the ignition times of DUC 40/0 and DUC 40/40 at an incident heat flux of 10 kW/m<sup>2</sup>. The critical heat flux of DUC 30/0 is therefore expected to be lower than the critical heat flux of DUC 40/0 and DUC 40/40.

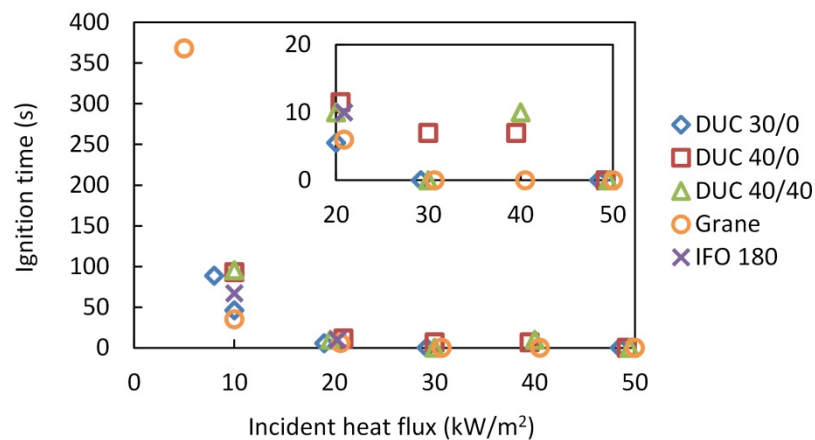


**Figure 4.24.** Ignition time as a function of the incident heat flux for DUC (weathered), Grane and IFO 180. The data points are jittered for incident heat fluxes  $\geq 20$  kW/m<sup>2</sup> for clarity purposes.

Temperature measurements at the fuel surface and at the bottom of the sample holder showed a clear temperature gradient in all the oil slicks, which confirms that the tested oils were thermally thick. This is also in agreement with temperature measurements of oil burning on water in the COFA setup (Fig. 4.10) and literature data from Wu et al. (2000). The ignition time results from Fig. 4.24 could therefore be plotted in the form of  $1/\sqrt{t_{ig}}$  as a function of the incident heat flux (Fig. 4.25), based on Eq. (1) (repeated here for convenience purposes, see also Section 2.1.1). The results for the critical heat flux derived from Fig. 4.25, the surface temperature upon ignition and the thermal inertia of the tested oils calculated with Eq. (1) are summarized in Table 4.5.

$$t_{ig} = \frac{\pi}{4} \cdot k\rho c_p \cdot \left( \frac{T_{ig} - T_{\infty}}{a \cdot \dot{q}_{inc}} \right)^2 \quad (1)$$

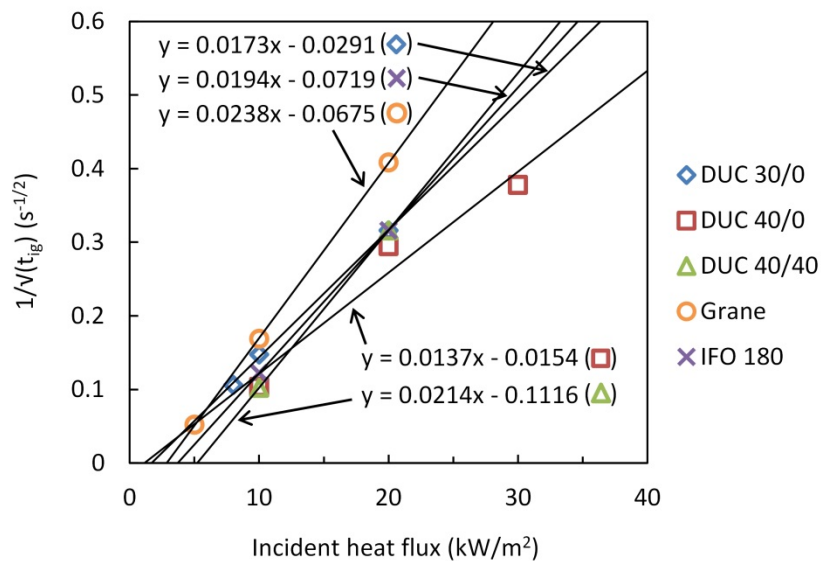


**Figure 4.25.** Ignition time as a function of the incident heat flux for DUC (weathered), Grane and IFO 180. The intercept of each trendline with the x-axis gives the critical heat flux of its respective oil.

**Table 4.5.** Thermal properties of the tested fresh and weathered oils

<i>Oil</i>	<i>Critical heat flux (kW/m<sup>2</sup>)</i>	<i>Temperature of ignition (°C)</i>	<i>Thermal inertia (Ws<sup>1/2</sup>/(m<sup>2</sup>K))<sup>a</sup></i>
DUC	< 0	< 18	-
DUC 30/0	1.7	113	8.2 · 10 <sup>2</sup>
DUC 40/0	1.1	110	1.1 · 10 <sup>3</sup>
DUC 40/40	5.2	127	8.3 · 10 <sup>2</sup>
Grane	2.8	125	7.2 · 10 <sup>2</sup>
IFO 180	3.7	145	6.4 · 10 <sup>2</sup>

<sup>a</sup> An ambient temperature of 18 °C was assumed.

The results for the calculated critical heat flux in Table 4.5 show a significant deviation from the experimentally observed critical heat flux (Fig. 4.25). Both DUC 40/0 and IFO 180 were not ignitable for an incident heat flux of 5 kW/m<sup>2</sup>, so critical heat fluxes of 1.1 and 3.7 kW/m<sup>2</sup>, respectively, cannot be correct. Similarly, the critical heat fluxes of DUC 30/0 and DUC 40/40 are most likely too low based on the time to ignition at incident heat fluxes of 8 kW/m<sup>2</sup> and 10 kW/m<sup>2</sup>, respectively. Only for Grane, the calculated critical heat flux shows a plausible value as it corresponds with Grane being ignitable at an incident heat flux of 5 kW/m<sup>2</sup>.

The deviations of the calculated critical heat flux results from the experimental results were possibly caused by preheating of the oil sample below the shutters of the cone. The thermocouples had to be positioned while the sample was in place under the hot cone. Although the shutters prevented the oil from being heated directly, the temperature of the oil samples still increased as a function of time and the temperature of the cone. For example, for Grane, the surface temperature varied from 30 °C to 130 °C for incident heat fluxes of 5 kW/m<sup>2</sup> and 30 kW/m<sup>2</sup>, respectively, right before the shutters were opened and the experiment was started. At incident heat fluxes ≥ 30 kW/m<sup>2</sup>, all crude oils ignited nearly instantly upon opening the shutters above the sample and turning on the spark igniter. Such instant ignitions are clearly an artifact of samples preheated above their flashpoint and do not reflect actual ignition times. While longer ignition times at high heat fluxes may not necessarily lead to an increase of the calculated critical heat flux, the results undoubtedly indicate that the experimental procedure should be refined.

In theory, the flashpoint (Table 3.1) could be used as the ignition temperature in Eq. (1). These flashpoints were obtained in a small, closed environment, however, where the combustible gases could build up in concentration and thus show a lower flashpoint than in open environments. In addition, due to the multicomponent character of crude oils, the oils practically weather when subjected to an incident heat flux and thus lose a fraction of the volatile components prior to ignition. Once the oil then ignites, the surface temperature at ignition will be higher than the flashpoint measured in a closed cup. For example, IFO 180 has a measured flashpoint of 90 °C, whereas the oil could not be ignited while it had a surface temperature of 110-120 °C at an incident heat flux of 5 kW/m<sup>2</sup>. The measured surface temperature at ignition was therefore used to calculate the thermal inertia for the tested oils (Table 4.5).

The results for the time to ignition (Fig. 4.24) and estimated thermal inertias (Table 4.5) of the tested oils matched reasonably well with the data from Wu et al. (2000). The results were within the same order of magnitude but lower ignition times and thermal inertia were systematically found in this study, which, based on the above discussion, was expected. The experimentally obtained limits for the critical heat flux for the 30-40 wt% evaporated oils (5-10 kW/m<sup>2</sup>) were well in line with the critical heat fluxes found for 20-25 wt% evaporated crude oils (4-6 kW/m<sup>2</sup>). These comparisons show that, although the observed ignition times were too low, these initial results can still be used to assess the relative ignition requirements among the tested oils.

The ignition times in Fig. 4.24 show that the ignition times increased most with increasing evaporative losses. Emulsification did not notably influence the time to ignition at incident heat fluxes of  $\geq 5$  kW/m<sup>2</sup>. When igniting the emulsion without an incident heat flux, however, it took several minutes to ignite compared to several seconds for any of the other oils. Ignition results of evaporated and emulsified oils in large scale field experiments, in contrast, showed that emulsification was the dominant weathering effect that decreased the ignitability of the tested oils (Bech et al., 1993). Large amounts of fresh oil ( $\geq 200$  L) were required to ignite and initiate flame spreading on oils with 18-45 vol% evaporative losses and 10-40 vol% water content. Oils with only evaporated losses, on the other hand, were reported to be easily ignitable.

The difference between the observed results and results reported in literature is probably due to the stability of the tested emulsions. The DUC 40/40 emulsion was very unstable and would start to naturally break up within an hour after shaking of the emulsion was stopped. It is therefore probable that an incident heat flux of only 5 kW/m<sup>2</sup> was already sufficient to break the emulsion prior to ignition, after which it essentially behaves as only the evaporated oil. This would explain why the results for DUC 40/40 and DUC 40/0 are nearly identical

in Fig. 4.24. The hand torch used to ignite the oils in the experiments without an incident heat flux is a much smaller ignition source than the conical heater. Breaking the emulsion would then take a much longer time and increase the time to ignition, as observed during the experiments. More stable emulsions, such as Grane emulsions (Fritt-Rasmussen et al., 2012), that require more heat to be broken prior to ignition are therefore expected to show more significant deviations from evaporated oils. Further testing is needed to be able to obtain a more accurate correlation between the weathering state and the time to ignition as a function of the incident heat flux.

Of the physical properties of the tested oils, only the volatility was relevant to the ignitability of the oils (Table 3.1). The density and viscosity did not show any correlation to the time to ignition and critical heat flux (Table 3.1 and Table 3.4). Because of the volatility controlled vaporization order (Section 4.2), the combustible gases evaporating from a crude oil when heated up for ignition originate mostly from the lightest, most volatile fraction of the oil. The density and viscosity, on the other hand, are mostly determined by the heavy, non-volatile fraction of a crude oil (Section 2.2). For example, the evaporated DUC samples had a lower density and viscosity than fresh Grane because Grane has, among others, a higher asphaltenic content. Grane had nevertheless a lower time to ignition, because it also contained a larger fraction of light components. The physical appearance of a spilled oil can thus not be used to estimate whether the oil will be ignitable.

#### **4.5.2 Heat release rate**

The heat release rates as a function of the burning time at an incident heat flux of  $10 \text{ kW/m}^2$  for each tested oil is shown in Fig. 4.26. The oils that did not feature a boilover during the burning (DUC, DUC 30/0, DUC 40/0 and IFO 180) all showed a declining heat release rate as a function of the burning time. These results correspond well with the proposed volatility controlled vaporization order for crude oils (Section 4.2). Equation (4) shows that the heat release rate depends on the burning rate and the heat of combustion of the fuel, which decrease for hydrocarbons with decreasing volatility (Section 2.2.2), and therefore the heat release rate decreases.

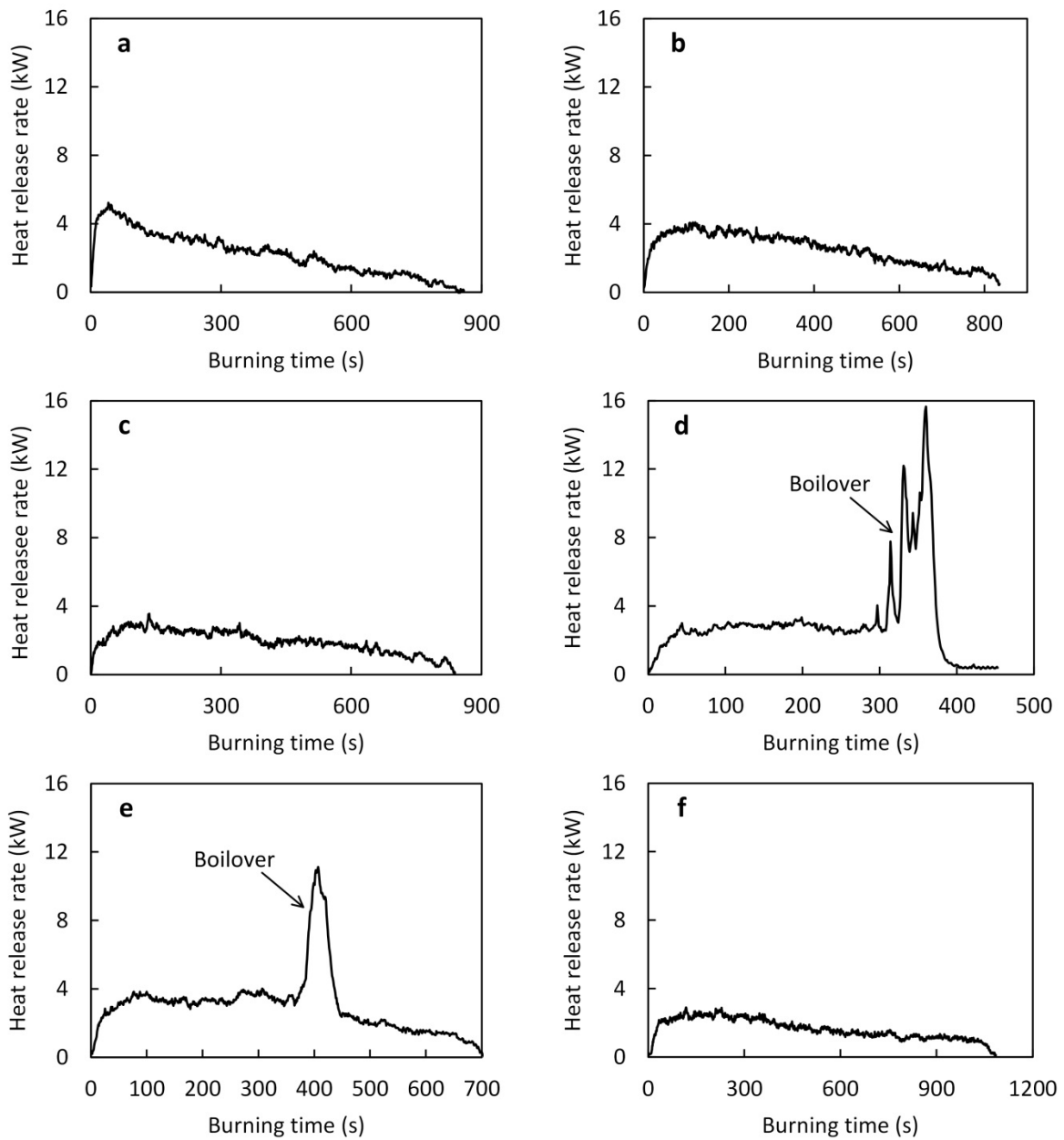


**Figure 4.26.** Heat release rate as a function of the burning time at an incident heat flux of  $10 \text{ kW/m}^2$  of DUC (a), DUC 30/0 (b), DUC 40/0 (c), DUC 40/40 (d), Grane (e) and IFO 180 (f). The presented curves were representative for all tested incident heat fluxes.

For DUC 40/40 and Grane, boilovers occurred in each experiment and dominated the heat release rates. Both the average and peak heat release rates increased significantly due to boilover compared to experiments

without boilover (Fig. 4.26). The near-constant heat release rate prior to boilover for DUC 40/40 and to a lesser degree for Grane suggests that these oils did not burn according to a volatility controlled vaporization order. As mentioned in Section 2.4, weathered oils could follow an onion skin model. Alternatively, the decrease in the heat release rate caused by the volatility controlled vaporization order is evened out by an increasing burning rate as the fire leads up to the boilover. These results are further discussed in Section 4.7.3 in relation to the burning efficiency as a function of the incident heat flux. The low heat release rates for Grane at high incident heat fluxes ( $\geq 30 \text{ kW/m}^2$ ) were caused by a combination of the rapid decrease of the heat release rate after boilover (see Fig. 4.26) and low initial heat release rates. The underlying causes for these asymmetric trends in the Grane data in Fig. 4.27 are the subject of further studies.

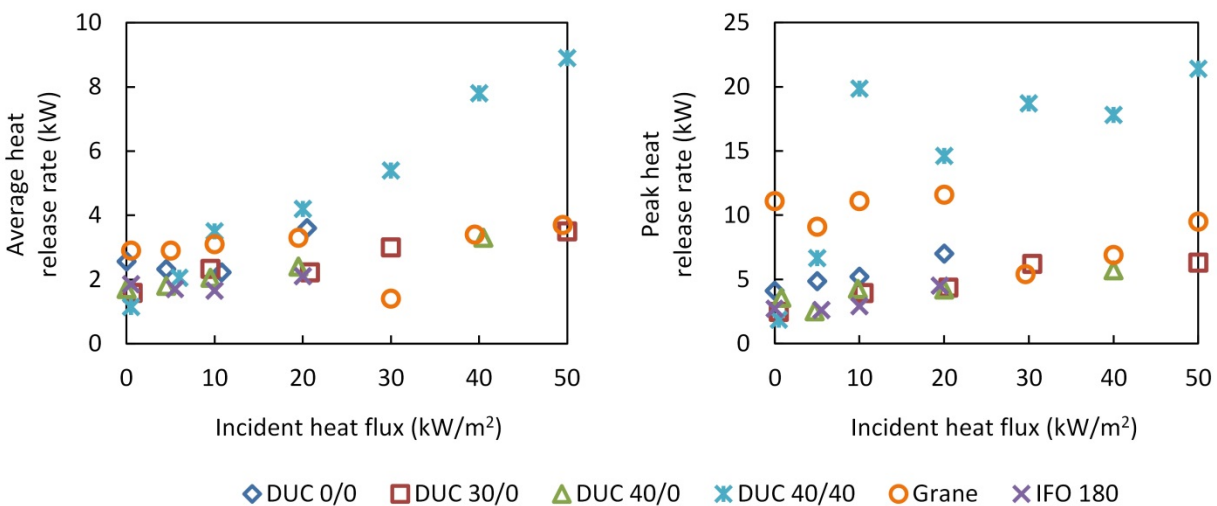


**Figure 4.27.** Average heat release rate and peak heat release rate as a function of the incident heat flux. Data points are jittered on the x-axis for clarity reasons.

The results of the average and peak heat release rate (Fig. 4.27) show that the evaporation of crude oil reduces the energy released during combustion. This confirms that the light, volatile components of crude oil, which are removed during evaporation, have a higher heat release rate than the medium and low volatility components. Similar to the ignition time results (Fig. 4.24), the weathering effect from emulsification (40 vol% water) of the oil only decreased the heat release rate without an incident heat flux. For incident heat fluxes of

$\geq 10 \text{ kW/m}^2$ , emulsification of the crude oil in fact increased the average and peak heat release rate due to the much higher boilover intensity, as indicated by the peak heat release rate. These results further support the theory that the weathering effect from emulsification mainly has an influence during the ignition of a cold oil slick (see also Section 4.2.4). Once an emulsion has been successfully ignited, the burning intensity is similar to or higher than the burning intensity of the fresh oil.

### 4.5.3 *In-situ* burning results

Ignition tests in the COFA setup confirmed that the minimum slick thickness required for ignition of an oil slick on water is approximately 1-2 mm, depending on the volatility of the oil. For *n*-octane and dodecane, two pure oils, the lowest ignitable slick thicknesses were < 1 mm and 2-3 mm, respectively. For REBCO and Grane, a light and heavy crude oil, the lowest ignitable slick thicknesses were 0.8-1.0 mm and 1.75-2.0 mm (Brogaard et al., 2014), respectively. These oils were ignited with a hand torch under ideal circumstances, with no wind or waves present, at room temperature and the oil slick was confined in a relatively small Pyrex glass cylinder. The oils with low volatilities (dodecane and Grane) could be heated up by concentrating the heat from the torch on one location of the oil slick, without the oil slick expanding or floating away. Only when the volatility of the oil was very low, the initial slick thickness had to be increased to be able to ignite the oil (e.g. > 10 mm for hexadecane). Since heat losses to the water layer were the only inhibiting factor for ignition, the ignitability of the oil was only depending on the initial slick thickness.

Under more challenging circumstances, e.g. wind and colder temperatures, the slick thickness is no longer the only controlling factor for successful ignition of an oil slick on water. While the slick thickness still needs to be above 1-2 mm for the oil to be ignitable, meeting this requirement does not guarantee successful ignition as it does in controlled laboratory experiments. The ignition results of herded crude oil slicks (Section 4.4.3) clearly showed that igniting of crude oil slicks was much more challenging in typical outdoor conditions. Considering that a fresh crude oil was used, wind speeds were low, there were no waves and outdoor temperatures were between 0-10 °C, the observed ignition challenges represent only a best case scenario for oil spills on sea. In addition, small oil slicks (< 0.5 m<sup>2</sup>) were often not ignitable, even when a strong ignition source (ignition gel) was used, because these slicks were dispersed rather than ignited by the ignition gel. As such, these results give a clear example of the ignition challenges in outdoor conditions, but combining these results with the ignition results in Section 4.5.1 is difficult because any quantitative information is lacking. Considering that the

environmental conditions play a substantial role in the ignitability of an oil slick on water, incorporating conditions such as wind in future ignition studies would greatly increase their relevance.

#### **4.5.4 Sub-conclusion**

The ignition results of fresh and weathered oils subjected to an incident heat flux suggested that evaporative weathering was the most determining parameter that reduced the ignitability of crude oils. Emulsification of evaporated crude oil only affected the ignition time when the oil was not subjected to an external heat flux. This result, however, was only obtained for an unstable emulsion and may change when more stable emulsions have been tested. Further testing is required to establish more accurate correlations between the weathering state of the oil and ignition requirements such as the critical heat flux and the thermal inertia.

In order to overcome the ignition limitations caused by weathering of an oil, a strong ignition source would be required that can subject the oil slick to an estimated heat flux of 5-10 kW/m<sup>2</sup>. These results are in line with the large ignition sources ( $\geq 200$  L of fresh oil) that were required to ignite weathered oil slicks in intermediate scale field experiments reported in literature. *In-situ* burning experiments also showed that the ignitability of oils on water is reduced by fracturing of an oil slick into multiple small oil slicks in combination with environmental conditions such as wind. Quantitative measures of the environmental effects and the slick size on the ignition requirements, however, could not be established from such *in-situ* burning experiments. Implementation of these factors into future ignition experiments would therefore make any quantitative results more representative of the ignition requirements for *in-situ* burning of oil under realistic conditions.

## **4.6 Boilover**

The results presented in this section were obtained with the COFA setup (Section 3.1), the burning rate setup (Section 3.1.1), the modified COFA setup (Section 3.5) and the cone setup (3.3), according to the methodologies described in Sections 3.1.4 and 3.1.6, 3.5, and 3.3, respectively.

#### 4.6.1 COFA setup and burning rate setup

All of the crude oils tested in the COFA (DUC, REBCO and Grane) and IFO 180 resulted in boilovers during *in-situ* burning in the COFA setup (Fig. 3.1) and in the burning rate setup. During boilover, the burning changed from a regular laminar-turbulent flame to an explosive burning state with a large increase of the burning rate (Fig. 4.12) and flame height (Fig. 4.17) as a consequence (Fig. 4.28). Explosions at the oil surface ejected oil droplets into the flames and outside of the Pyrex glass cylinder, up to a meter from the oil pool, and caused residue to spill over the cylinder edge. After the boilover, the residue was spread over a large portion of the water surface and the residue outside the Pyrex glass cylinder could contain over 50 wt% of the total residue mass.



**Figure 4.28.** Regular burning of REBCO (left) followed by a boilover (middle) and the resulting spreading of the residue, after flame extinction (right). The frames are 77 cm wide and 91 cm high.

As discussed in Section 1.5.5, the boilover phenomenon is attributed to the explosive boiling of the water layer below the burning oil due to superheating of the water (Arai et al., 1990; Garo et al., 1994). In order to reach a superheated water layer of 120-150 °C, it is essential that the fuel has a boiling point considerably higher than that of the underlying water, i.e. considerably higher than 120 °C. Experiments with *n*-octane, dodecane and gasoline, which have relatively low boiling points (Table 3.1), confirmed this theory. No boilover was observed

for experiments with *n*-octane and explosions at the oil surface only occurred in very limited form for some of the experiments with dodecane. These results for dodecane indicate that its boiling point of approximately 225 °C lies at the borderline between occurrence and no occurrence of boilover. Experiments with hexadecane, the alkane mixture and diesel, that have higher boiling points than dodecane, indeed showed boilovers, although the boilover duration was only very brief compared to the crude oils.

The borderline between boilover and no-boilover for dodecane experiments was also confirmed by the oil-water interface temperatures, which reached between 100-120 °C. For comparison, experiments with REBCO that ended in a boilover reached oil-water interface temperatures of 120-150 °C, while for experiments with *n*-octane featuring no boilover the interface temperature did not exceed 100 °C (Fig. 4.29). These results correspond well with previous studies on the boilover phenomenon (Garo et al., 1994; Garo et al., 1999a).

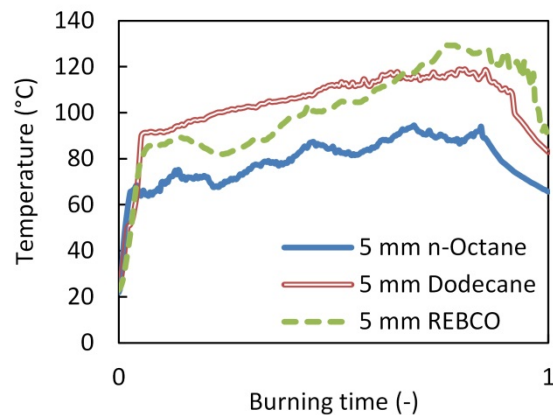


**Figure 4.29.** The oil-water interface temperature over the burning progression for *n*-octane, dodecane and REBCO at an initial slick thickness of 5 mm.

The two data points in Fig. 4.11 for 20 mm Grane and 40 mm REBCO represent the experiments with and without boilover. A possible explanation for the failure to boilover is that the oil slick is too thick or becomes too dense during the burning to conduct the amount of heat from the burning surface required for superheating the underlying water layer. The burning residue was furthermore much more viscous (and dense) than the initial crude oil, due to the volatility controlled vaporization order, which could further amplify the insulating effect of the oil slick. Thus, with the viscosity of the slick increasing during the burning and the

insulating effect increasing with thicker initial slicks, a certain initial slick thickness might result in a sufficiently insulating slick to prevent the water from superheating. It seems that this 'boundary thickness' is around 20 mm for Grane and 40 mm for REBCO, considering that only half of these experiments went into boilover and no boilover occurred for 40 mm Grane. The difference in boundary thickness is most likely caused by the properties of the oil (Table 3.1), e.g. Grane is much more viscous than REBCO.

For the 10 mm experiments with REBCO and Grane, the boilover was extremely violent and had a significant effect on the burning efficiency and regression rate. These violent boilovers resulted in more scattered data upon repetition, but the individual data points were still matching the presented trends in Fig. 4.11 and Fig. 4.15. A possible explanation for the extremity of the boilover is that an initial slick thickness of 10 mm is sufficiently thick to superheat the water but is not yet functioning as an insulating layer. For initial slicks of 2-5 mm the water layer might already penetrate the oil layer just after it reaches a temperature of 120 °C, instead of heating up to 150 °C, leading to less violent boilovers. For slicks thicker than 10 mm, the insulating effect of the oil (as described above) might hinder the superheating and penetration of the water.

#### **4.6.2 Modified COFA setup**

Experiments in the modified COFA setup (Fig. 3.7) featured circulation of the water below the oil, which allowed for testing the boilover tendency of oils on moving water, such as on open sea. Initial testing of DUC crude oil with an initial slick thickness of 5 mm showed no signs of boilover and the fire simply extinguished when the flames were too small to sustain the fire. DUC experiments in the COFA with an initial thickness of 5 mm, on the other hand, showed clear boilovers that lasted for 15-30 seconds before extinguishing the fire. These results clearly show that a current in the water prevents boilovers of crude oil burning on water. Because the current did not notably affect the surface of the oil, the current was deemed representative of the current on sea. The results thus provide an initial confirmation of the theory that boilovers do not occur for *in-situ* burning of crude oil on sea due to the sea current (Buist et al., 2013).

Compared to the experiments in the COFA, the burning time increased from 5-6 to 8 minutes and the burning efficiency increased from 40% to 50% for experiments with a water current. These results show that boilovers can also have a negative effect on the burning of crude oil by prematurely ending the burning. This decrease in burning efficiency is contrary to the results presented for thick slicks of REBCO (Fig. 4.15) and indicates that the

influence of boilovers on the burning of crude oils is unpredictable. Since boilovers are unlikely to occur on sea and the effect of boilovers on the burning efficiency is difficult to control, laboratory experiments should thus aim to prevent boilovers to better represent full scale operations.

#### **4.6.3 Cone setup**

The experiments conducted in the cone setup did not contain a water layer below the oil and thus the boilovers observed for DUC 40/40 and Grane were directly related to the properties of the oils. For DUC 40/40, the boilover occurrence was expected because of the water present in the fuel. By applying heat to the emulsion in order to ignite it, the emulsion will break (Section 2.3.2). Because the water had a higher density than the emulsion, it formed a sub-layer below the fuel which could then superheat. The Boilovers for the emulsion were extremely violent (Fig. 4.30) compared to the boilovers for fresh oils in the COFA, with often multiple instances of boilover, which can be seen from the multiple peaks in Fig. 4.26d. After the fire extinguished, sometimes additional explosions released a white smoke plume, most likely consisting of combustible gases (as the plume could ignite) and water vapor. This relatively violent boilover behavior of DUC 40/40 was probably the effect of the water being distributed throughout the fuel, creating multiple layers of water (droplets) that could superheat one after the other.

The boilover occurrence for Grane, which was observed in each experiment with Grane, was not expected because fresh Grane does not contain a significant amount of water. The boilovers could therefore not be caused by the superheating of a water sub-layer. These boilovers without a water layer provide strong evidence that boilovers are similar to the microexplosions observed during the combustion of multicomponent droplets results (Law, 1978; Wang et al., 1984; Ikegami et al., 2003). During the combustion of multicomponent droplets with a volatile and non-volatile component, the volatile component burned more rapidly at the surface than the non-volatile component. This resulted in the depletion of the volatile component at the surface of the droplet, so that the volatile component became concentrated in the core of the droplet. The temperature of the burning droplet then became dominated by the high boiling point of the more abundant non-volatile component at the droplet surface. This finally caused the volatile component trapped in the droplet core to superheat, which lead to the microexplosion of the droplet (Wang et al., 1984). The boilover phenomenon of Grane would thus be caused by (relatively) light components trapped inside the viscous oil slick, which superheat and then lead to a multitude of microexplosions.



**Figure 4.30.** Regular burning (left), boilover (middle) and vapor explosion after the fire extinguished (right) of emulsified DUC (40/40) in the cone setup with an incident heat flux of  $50 \text{ kW/m}^2$ .

For microexplosions to occur in multicomponent droplet combustion there has to be a large difference in the boiling points of the components and the vaporization order has to be volatility controlled. Both of these conditions are met by fresh Grane, which has a high asphaltenic content and a substantial amount of light components, as seen from its relatively low flashpoint (Table 3.1). In addition, Grane is a viscous crude oil, which increases the plausibility that unburned, light components can become trapped inside the burning slick. Fresh DUC, in comparison, has a lower concentration of heavy components and a lower viscosity, so light components are not as easily trapped and superheated. IFO 180 is a heavier oil than Grane, but lacks a substantial light fraction that could be superheated. Theoretically, Grane would therefore be the only of the tested fresh oils to result in boilover without a water sub-layer.

Due to its high asphaltenic content, however, Grane has a large affinity for water and there is a possibility that the Grane used in the experiments contained a small fraction of water in the form of a stable water-in-oil emulsion. Temperatures at the bottom of the sample holder at the time of boilover varied between  $135\text{-}270 \text{ }^\circ\text{C}$  and could not be used as an indication of when boilover started or which type of components superheated. These temperatures, however, are much higher than the superheating temperature of water ( $120\text{-}150 \text{ }^\circ\text{C}$ ),

which provides some proof that water did not cause the boilovers observed in Grane experiments. Further testing will be required to confirm that the superheating of water was not the cause for the Grane boilovers.

The boilover results of Grane are relevant because they indicate that boilovers could theoretically happen during *in-situ* burning operations on sea for oils with both a substantial light and heavy fraction. A current in the water sub-layer was shown to prevent the superheating of water, and thereby boilover (Section 4.6.2), which suggested that boilovers would not occur on sea. However, if boilovers can occur independent of interaction with a water sub-layer, then the boilover phenomenon they cannot be excluded for *in-situ* burning of oil on sea. This would mean that boilovers have to be taken into account during the safety planning of any *in-situ* burning operations, which complicates the planning and execution of this oil spill response method. A logical next step will therefore be to study the boilover tendency of Grane in the modified COFA setup, to test whether the boilovers also occur under more representative testing conditions.

#### **4.6.4 Sub-conclusion**

Boilovers were observed for pure, refined and crude oils in the COFA setup and for emulsified crude oil and a heavy crude oil in the cone setup. In the COFA setup, temperature measurements of the oil-water interface suggested that boilovers were caused by the superheating of water (120-150 °C), which required a fuel with a boiling point > 220 °C. For thick initial slick thicknesses of REBCO and Grane (20-40 mm), boilover was not always observed, possibly because the viscosity of the oil became too high during the burning for water vapor to penetrate the oil. Introducing a current in the water that refreshed the water below the oil continuously prevented boilover occurrence, which is in accordance to observations of *in-situ* burning of crude oil on sea.

Boilover occurrence for emulsified DUC in the cone setup was expected because of the water inside the emulsion. The burning of emulsified DUC was extremely violent, with multiple instances of boilover, and explosions even occurred after the fire extinguished. Boilover occurrence of Grane in the cone setup was unexpected, because fresh Grane contains no significant amount of water. The results indicated that the boilover phenomenon is similar to microexplosions observed during the multicomponent droplets combustion. Such microexplosions are caused by a volatile component that is trapped in the droplet core and superheats as the temperature of the droplet increases when less volatile components burn at the fuel surface. The implications of these results are that boilovers could occur during *in-situ* burning operations of crude oil on sea,

because a superheating water sub-layer is then not a requirement for boilover. Further studies are required to determine the conditions under which (crude) oils can lead to boilover, independent of a superheating water sub-layer.

## **4.7 Burning efficiency**

The results presented in this section were obtained with the COFA setup (Section 3.1), the burning rate setup (Section 3.1.1), the ice cavity setups (Section 3.4.2) and the cone setup (3.3), according to the methodologies described in Sections 3.1.4, 3.1.6, 3.4.1, 3.4.2 and 3.3.

### **4.7.1 Oil types in COFA setup**

Figure 4.31 shows the burning efficiency of all the different oil types tested in the COFA setup at initial slick thicknesses of 5 and 10 mm, apart from the alkane mixture (15 mm) and hexadecane (20 mm). The results clearly show that the burning efficiency decreases with a decreasing amount of volatile components and an increasing amount of non-volatile components in the oils. These results were expected based on the heat loss and vaporization order theories discussed in Section 4.2 for the burning efficiency of small scale pool fires on water and provide further evidence for the proposed theories.

The lowest burning efficiencies were obtained for diesel and IFO 180, i.e. refined oils with little light components. The burning of heavy oil fractions was shown to become quickly dominated by heat losses to the underlying water layer, which cause the fire to extinguish prematurely. Compared to light components such as *n*-octane, heavy components have lower burning rates, lower flame heights (Fig. 4.4) and therefore less heat feedback to the fuel surface to accommodate for the heat losses. Although crude oils contain heavier components than diesel and have higher densities, they also contain a more substantial light fraction, as indicated by their lower flashpoints (Table 3.1). Crude oil burning efficiencies were therefore higher because they are an average value of the high burning efficiencies of their light components and the low burning efficiencies of their heavy components.

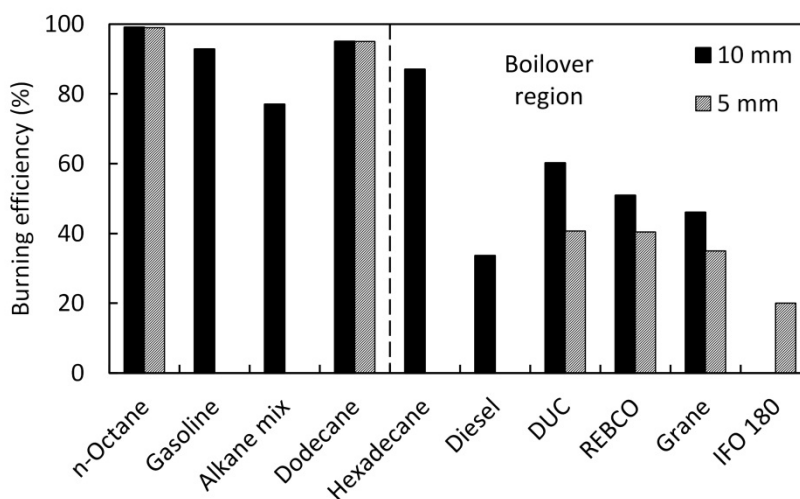


**Figure 4.31.** Burning efficiency as a function of the oil type. The oils are ordered from left to right by increasing density. All oils on the right of the vertical dashed line ended in boilover. Burning efficiencies of the alkane mixture and hexadecane were obtained for an initial slick thickness of 15 and 20 mm, respectively.

A similar behavior was observed for the alkane mixture, which had a relatively low burning efficiency. Once the majority of the *n*-octane and dodecane were burned from the mixture, the slick thickness of the remaining hexadecane (< 5 mm) was insufficient to sustain the fire. The burning efficiency of the alkane mixture with a 15 mm initial slick thickness thus mainly consisted of the burned *n*-octane and dodecane fractions (65 wt%), as hardly any of the hexadecane was burned. At a higher initial slick thickness, the burning efficiency was more in line with the burning efficiencies of gasoline and dodecane, because a higher fraction of the hexadecane could be burned (Table 4.1).

Boilovers occurred for all oils with a boiling point of  $\geq 287$  °C, although with varying intensity. While it is difficult to assess the boilover intensity without heat release rate measurements, visual observations and video recordings could still be used to obtain an impression of the boilover intensity. The boilover intensity seemed to increase with increasing boiling point of the fuel. Boilovers were clearly less intense for hexadecane and diesel than for the crude oils and IFO 180 seemed to have the most violent boilovers. It was shown that the effect of boilovers on the burning efficiency could be both positive (Fig. 4.15) and negative (Section 4.6.2) at initial slick thicknesses of 40 mm and 10 mm, respectively. The deviations caused by boilovers from burning efficiencies without boilover, however, did not exceed a  $\pm 10\%$  burning efficiency interval. Experiments with

DUC and REBCO showed good repeatability in terms of the time to boilover and the burning efficiency at an initial slick thickness of 10 mm. These results indicate that boilovers do not randomly affect the burning efficiency, but that this influence is likely correlated to the initial slick thickness. It seems therefore improbable that at the same initial slick thickness, boilovers will affect the burning efficiency of the tested oils positively for some oils and negatively for others. It is thus expected that the relative burning efficiencies among the different oil types as shown in Fig. 4.31 were not significantly affected by boilovers.

#### **4.7.2 Scaling in ice cavities**

The burning efficiency of ANS with an initial slick thickness of 10 mm as a function of the ice cavity diameter is shown in Fig. 4.32. The burning efficiencies are also plotted as a function of the oil amount with respect to the data in Fig. 4.23, for a comparison between the ice cavity results and (herded) oil burned in ice-infested water (Section 4.4.4). The results clearly show that the burning efficiency increased with increasing pool diameter. Because the ice cavity experiments were conducted under very similar conditions, these results provide strong evidence that the burning efficiency is a function of the diameter. Compared to *in-situ* burning experiments in ice-infested water, the ice cavity results show similar burning efficiencies as a function of the oil amount. This indicates that the burning oil in ice cavities is not notably different from burning oil on water and that the results can be considered to be representative of the other results presented in this thesis.

The relatively high burning efficiency of the 1.1 m diameter experiment as a function of the oil amount was probably caused by both the indoor conditions and limited spreading opportunity for the burning oil slick. The main spreading mechanism of oil burning in an ice cavity is due to melting of the cavity that increases the diameter (Fig. 4.33) and formation of a lateral cavity in the ice (Farmahini Farahani et al., 2015a; Farmahini Farahani et al., 2015b; Shi et al., 2016). Compared to the intermediate scale herding experiments, wind was shown to have a significant impact on the burning efficiency and herded oil slicks were observed to spread out during the burning (Section 4.4.4). Because the slick thickness of spreading slicks decreases faster, the heat losses to the water increase faster resulting in faster extinction of the flames and thus a lower burning efficiency. Spreading of herded slicks was, however, less common in experiments with an ice coverage, while the burning efficiencies were still much lower than the ice cavity experiments. It is therefore most likely that the absence of wind in the ice cavity experiments was the dominating factor of the increased burning efficiency.

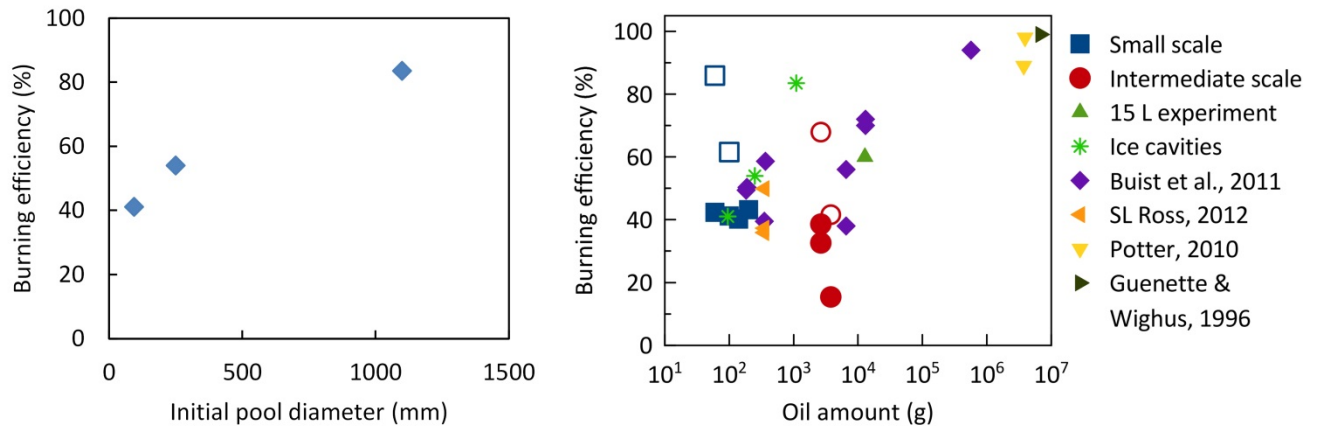


**Figure 4.32.** Burning efficiency of ANS with an initial slick thickness of 10 mm as a function of the ice cavity diameter (left) and relative to burning efficiencies of (herded) oil slicks in ice-infested water (right) (Fig. 4.23). Open symbols show the effective burning efficiency, which is relative to the oil area that was set on fire. Literature data was taken from Buist et al. (2011), SL Ross (2012), Potter (2010b) and Guénette and Wighus (1996).

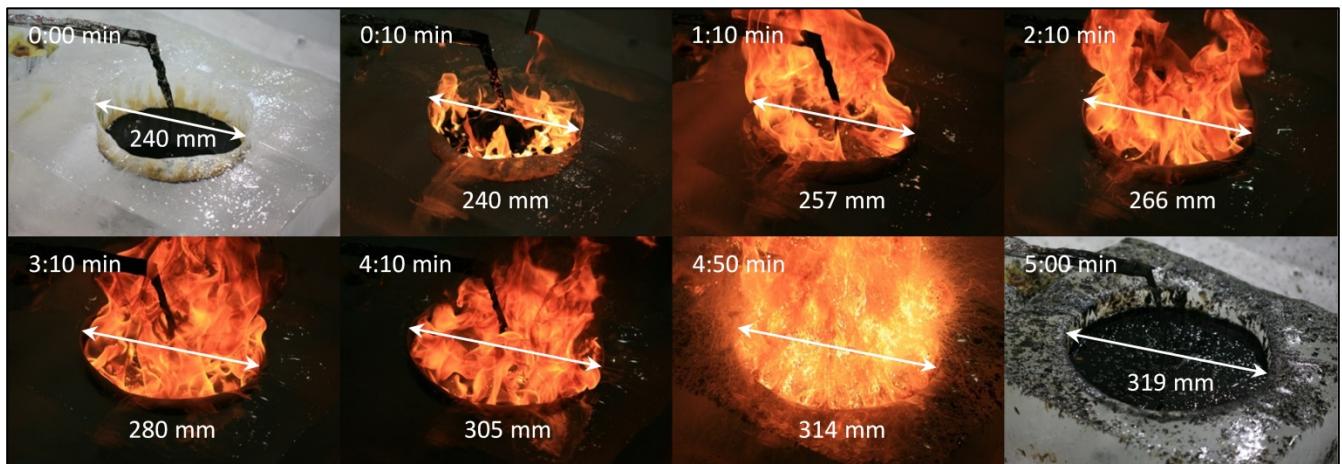


**Figure 4.33.** Snapshots of ANS burning in a 240 mm diameter ice cavity. The arrows in each frame give an indication of the size of the cavity diameter, which increased as a function of the burning time. The decrease in the ullage height due to meltwater accumulating below the oil can also be observed between the first and last frame.

Melting of the ice cavity caused water to accumulate below the oil because the water had a higher density than the crude oil. The ullage height therefore decreased as a function of the burning time (Fig. 4.33) and had to be deep enough to prevent the oil from overflowing from the cavity during the burning. In the ice cavity

experiments with  $D = 0.25$  m and 1.1 m, boilovers were observed as a consequence of the water layer accumulating below the oil (4:50 min in Fig. 4.33). The flow of water from melting ice into the water layer was clearly not sufficient to prevent the superheating of the water in these experiments. In the smallest ice cavities ( $D = 0.1$  m), the size of the crude oil fire was likely too small to superheat the water sub-layer because of the constant inflow of cold water. In ice cavities (or melt pools) of any substantial size ( $D > 0.1$  m), the forming water layer under burning oil should as such be considered to be a still water layer that facilitates boilover. Contrary to *in-situ* burning of crude oil on open water, boilovers in ice cavities are thus not an artefact of the experimental design but are part of the burning process and the resulting burning efficiency.

The effects of the initial slick thickness and initial ullage height on the burning efficiency in small scale cavities ( $D = 0.1$  m) are shown in Fig. 4.34. The burning efficiencies of the experiments with varying initial slick thicknesses were taken for the initial ullage heights that resulted in similar final ullage heights (just below the cavity edge) for each initial slick thickness. A fixed initial ullage height for these experiments would either result in oil overflowing from the cavity for thick initial slick thicknesses or reduce the burning efficiency for thin initial slick thicknesses (as discussed below). An initial water layer under the oil did not show any effect on the burning efficiency and this parameter is therefore not further discussed.

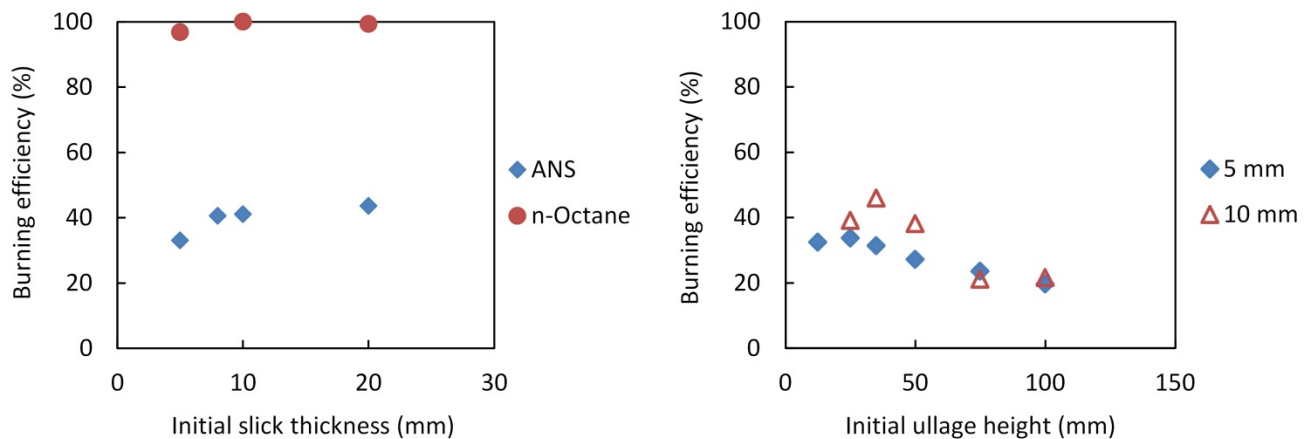


**Figure 4.34.** Burning efficiency as a function of the initial slick thickness for ANS and *n*-octane (left) and as a function of the initial ullage height for ANS (right).

The burning efficiencies as a function of the initial slick thickness (Fig. 4.34) showed very similar results compared to the results obtained in the COFA setup (Fig. 4.15). The burning efficiency showed an asymptotic increase with increasing initial slick thickness, reaching a maximum at an initial slick thickness of 10 mm for *n*-octane and 20 mm for ANS. As for the results obtained in the COFA, *n*-octane burned to near completion, whereas the crude oil was limited to a burning efficiency of 44%. These results indicate that the burning behavior (e.g. vaporization order) and the heat losses are similar for oil burning in ice cavities and confined oil burning on water.

By increasing the ullage height, the burning efficiency initially remained near-constant, after which the burning efficiency decreased by further increasing the ullage height (Fig. 4.34). The negative effect of the ullage height on the burning efficiency was attributed to an oxygen deficiency inside the cavity as air is less capable of flowing into deep cavities to provide the oxygen required for combustion. For minor increases in the ullage height, this effect was not noticeable because the burning efficiency was more limited by other factors (e.g. heat losses). For relatively large ullage heights ( $\geq 50$  mm), the limitation of the air supply to the burning fuel started to play a factor and reduce the oxygen available for combustion. This means that more CO and soot is formed instead of CO<sub>2</sub>, which have a lower heat of combustion, and thus the heat release rate decreases. This in turn lowers the heat feedback to the fuel, which causes the heat losses to the water layer below the oil to dominate the heat transfer mechanics faster and as a consequence reduces the burning efficiency. For ice cavities with a high initial ullage height, the burning of crude oil would thus no longer be comparable to confined oil slicks burning on open water. Based on the final ullage height (relative to the pool diameter), however, the influence of the ullage height on the burning efficiency of the  $D = 0.25$  m and 1.1 m ice cavity experiments was considered to be negligible.

#### 4.7.3 Cone setup

The burning rate and burning efficiency of weathered and fresh oils as a function of the incident heat flux are shown in Fig. 4.35. For all the tested oils, the burning rate and burning efficiency increased with increasing incident heat flux. The burning efficiency results show that the weathering state of crude oil and a lack of volatile components (IFO 180) mostly reduce the burning efficiency at low incident heat fluxes ( $\leq 5$  kW/m<sup>2</sup>). Because the heat release rate increases with increasing pool diameter (Section 2.1.3 and Eq. (4)), the heat feedback to the fuel surface also increases (Eq. (9)). These results thus suggest that as the diameter of an oil

pool fire increases, the burning efficiency of the oil becomes less dependent of its weathering state and chemical composition. This theory is supported by the high burning efficiencies that have been observed for evaporated and emulsified oil in large scale experiments and full scale *in-situ* burning operations (Allen, 1990; Guénette et al., 1995; Guénette and Wighus, 1996). The results therefore further suggest that the detailed fire science aspects associated with ignition are the main issues related to *in-situ* burning of oil spills (see also Sections 4.3.3 and 4.4.4). Once an oil slick is ignited, high burning efficiencies have been obtained for *in-situ* burning of spilled crude oil under most conditions tested to date.

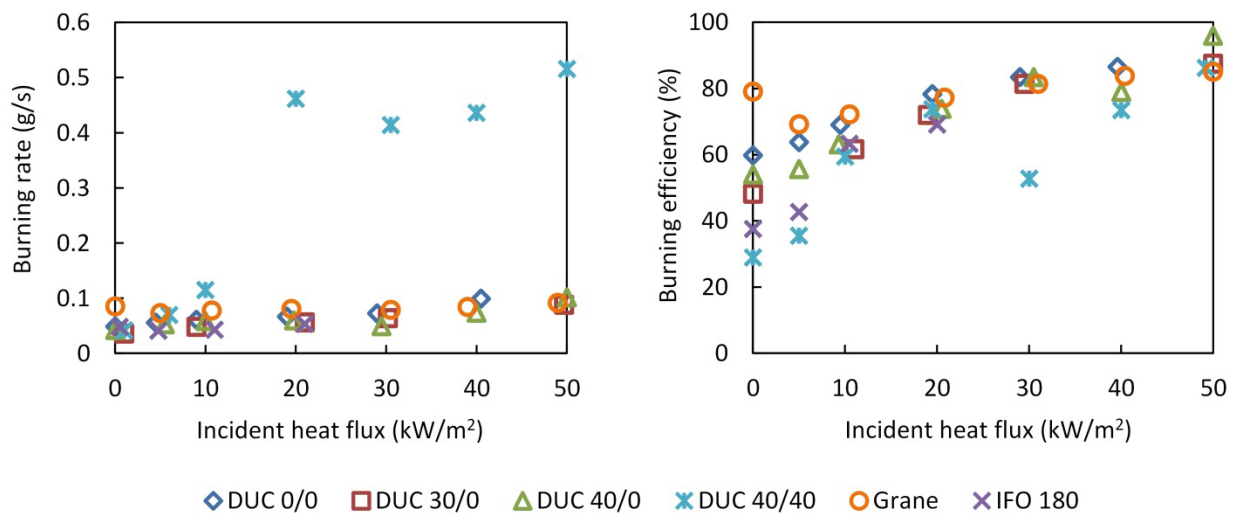


**Figure 4.35.** Burning rate and burning efficiency as a function of the incident heat flux. Data points are jittered on the x-axis for clarity reasons.

Similar to the heat release rate results (Fig. 4.27), the boilover occurrence of DUC 40/40 dominated its burning rate, showing a large jump in the burning rate from an incident heat flux of 10 kW/m<sup>2</sup> to 20 kW/m<sup>2</sup>. Based on the peak heat release rate (Fig. 4.27), however, this increase in burning rate was expected already at an incident heat flux of 10 kW/m<sup>2</sup>. The low burning efficiency at an incident heat flux of 30 kW/m<sup>2</sup> was most likely related to the boilover phase, although the boilover intensity and burning time did not stand out compared to the other DUC 40/40 experiments. For Grane, the burning rate and burning efficiency were not notably affected by the occurrence of boilovers, most likely because the boilovers were less violent and the burning continued after the boilover phase. Apart from the relatively high burning efficiency for the experiment

without an incident heat flux, the Grane results were similar to the other fresh oils. The reason for the observed anomalies are currently unknown but will be investigated in future studies.

The increasing burning efficiency for increasing incident heat fluxes (Fig. 4.35) provides further evidence that the vaporization order of crude oils, including weathered crude oils, is volatility controlled (Section 4.2). This vaporization order causes the heat losses to the cooled sample holder to increase as a function of the burning time and consequently limit the burning efficiency (Section 4.2.4). By increasing the incident heat flux, this limiting of the increasing heat losses effect on the burning efficiency is mitigated, which results in the higher observed burning efficiencies with increasing incident heat fluxes.

For most of the oils in Fig. 4.35, however, the burning efficiencies do not reach the  $\geq 90\%$  that has typically been observed in large scale crude oil fires on water (Allen, 1990; Guénette and Wighus, 1996; Brandvik et al., 2010a; Potter, 2010b). An estimate of the heat feedback to the fuel surface in large scale pool fires was calculated using Eq. (19) (from Eq. (4) and (9)) to determine whether the tested incident heat fluxes are representative of large scale pool fires.

$$\dot{Q}_{net} = \chi_s \cdot \dot{Q} = \chi_s \cdot A \cdot \dot{m}'' \cdot \chi_c \cdot \Delta H_c \quad (19)$$

The heat feedback fraction of crude oil was assumed to be 0.011, based on the reported heat feedback fractions of heptane (0.010) and toluene (0.012) in Hamins et al. (1994). The fraction accounting for incomplete combustion was assumed to be 0.7 (similar to heptane (Tewarson, 1982)) (see also Section 2.1.3) and the heat of combustion of crude oil was taken as 44 kJ/g (Section 2.2.2). According to Buist et al. (2013), the regression rate of a large, unemulsified oil fire on water is 3.5 mm/min. This translates to a burning rate of 3.9 kg/s for a 10 m diameter pool fire of a crude oil with a density of 0.85 g/ml. The heat feedback to the fuel surface for such a crude oil fire on water would then be approximately 17 kW/m<sup>2</sup>.

The main uncertainty in this estimate originates from the heat feedback fraction, because the reported values were based on 0.30 m pool fires (Hamins et al., 1995). The other parameters are either relatively well-known, or have less influence on the calculated heat feedback. It was shown, however, by Hamins et al. (1995) that the mass transfer number ( $B = 1/\chi_s$ ) is relatively constant with increasing diameter for hydrocarbon pool fires. It is therefore deemed unlikely that the used heat feedback fraction contains a factor three error margin, which is the ratio between the calculated heat flux and the highest incident heat flux tested in this study. The estimated

heat feedback thus strongly suggests that the very high heat fluxes tested ( $\geq 30 \text{ kW/m}^2$ ) in this study are not representative of the heat feedback to the fuel surface in large scale crude oil fires.

For an incident heat flux of  $20 \text{ kW/m}^2$ , the burning efficiency for the tested oils varied between 69-77% (Fig. 4.35). As such, these results suggest that the high burning efficiencies observed for large scale crude oil fires on water are not only caused by the increased heat feedback to the fuel surface compared to small scales. One possible additional factor that could contribute to the high burning efficiencies in large scale fires is the wind induced herding of surrounding oil into the fire (Allen et al., 2011). The buoyancy controlled rise of a hot smoke plume from a pool fire causes entrained flows of air into the fire and the plume (Heskestad, 2016), which become stronger with increasing pool diameter. During the *in-situ* burning operations that were part of the response to the Macondo spill, it was observed that oil on the sea surface around the fire was herded into the fire by these entrained flows into the fire. By feeding oil to the fire, the oil slick thickness increases which counteracts the reduction of the slick thickness, as oil is consumed by the fire. More oil can then be burned before the oil slick reaches its critical thickness, for which the heat losses to the water dominate the heat transfer mechanics (Section 4.2.4), and the fire is extinguished. As such, the herding of oil into the fire increases the burning efficiency. This oil herding phenomenon, induced by entrained flows, could therefore possibly contribute to the high burning efficiencies observed for large scale crude oil fires on water.

Overall, there is only very limited experimental data available on the differences between the fire dynamics of small and large scale crude oil fires on water. There is therefore currently no reason to assume that the two factors discussed above (increased heat feedback and herding of oil into the fire) are the only two factors that increase the burning efficiency for large scale crude oil fires on water compared to smaller scales. Further studies should be conducted that focus on the fire dynamics of large scale crude oil fires on water to accurately determine the driving factors behind the very high burning efficiencies observed for such operations.

#### **4.7.4 Sub-conclusion**

The burning efficiencies of pure oils, refined oils, crude oils and weathered crude oils were studied on water, in ice cavities and in a cooled sample holder subjected to an incident heat flux. All of the burning efficiency results supported the proposed volatility controlled vaporization order (Section 4.2.5). The burning efficiency decreased from 99% to 20% with decreasing amount of volatile components and increasing amount of non-

volatile components in the oil composition for small scale experiments on water. Burning efficiency results of oil burning in ice cavities showed similar burning behavior and heat losses as confined oil burning on open water. The main difference between crude oil burning in ice cavities and on open water is that crude oil burning in ice cavities is expected to end in a boilover, because the water layer is by definition still. Scaling experiments in ice cavities clearly showed that the burning efficiency increases with increasing pool diameter under similar testing conditions. These results confirm that the burning efficiency is a function of the pool diameter for crude oils burning on water.

Burning efficiencies increased with increasing incident heat flux for fresh and weathered oils, as expected. These results support the theory that the high burning efficiencies observed in large scale *in-situ* burning experiments ( $\geq 90\%$ ) are due to an increased heat feedback to the fuel surface compared to small scale fires. Such high burning efficiencies, however, were not reached for the conducted small scale experiments. Even at incident heat fluxes of 40-50 kW/m<sup>2</sup>, which are much higher than the estimated 20 kW/m<sup>2</sup> heat feedback to the fuel surface for large scale crude oil fires on water, the burning efficiency did not reach above 85%. The high burning efficiencies observed in large scale crude oil fires on water are therefore probably caused by a combination of multiple factors. One such factor that could possibly increase the burning efficiency of large scale fires compared to small scale fires is the herding of surrounding oil into the fire, induced by entrainment flows into the fire and the plume.

## **4.8 Composition analysis of byproducts**

The results presented in this section were obtained with the modified COFA setup (Section 3.5), according to the methodologies described in Sections 3.5.1 and 3.5.2.

### **4.8.1 Smoke analysis test**

The gas chromatogram of the analytes adsorbed on one of the thermal desorption tubes (number 1) is shown in Fig. 4.36, which was representative of the results for all thermal desorption tubes. The result shows that the analytes on the thermal desorption tubes mainly consisted of water and components corresponding to the sorbent materials in the tubes. The concentration of the hydrocarbon combustion products was very low and

therefore difficult to analyze. Because water is also one of the combustion products (Section 2.1.2), this is an inherent problem to sampling the combustion gases in the smoke plume. It was attempted during the gas chromatography analysis to remove the water by heating the tubes at 70 °C prior to injecting the samples on the column, but this could not prevent water from dominating the results. Heating tape was therefore added around the thermal desorption tubes in the experimental design (Fig. 3.7) to heat up the sorbent material during the sampling. By elevating the temperature inside the tubes, water is less likely to be adsorbed on the sorbent materials in the tubes. The downside of this method is that volatile hydrocarbon combustion products with boiling points similar to water are also less likely to be absorbed on the sorbent material in the tubes. Alternative methods to reduce the water concentration on the thermal desorption tubes are installing a water trap before the tubes or testing alternative sorbent materials that may have a lower affinity for adsorbing water.

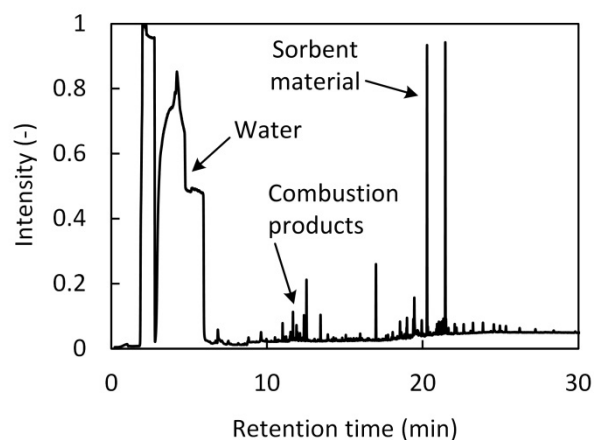


**Figure 4.36.** Gas chromatogram of the analytes on the first thermal desorption tube. The analytes were mainly dominated by water and components corresponding to the sorbent materials, as annotated.

Despite the high concentration of water in the thermal desorption tubes, hydrocarbon combustion products could be sampled from the smoke plume. The use of thermal desorption tubes is as such a promising method for sampling combustion gases from the smoke plume of burning crude oil on water. Further testing to optimize the water to hydrocarbon ratio on the sorbent material will be required to be able to properly analyze chemical composition of the hydrocarbon byproducts in the smoke plume.

Analysis of soot particles was not possible because no visible amount of soot was collected by the filter before the thermal desorption tubes. The thermal desorption tubes, however, contained a sufficient amount of sampled gases. Increasing the smoke inlet or increasing the flow through the tubes to increase the collection of smoke thus risks that the thermal desorption tubes are overdosed with sampling gases. This could lead to differences between the relative concentrations of the byproducts on the tubes and in the smoke plume. The collected sample would then no longer be representative of the actual smoke plume composition. A separate filter may thus be necessary to sample the soot from the smoke plumes for chemical analysis of the soot composition.

#### **4.8.2 Water fraction test**

The total petroleum content (hydrocarbon oil index from  $C_{10}$  to  $C_{40}$ ) in the water samples was measured to be 6.35 mg/l for the experiment with a burning efficiency of 10% and < 5 mg/l for the other experiments. These values correspond well with reported values in literature (Faksness et al., 2008; Faksness et al., 2012), which indicates that the water body is being properly homogenized by the current. The experimental design with the low Pyrex glass cylinder and a mild water current is thus suitable for further analysis of the chemical composition of the hydrocarbon fraction in the water body below burning oil.

#### **4.8.3 Residue composition test**

The burning efficiency, burning time, density and viscosity of the residues that were intentionally stopped to match burning efficiency intervals of 10% are shown in Table 4.6. The relationship between the burning time and the burning efficiency, density and viscosity corresponds very well with the results of the burning series conducted in the COFA setup (Table 4.2). This clearly shows that the burning of crude oil in the modified COFA setup is not notably affected by introducing a water current, apart from the lack of boilover (Section 4.6). The chemical compositions of the residues also showed the expected reduction in relative concentration of the volatile components as a function of the burning time (Fig. 4.37). These results thus show that the modified COFA is a suitable setup for studying the chemical composition of burning residues as a function of the burning efficiency, for example using a principal component analysis (Section 4.2.3).

**Table 4.6.** Density and viscosity of burned DUC residues

<i>Burning efficiency (%)</i>	<i>Burning time (min)</i>	<i>Density (g/ml)<sup>a</sup></i>	<i>Viscosity (cP)<sup>a</sup></i>
Fresh	0:00	0.853	6.750
13	0:56	0.877	16.62
24	2:23	0.896	49.13
30	3:42	0.916	117.0
45	6:02	0.949	665.0
51	8:10	0.929	3170

<sup>a</sup> Measured at 25 °C using an Anton Paar SVM 3000 viscometer.

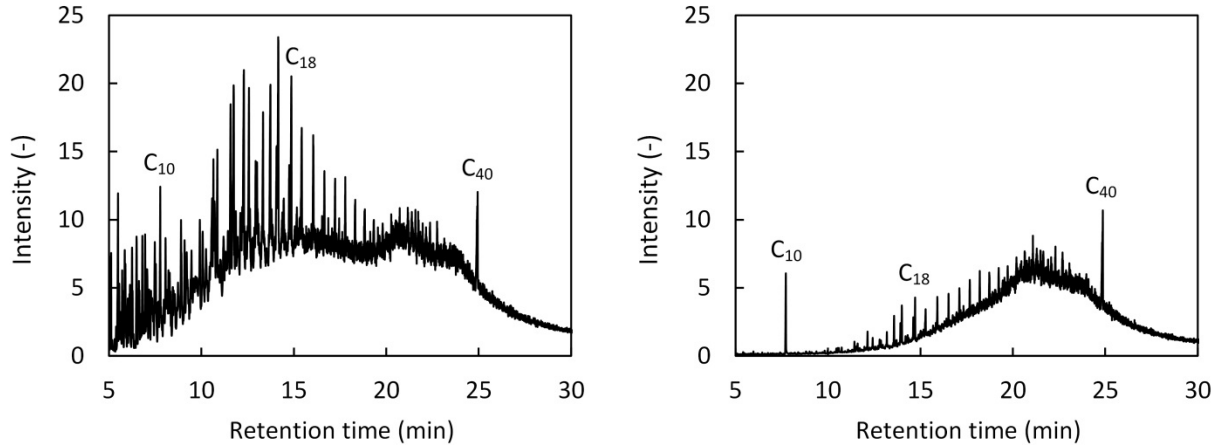


**Figure 4.37.** Gas chromatograms of DUC burn residues with a burning efficiency of 13% (left) and 51% (right). The reduced concentration of the volatile components as a function of the burning efficiency observed between these samples was representative of all residue samples.

Based on the burning efficiency results as a function of the incident heat flux in the cone setup (Section 4.7.3), it is expected that the current limit of the burning efficiency (50%) can be increased by the infrared heaters (Fig. 3.7). Although the very high tested heat fluxes ( $\geq 30 \text{ kW/m}^2$ ) may not be representative of the heat feedback to the fuel surface for large scale oil fires on water, these heat fluxes did result in high burning efficiencies ( $> 85\%$ ). As such, the factors that increase the burning efficiency with increasing pool diameter, besides an increased heat feedback, (Section 4.7.3) could possibly be simulated by increasing the incident heat

flux to 30-50 kW/m<sup>2</sup>. The modified COFA setup will then allow for studying the chemical composition of byproducts from *in-situ* burning of oil on water at burning efficiencies representative of large scale fires.

#### **4.8.4 Sub-conclusion**

Sampling tests of the water fraction, residue and smoke plume from oil burning experiments on water in the modified COFA setup showed that this setup is suitable for studying the chemical composition of the byproducts as a function of the burning efficiency. Only with respect to the sampling of soot and combustion gases should the setup be optimized to reduce the concentration of water in the thermal desorption tubes and allow for sampling higher concentrations of soot. The burning efficiency results for an increased heat flux to the fuel surface indicated that increased burning efficiencies could be obtained for small scale experiments that are representative of large scale oil fires on water. With the use of infrared heaters, it is thus expected that the modified COFA can be used to study the chemical balance between byproducts of *in-situ* burning as a function of burning efficiencies representative for operational scales.



## 5 Conclusion

The main results of all the sub-conclusions in the results sections are summarized here. Section 5.1 shows the main highlights of the results presented throughout this thesis. Section 5.2 gives a full summary of the experimental results and the main conclusions. These conclusions are then placed into the perspective of the research objective in Section 5.3. Finally, based on the presented conclusions, recommendations are made for future work in Section 5.4.

### 5.1 Result highlights

- Crude oils burn with a volatility controlled vaporization order which means that the components in crude oils are burned in the order of decreasing volatility.
- Crude oils are a unique type of fuel that cannot be simulated with simplified multicomponent fuels.
- Chemical herders were shown to successfully thicken simulated oil spills to ignitable thicknesses in ice coverages of 3/10-7/10, but ignition issues with fractured oil slicks should be solved to improve the burning efficiencies of herder oil slicks.
- Strong ignition sources that translate to substantial ignition gel pool fires are required to provide the heat flux required for ignition of weathered and non-volatile oils.
- Boilover tendency depended on both the superheating of an underlying water layer and the chemical composition of the oil and could therefore not be excluded from occurring for *in-situ* burning operations on sea.
- The primary conclusion of this thesis is that once a large oil slick has been ignited, it is expected to result in a high burning efficiency, independent of the properties of the oil and environmental conditions.

### 5.2 Summary of experimental results

*In-situ* burning experiments of crude oil on water were conducted under various laboratory and outdoor conditions to study the fire dynamics and fire chemistry of burning crude oil on water. The results showed that

crude oil, being a multicomponent fuel with a large range of components, has a distinct vaporization order in which its components evaporate during combustion. The components in crude oils are burned in order of decreasing volatility, as indicated by an increasing surface temperatures and decreasing burning rates and flame heights as a function of the burning time. A principal component analysis of the composition of burned crude oil residues with different burning efficiencies confirmed that the (relative) concentration of volatile components decreased with increasing burning efficiency. Because of this volatility controlled vaporization order, the crude oils never reached the steady-state burning phase that was observed for the reference fuels (pure oils and the pure oil mixture) burning on water. This shows that crude oils are a unique type of fuel that cannot be simulated with simplified multicomponent fuels.

A mathematical analysis of the heat transfer mechanics showed that the heat losses to the water layer increase as a function of the burning time for crude oil burning on water due to the volatility controlled vaporization order. Furthermore, the flame height, and thus the heat feedback to the fuel surface, decreased as a function of the burning time. The burning efficiencies of the crude oils in the small scale experiments (20-75%) were probably limited by these increasing heat losses that led to premature extinction of the flame. It was proposed that the higher burning efficiencies observed for large scale crude oil fires were due to their higher heat feedback to the fuel surface that balanced out against the increasing heat losses. In fact, small scale crude oil burning experiments subjected to an incident heat flux showed increased burning efficiencies. At incident heat fluxes representative of large scale pool crude oil fires on water ( $20 \text{ kW/m}^2$ ), however, the burning efficiencies did not reach above 80%. It was therefore deduced that the high burning efficiencies observed in large scale crude oil fires on water are not only caused by an increased heat feedback, but by other factors inherent to large scale fires as well. One of such additional factors could be the herding of surrounding oil into the fire by air entrainment flows. It is, however, likely that there are additional, currently unknown, complex factors related with the fire dynamics of the problem that lead to the high burning efficiencies for large scale fires. Further studies on the fire dynamics of large scale crude oil fires on water should be conducted to identify the factors associated with a large pool diameter that are responsible for the high burning efficiencies.

The initial slick thickness was found to be mainly relevant for the ignitability of crude oil slicks on water. Once ignited, the diameter of the pool fire was a more dominating parameter, which limits the burning efficiency more than the initial slick thickness. An ignitable slick thickness ( $> 1\text{-}2 \text{ mm}$ ), however, does not guarantee that the oil slick can in fact be ignited. Ignition attempts of herded oil slicks showed that the combination of the slick size and wind also play an important role in the ignitability of (herded) oil slicks. Ignitability tests showed that

for oils with a low amount of volatile components (e.g. weathered oils), an ignition source of 5-10 kW/m<sup>2</sup> was required to ignite the oil. In terms of the current ignition methods, such as ignition oil, this means that the ignition source needs to have a substantial fire diameter to provide this critical heat flux to the oil. Oil slicks need to have large enough sizes to accommodate the ignition source spreading over the oil, rather than dissipating the slick. Experimental results of herded oil suggested that oil slicks need to be larger than 0.5 m<sup>2</sup> to support ignition by ignition gel.

Chemical herders were shown to successfully thicken simulated oil spills to ignitable thicknesses in ice coverages of 3/10-7/10. Interaction with the ice, however, caused the oil slicks to break up into multiple oil slicks during the herding process. Because the smaller slicks of these fractured oil slicks were difficult to ignite, the burning efficiencies of the herded oil slicks were low (15-43%) compared to other experiments with similar oil volumes and experimental conditions (36-59%). Herders could thus be a potentially valuable tool for *in-situ* burning as oil spill response method, also in ice-infested waters, if the ignitability issues inherent to fractured oil slicks can be resolved.

The boilover phenomenon, i.e. the explosive burning of crude oil, observed during the burning of oils with a high boiling point on a still water layer was shown to depend on the superheating of the water below the oil. Introducing a current in the water body of the small scale water basin to continuously refresh the water layer directly below the burning oil prevented boilovers from occurring. Boilovers are therefore only expected on still water, such as in ice cavities or melt pools. During ignition studies on fresh and weathered oils without an underlying water layer, however, boilovers were also observed for a fresh heavy crude oil with both an abundant light and heavy fraction. The lack of a water layer suggests that the light components in the oil were the cause for the boilover, which means that the tendency to boilover is also depending on the chemical composition of the burning oil. Boilovers can thus not be excluded from occurring during *in-situ* burning operations on sea, which could complicate the safety planning of *in-situ* burning operations due to the increased fire intensity of boilovers. Further studies are required to determine the conditions under which these boilovers without a water layer can occur.

All of the experimental results supported the observation from literature data that the burning efficiency is depending on the pool diameter. The dependency on the pool diameter for crude oil fires on water was shown to be partially due to a combination of the volatility controlled vaporization order and increasing heat losses to the underlying water layer. Other parameters such as the initial slick thickness, presence of ice, chemical

composition of the oil and weathering state of the oil mostly influenced the burning efficiency in small scale experiments. The primary conclusion of this thesis is therefore that once a large oil slick has been ignited, it is expected to result in high burning efficiencies, independent of the properties of the oil and environmental conditions.

### 5.3 Research objective

In terms of the research objective, the results show that most of the operational parameters, apart from the pool diameter, will only have a limited effect on the efficiency of *in-situ* burning as oil spill response method. This strongly suggests that high burning efficiencies are inherent to operational scale crude oil fires on water. Once both ignition and flame spread on a large oil slick are successful, high burning efficiencies are expected simply due to the scale of the fire. As such, the main parameter that determines the suitability of *in-situ* burning as oil spill response method becomes the ignitability of the oil.

The ignitability parameter is depending on complex fire dynamics aspects, but can be expressed in terms of the heat flux that the ignition source needs to be able to provide to the oil surface to ignite the oil. At high heat fluxes ( $\geq 20 \text{ kW/m}^2$ ), ignition was nearly instantaneous for all tested oils, independent of the weathering state or volatile components present in the oil. An estimate of the heat feedback to the fuel surface in crude oil pool fires on water with a 10 m diameter, however, showed that such large scale fires only reach heat fluxes of approximately  $17 \text{ kW/m}^2$ . While heavily weathered oils could thus be ignitable when subjected to heat fluxes of  $20 \text{ kW/m}^2$ , it would require an enormous amount of ignition gel to create an ignition source large enough to provide this heat flux. The ignitability of oil slicks should thus not be considered as a binary question of whether an oil slick is ignitable or non-ignitable, but as a function of the strength of the ignition sources available to ignite the oil slick. From an operational point of view, predicting the suitability of *in-situ* burning as oil spill response method can thus be reduced to answering the question whether the required strength (e.g. ignition gel volume) of the ignition source is practically feasible.

## 5.4 Recommendations for future work

Based on the results from this study, the recommendations for future work can be divided into scientific problems and practical problems. It would be valuable for suitability predictions of *in-situ* burning as response method to oil spills to confirm the postulated theories regarding the burning efficiencies of large scale crude oil fires on water. This works should focus on the factors that increase the burning efficiency with increasing diameter, such as the increased heat feedback to the fuel surface as compared to small scales.

Once the burning efficiency can be predicted with a high certainty, the suitability of *in-situ* burning will be mainly depending on the ignition of the oil slick and the net impact of the byproducts on the environment. The fundamentals of ignition studies should aim to take into account realistic field conditions as these conditions are known to notably affect the ignitability of crude oil on water. Such studies should then translate to functional field methods that are capable of igniting weathered oils under challenging weather conditions.

The (relatively) low capacity of *in-situ* burning is also a problem that should be addressed to make *in-situ* burning an effective oil spill response method. Chemical herders are a promising measure to contain oil spills, even in ice-infested waters, that can facilitate *in-situ* burning of spread oil on water. Further research on the fracturing of oil slicks during the herding process and ignition of fractured oil slicks could improve the viability of herders, and thereby *in-situ* burning, as oil spill response method.

Fundamental research can aim to improve the understanding of the boilover phenomenon during the combustion of crude oils with and without underlying water layers. A better understanding of this phenomenon would allow for predictions under which conditions boilovers become plausible during operational scale *in-situ* burning of crude oil. This is a relevant problem for the safety planning of oil spill response operations and as such would make suitability predictions of *in-situ* burning more accurate.

Finally, to determine the net environmental impact of the byproducts, it would be valuable to determine the chemical balance of the byproducts that form during *in-situ* burning at large scale crude oil fires on water. Studies should therefore focus on representative burning efficiencies for such large scale fires. The new experimental setup developed for this purpose showed promising results and provides a suitable experimental setup for such studies. On the practical side, one aspect that seems relatively less studied is the impact of precipitating soot in the environment, on for example snow and ice. Together with the residue, these two

products seem to have the largest potential to negatively impact the environment, although further studies are required to determine the extent of their environmental impact.

## Bibliography

ACIA, 2005. Arctic Climate Impact Assessment, Cambridge University Press, New York, 1042 p.

Adams, J., Sweezey, M. and Hodson, P. V., 2014. Oil and Oil Dispersant Do Not Cause Synergistic Toxicity to Fish Embryos, *Environmental Toxicology and Chemistry*, 33(1): 107-114.

Allen, A. A., 1990. Contained Controlled Burning of Spilled Oil During the Exxon Valdez Oil Spill, in *Proceedings of the Thirteenth Arctic and Marine Oilspill Program (AMOP) Technical Seminar*, Environment Canada, Ottawa, ON, p. 305-313.

Allen, A. A. and Ferek, R. J., 1993. Advantages and Disadvantages of Burning Spilled Oil, *International Oil Spill Conference Proceedings*, 1993(1): 765-772.

Allen, A. A., Jaeger, D., Mabile, N. J. and Costanzo, D., 2011. The Use of Controlled Burning During the Gulf of Mexico Deepwater Horizon MC-252 Oil Spill Response, *International Oil Spill Conference Proceedings*, 2011(1): 1-13.

Allen, A. A., 2016. Tech File: Fire Boom for the US' Worst Oil Spill. Marine Link, Retrieved 31st of December, 2016, from [www.marinelink.com/news/worst-spill-fire411277](http://www.marinelink.com/news/worst-spill-fire411277).

Almeda, R., Baca, S., Hyatt, C. and Buskey, E. J., 2014. Ingestion and Sublethal Effects of Physically and Chemically Dispersed Crude Oil on Marine Planktonic Copepods, *Ecotoxicology*, 23(6): 988-1003.

AMAP, 1998. AMAP Assessment Report: Arctic Pollution Issues, Arctic Monitoring and Assessment Programme (AMAP), Oslo, Norway, xii+ 859 p.

AMAP, 2010a. Assessment 2007: Oil and Gas Activities in the Arctic - Effects and Potential Effects, Arctic Monitoring and Assessment Programme (AMAP), Oslo, Norway, Vol. 1, I: 423 p.

AMAP, 2010b. Assessment 2007: Oil and Gas Activities in the Arctic - Effects and Potential Effects, Arctic Monitoring and Assessment Programme (AMAP), Oslo, Norway, Vol. 2, II: 277 p.

AMAP, 2012. Arctic Climate Issues 2011: Changes in Arctic Snow, Water, Ice and Permafrost, Arctic Monitoring and Assessment Programme (AMAP), Oslo, Norway, 97 p.

Arai, M., Saito, K. and Altenkirch, R. A., 1990. A Study of Boilover in Liquid Pool Fires Supported on Water Part I: Effects of a Water Sublayer on Pool Fires, *Combustion Science and Technology*, 71(1-3): 25-40.

Arctic Council, 2013. Agreement on Cooperation on Marine Oil Pollution Preparedness and Response in the Arctic, Arctic Council Secretariat, Tromsø, Norway, 230 p.

Arctic Council, 2016. Ratification Completed for Agreement on Oil Pollution Preparedness and Response Arctic Council Secretariat, *Retrieved 14th of October, 2016*, from [www.arctic-council.org/index.php/en/our-work2/8-news-and-events/401-mospa-ratification](http://www.arctic-council.org/index.php/en/our-work2/8-news-and-events/401-mospa-ratification).

Aske, N., Kallevik, H. and Sjöblom, J., 2002. Water-in-Crude Oil Emulsion Stability Studied by Critical Electric Field Measurements. Correlation to Physico-Chemical Parameters and near-Infrared Spectroscopy, *Journal of Petroleum Science and Engineering*, 36(1–2): 1-17.

Babrauskas, V., 1983. Estimating Large Pool Fire Burning Rates, *Fire Technology*, 19(4): 251-261.

Babrauskas, V., 2016a. The Cone Calorimeter in *SFPE Handbook of Fire Protection Engineering*, M. J. Hurley, D. T. Gottuk, J. R. Hall Jr, K. Harada, E. D. Kuligowski, M. Puchovsky, J. L. Torero, J. M. Watts Jr and C. J. Wieczorek (Eds.), Springer New York, New York, NY, pp. 952-980.

Babrauskas, V., 2016b. Heat Release Rates in *SFPE Handbook of Fire Protection Engineering*, M. J. Hurley, D. T. Gottuk, J. R. Hall Jr, K. Harada, E. D. Kuligowski, M. Puchovsky, J. L. Torero, J. M. Watts Jr and C. J. Wieczorek (Eds.), Springer New York, New York, NY, pp. 799-904.

Baker, J. M., 1995. Net Environmental Benefit Analysis for Oil Spill Response, *International Oil Spill Conference Proceedings*, 1995(1): 611-614.

Bech, C. M., Sveum, P. and Buist, I. A., 1993. The Effect of Wind, Ice and Waves on the In-Situ Burning of Emulsions and Aged Oils, in *Proceedings of the Sixteenth Arctic and Marine Oilspill Program (AMOP) Technical Seminar*, Environment Canada, p. 735-748.

Bejarano, A. C., Clark, J. R. and Coelho, G. M., 2014. Issues and Challenges with Oil Toxicity Data and Implications for Their Use in Decision Making: A Quantitative Review, *Environmental Toxicology and Chemistry*, 33(4): 732-742.

Benner, B. A., Bryner, N. P., Wise, S. A., Mulholland, G. W., Lao, R. C. and Fingas, M. F., 1990. Polycyclic Aromatic Hydrocarbon Emissions from the Combustion of Crude Oil on Water, *Environmental Science & Technology*, 24(9): 1418-1427.

Blander, M. and Katz, J. L., 1975. Bubble Nucleation in Liquids, *AIChE Journal*, 21(5): 833-848.

Blenkinsopp, S., Sergy, G., Doe, K., Wohlgeschaffen, G., Li, K. and Fingas, M., 1997. Evaluation of the Toxicity of the Weathered Crude Oil Used at the Newfoundland Offshore Burn Experiment (NOBE) and the Resultant Burn Residue, in *Proceedings of the Twentieth Arctic and Marine Oilspill Program (AMOP) Technical seminar*, Environment Canada, p. 677-684.

Blinov, V. I. and Khudiakov, G. N., 1957. Certain Laws Governing Diffusive Burning of Liquids, *Academiia Nauk, SSSR Doklady*, 113: 1094-1098.

Bobra, M., 1991. Water-in-Oil Emulsification: A Physicochemical Study, *International Oil Spill Conference Proceedings*, 1991(1): 483-488.

BP, 2011. Diesel Material Safety Data Sheet, BP Oil International Limited, MSDS NR: SMI2110, 10 p.

BP, 2015. Alaskan North Slope - Summary Crude Oil Assay Report. BP Oil International Limited, *Retrieved 1st of January, 2017*, from [www.bp.com/content/dam/bp-crudes/en/Assays/Alaskan\\_North\\_Slope\\_Aug\\_2015.xls](http://www.bp.com/content/dam/bp-crudes/en/Assays/Alaskan_North_Slope_Aug_2015.xls).

Bradford, M. L. and Thodos, G., 1967. Latent Heats of Vaporization Hydrocarbons, *Journal of Chemical & Engineering Data*, 12(3): 373-376.

Brandvik, P. J., Singasaas, I. and Daling, P. S., 2004. Oil Spill R&D in Norwegian Arctic Waters with Special Focus on Large-Scale Oil Weathering Experiments, in *Interspill Conference Proceedings*, Interspill, p. 1-18.

Brandvik, P. J., Sørheim, K. R., Singasaas, I. and Reed, M., 2006. Short State-of-the-Art Report on Oil Spills in Ice-Infested Waters, SINTEF, Report No. 1, 59 p.

Brandvik, P. J., Daling, P. S., Faksness, L.-G., Fritt-Rasmussen, J., Daae, R. L. and Leirvik, F., 2010a. Experimental Oil Release in Broken Ice - a Large-Scale Field Verification of Results from Laboratory Studies of Oil Weathering and Ignitability of Weathered Oil Spills, SINTEF, Trondheim, Report No. 26, 34 p.

Brandvik, P. J., Fritt-Rasmussen, J., Daniloff, R., Leirvik, F. and Resby, J. L., 2010b. Establishing, Testing and Verification of a Laboratory Burning Cell to Measure Ignitability for In-Situ Burning of Oil Spills, SINTEF, Trondheim, Report No. 20, 26 p.

Brandvik, P. J., Myrhaug Resby, J. L., Daling, P. S., Leirvik, F. and Fritt-Rasmussen, J., 2010c. Meso-Scale Weathering of Oil as a Function of Ice Conditions. Oil Properties, Dispersibility and In Situ Burnability of Weathered Oil as a Function of Time, SINTEF, Trondheim, Report No. 19, 112 p.

Brogaard, N. L., Sørensen, M. X., Fritt-Rasmussen, J., Rangwala, A. S. and Jomaas, G., 2014. *A New Experimental Rig for Oil Burning on Water - Results for Crude and Pure Oils*. Paper presented at the 11th International Symposium for Fire Safety Science, IAFSS, Christchurch, NZ, p. 1481-1494.

Bromley, L. A., Diamond, A. E., Salami, E. and Wilkins, D. G., 1970. Heat Capacities and Enthalpies of Sea Salt Solutions to 200.Deg, *Journal of Chemical & Engineering Data*, 15(2): 246-253.

Brzustowski, T. A. and Twardus, E. M., 1982. A Study of the Burning of a Slick of Crude Oil on Water, *Symposium (International) on Combustion*, 19(1): 847-854.

BSEE, 2012. BSEE Authorizes Shell Preparatory Activities in Chukchi Sea. Bureau of Safety and Environmental Enforcement (BSEE), *Retrieved 18th of October, 2016*, from [www.bsee.gov/newsroom/latest-news/statements-and-releases/press-releases/bsee-authorizes-shell-preparatory-0](http://www.bsee.gov/newsroom/latest-news/statements-and-releases/press-releases/bsee-authorizes-shell-preparatory-0).

- BSEE, 2015. BSEE Approves Updated Permit for Exploration Activities in Arctic Waters under Rigorous Safety Requirements. Bureau of Safety and Environmental Enforcement (BSEE), *Retrieved 18th of October, 2016*, from [www.bsee.gov/newsroom/latest-news/statements-and-releases/press-releases/bsee-approves-updated-permit-for](http://www.bsee.gov/newsroom/latest-news/statements-and-releases/press-releases/bsee-approves-updated-permit-for).
- Buist, I., Trudel, K., Morrison, J. and Aurand, D., 1997. Laboratory Studies of the Properties of In-Situ Burn Residues, *International Oil Spill Conference Proceedings*, 1997(1): 149-156.
- Buist, I., McCourt, J., Potter, S., Ross, S. and Trudel, K., 1999. *In Situ* Burning, *Pure and Applied Chemistry*, 71(1): 43-65.
- Buist, I., 2003. Window-of-Opportunity for In Situ Burning, *Spill Science & Technology Bulletin*, 8(4): 341-346.
- Buist, I., Potter, S., Nedwed, T. and Mullin, J., 2011. Herding Surfactants to Contract and Thicken Oil Spills in Pack Ice for In Situ Burning, *Cold Regions Science and Technology*, 67(1-2): 3-23.
- Buist, I. A. and Glover, N., 1995. In Situ Burning of Alaska North Slope Emulsions, *International Oil Spill Conference Proceedings*, 1995(1): 139-146.
- Buist, I. A., Canevari, G. and Nedwed, T., 2010a. New Herding Agents for Thickening Oil Slicks in Drift Ice for *In Situ* Burning, in *Proceedings of the Thirty-third Arctic and Marine Oilspill Program (AMOP) Technical Seminar*, Environment Canada, Ottawa, ON, p. 725-742.
- Buist, I. A., Potter, S. and Sørstrøm, S. E., 2010b. Barents Sea Field Test of Herder to Thicken Oil for In Situ Burning in Drift Ice, in *Proceedings of the Thirty-third Arctic and Marine Oilspill Program (AMOP) Technical Seminar*, Environment Canada, Ottawa, Ontario, p. 725-742.
- Buist, I. A., Potter, S. G., Trudel, B. K., Shelnutt, S. R., Walker, A. H., Scholz, D. K., Brandvik, P. J., Fritt-Rasmussen, J., Allen, A. A. and Smith, P., 2013. In Situ Burning in Ice-Affected Waters: State of Knowledge Report, Arctic Response Technology, Final Report 7.1.1, 293 p.
- Buist, I. A., Cooper, D., Trudel, B. K., Fritt-Rasmussen, J., Wegeberg, S., Gustavson, K., Lassen, P., Rojas Alva, W. U., Jomaas, G. and Zabilansky, L., 2016. Research Investigations into Herder Fate, Effects and Windows-of-Opportunity, Arctic Response Technology, under review.
- Burgess, D. S., Strasser, A. and Grumer, J., 1961. Diffusive Burning of Liquids in Open Trays, *Fire Research Abstracts and Reviews*, 3: 177-192.
- Caldwell, D. R., 1974. Thermal Conductivity of Sea Water, *Deep Sea Research and Oceanographic Abstracts*, 21(2): 131-137.
- Canevari, G. P., 1982. The Formulation of an Effective Demulsifier for Oil Spill Emulsions, *Marine Pollution Bulletin*, 13(2): 49-54.

- Carmichael, L. T., Berry, V. M. and Sage, B. H., 1964. Viscosity of Hydrocarbons. Propane, *Journal of Chemical & Engineering Data*, 9(3): 411-415.
- Çengel, Y. A. and Ghajar, A. J., 2011. *Heat and Mass Transfer: Fundamentals and Applications* (4th Edition ed.), McGraw-Hill, New York, 928 p.
- Chang, S. E., Stone, J., Demes, K. and Piscitelli, M., 2014. Consequences of Oil Spills: A Review and Framework for Informing Planning, *Ecology and Society*, 19(2): 26.
- Chen, X., Lu, S., Li, C., Zhang, J. and Liew, K. M., 2014. Experimental Study on Ignition and Combustion Characteristics of Typical Oils, *Fire and Materials*, 38(3): 409-417.
- Chevron, 2011. AODR Submission Part 2: Responses to NEB Calls for Information 1 and 2, Chevron Canada Limited, Calgary, Alberta, 88 p.
- Chickos, J. S. and Hanshaw, W., 2004. Vapor Pressures and Vaporization Enthalpies of the N-Alkanes from C21 to C30 at T = 298.15 K by Correlation Gas Chromatography, *Journal of Chemical & Engineering Data*, 49(1): 77-85.
- Christensen, J. H., Hansen, A. B., Karlson, U., Mortensen, J. and Andersen, O., 2005. Multivariate Statistical Methods for Evaluating Biodegradation of Mineral Oil, *Journal of Chromatography A*, 1090(1–2): 133-145.
- Christensen, J. H. and Tomasi, G., 2007. Practical Aspects of Chemometrics for Oil Spill Fingerprinting, *Journal of Chromatography A*, 1169(1–2): 1-22.
- Christensen, J. H., Tomasi, G., Scofield, A. d. L. and Meniconi, M. d. F. G., 2010. A Novel Approach for Characterization of Polycyclic Aromatic Hydrocarbon (Pah) Pollution Patterns in Sediments from Guanabara Bay, Rio De Janeiro, Brazil, *Environmental Pollution*, 158(10): 3290-3297.
- Clarke, A. D. and Noone, K. J., 1985. Soot in the Arctic Snowpack: A Cause for Perturbations in Radiative Transfer, *Atmospheric Environment (1967)*, 19(12): 2045-2053.
- Council, A., 2016. The Arctic Council: A Background. Arctic Council Secretariat, Retrieved 24th of December, 2016, from [www.arctic-council.org/index.php/en/about-us](http://www.arctic-council.org/index.php/en/about-us).
- Daling, P. S., Faksness, L.-G., Hansen, A. B. and Stout, S. A., 2002. Improved and Standardized Methodology for Oil Spill Fingerprinting, *Environmental Forensics*, 3(3-4): 263-278.
- Daling, P. S., Moldestad, M. Ø., Johansen, Ø., Lewis, A. and Rødal, J., 2003. Norwegian Testing of Emulsion Properties at Sea—the Importance of Oil Type and Release Conditions, *Spill Science & Technology Bulletin*, 8(2): 123-136.

- Daling, P. S., Holumsnes, A., Rasmussen, C., Brandvik, P. J. and Leirvik, F., 2010. Development and Testing of a Containerized Dispersant Spray System for Use in Cold and Ice-Covered Area, SINTEF, Trondheim, Norway, 13, 61 p.
- Day, T., Mackay, D., Nadeau, S. and Thurier, R., 1979. Emissions from In Situ Burning of Crude Oil in the Arctic, *Water, Air, and Soil Pollution*, 11(2): 139-152.
- Daykin, M., Sergy, G., Aurand, D., Shigenaka, G., Want, Z. and Tang, A., 1994. Aquatic Toxicity Resulting from *In Situ* Burning of Oil-on-Water, in *Proceedings of the Seventeenth Arctic and Marine Oil Spill Program (AMOP) Technical Seminar*, Environment Canada, p. 1165-1193.
- DG environment, 2009. Properties of Russian Oils and the Applicability of Dispersants, European Commission, 67 p.
- Drysdale, D., 2011. Diffusion Flames and Fire Plumes in *An Introduction to Fire Dynamics*, John Wiley & Sons, Ltd, New York, pp. 121-179.
- Drysdale, D. D., 2016. Ignition of Liquids in *SFPE Handbook of Fire Protection Engineering*, M. J. Hurley, D. T. Gottuk, J. R. Hall Jr, K. Harada, E. D. Kuligowski, M. Puchovsky, J. L. Torero, J. M. Watts Jr and C. J. Wieczorek (Eds.), Springer New York, New York, NY, pp. 554-580.
- Egloff, G., Sherman, J. and Dull, R. B., 1940. Boiling Point Relationships Among Aliphatic Hydrocarbons, *The Journal of Physical Chemistry*, 44(6): 730-745.
- Emmons, H. W., 1956. The Film Combustion of Liquid Fuel, *ZAMM - Journal of Applied Mathematics and Mechanics / Zeitschrift für Angewandte Mathematik und Mechanik*, 36(1-2): 60-71.
- EPPR, 2015. Guide to Oil Spill Response in Snow and Ice Conditions in the Arctic, Emergency Prevention, Preparedness and Response (EPPR), 184 p.
- Evans, D. D., Mulholland, G. W., Gross, H., Baum, H. and Saito, K., 1988. Burning, Smoke Production, and Smoke Dispersion from Oil Spill Combustion, in *Proceedings of the Eleventh Arctic and Marine Oilspill Program (AMOP) Technical Seminar*, Environment Canada, Ottawa, ON, Canada, p. 41-87.
- Evans, D. D., Walton, W., Baum, H., Notarianni, K. A., Lawson, J. R., Tang, H. C., Keydel, K. R., Rehm, R. G., Madrzykowski, D. and Zile, R. H., 1992. In Situ Burning of Oil Spills: Mesoscale Experiments, in *Proceedings of the Fifteenth Arctic and Marine Oilspill Program (AMOP) Technical Seminar*, Environment Canada, Ottawa, ON, Canada, p. 593-657.
- Faksness, L.-G., Brandvik, P. J. and Sydnes, L. K., 2008. Composition of the Water Accommodated Fractions as a Function of Exposure Times and Temperatures, *Marine Pollution Bulletin*, 56: 1746-1754.
- Faksness, L.-G., Hansen, B. H., Altin, D. and Brandvik, P. J., 2012. Chemical Composition and Acute Toxicity in the Water after In Situ Burning - a Laboratory Experiment, *Marine Pollution Bulletin*, 64(1): 49-55.

- Fan, T., Wang, J. and Buckley, J. S., 2002. *Evaluating Crude Oils by SARA Analysis*. Paper presented at the SPE/DOE Improved Oil Recovery Symposium, Society of Petroleum Engineers, p. 1-7.
- Farmahini Farahani, H., Jomaas, G. and Rangwala, A. S., 2015a. Effects of Convective Motion in n-Octane Pool Fires in an Ice Cavity, *Combustion and Flame*, 162(12): 4643-4648.
- Farmahini Farahani, H., Shi, X., Simeoni, A. and Rangwala, A. S., 2015b. A Study on Burning of Crude Oil in Ice Cavities, *Proceedings of the Combustion Institute*, 35(3): 2699-2706.
- Federal Interagency Solutions Group, 2010. Oil Budget Calculator Deepwater Horizon, NOAA, 217 p.
- Fingas, M., Fieldhouse, B. and Wang, Z., 2003. The Long Term Weathering of Water-in-Oil Emulsions, *Spill Science & Technology Bulletin*, 8(2): 137-143.
- Fingas, M. and Fieldhouse, B., 2009. Studies on Crude Oil and Petroleum Product Emulsions: Water Resolution and Rheology, *Colloids and Surfaces A: Physicochemical and Engineering Aspects*, 333(1-3): 67-81.
- Fingas, M., 2011a. Introduction to Oil Chemistry and Properties in *Oil Spill Science and Technology*, M. Fingas (Ed.), Gulf Professional Publishing, Oxford, pp. 51-59.
- Fingas, M., 2011b. Introduction to Oil Chemical Analysis in *Oil Spill Science and Technology*, M. Fingas (Ed.), Gulf Professional Publishing, Oxford, pp. 87-109.
- Fingas, M., 2011c. Chapter 12 - Physical Spill Countermeasures in *Oil Spill Science and Technology*, Gulf Professional Publishing, Boston, pp. 303-337.
- Fingas, M. F., Li, K., Ackerman, F., Bissonnette, M. C., Lambert, P., Nelson, R., Halley, G., Campagna, P. R., Laroche, N., Jokuty, P., Turpin, R. D., Trespalacios, M. J., Belanger, J., Vanderkooy, N., Tennyson, E. J., Aurand, D. and Hiltrabrand, R., 1994a. The Newfoundland Offshore Burn Experiment - NOBE, in *In Situ Burning Oil Spill Workshop Proceedings*, NIST, Gaithersburg, p. 63-70.
- Fingas, M. F., Li, K., Campagna, P. R., Turpin, R. D., Ackerman, F., Bissonnette, M. C., Lambert, P., Getty, S. J., Trespalacios, M. J., Belanger, J. and Tennyson, E. J., 1994b. Emissions from In Situ Oil Fires, in *In Situ Burning Oil Spill Workshop Proceedings*, National Institute of Standards and Technology and Minerals Management Service, p. 39-46.
- Fitzpatrick, M., 1985. *U.S. Coast Guard Arctic Pollution Response Research and Development*. Paper presented at the OCEANS '85 - Ocean Engineering and the Environment, IEEE, San Diego, CA, USA, p. 863-865.
- Free, A. P., Cox, J. C. and Schultz, L. A., 1981. Laboratory Studies of Oil Spill Behaviour in Broken Ice Fields, Environment Canada, Ottawa, ON, 1-21 p.

- Fritt-Rasmussen, J. and Brandvik, P. J., 2011. Measuring Ignitability for In Situ Burning of Oil Spills Weathered under Arctic Conditions: From Laboratory Studies to Large-Scale Field Experiments, *Marine Pollution Bulletin*, 62(8): 1780-1785.
- Fritt-Rasmussen, J., Brandvik, P. J., Villumsen, A. and Stenby, E. H., 2012. Comparing Ignitability for In Situ Burning of Oil Spills for an Asphaltenic, a Waxy and a Light Crude Oil as a Function of Weathering Conditions under Arctic Conditions, *Cold Regions Science and Technology*, 72(0): 1-6.
- Fritt-Rasmussen, J., Ascanius, B. E., Brandvik, P. J., Villumsen, A. and Stenby, E. H., 2013a. Composition of In Situ Burn Residue as a Function of Weathering Conditions, *Marine Pollution Bulletin*, 67(1-2): 75-81.
- Fritt-Rasmussen, J., Wegeberg, S., Boertmann, D., Clausen, D. S., Johansen, K. L. and Mosbech, A., 2013b. Net Environmental Benefit Analysis as a Decision Tool for Greenlandic Oil Spill Response, in *Proceedings of the Thirty-sixth Arctic and Marine Oilspill Program (AMOP) Technical Seminar*, Environment Canada, Ottawa, ON, p. 765-776.
- Fritt-Rasmussen, J., Wegeberg, S. and Gustavson, K., 2015. Review on Burn Residues from In Situ Burning of Oil Spills in Relation to Arctic Waters, *Water, Air, & Soil Pollution*, 226(10): 329.
- Fritt-Rasmussen, J., Linnebjerg, J. F., Sørensen, M. X., Brogaard, N. L., Rigét, F. F., Kristensen, P., Jomaas, G., Boertmann, D. M., Wegeberg, S. and Gustavson, K., 2016. Effects of Oil and Oil Burn Residues on Seabird Feathers, *Marine Pollution Bulletin*, 109(1): 446-452.
- Gallotta, F. D. C. and Christensen, J. H., 2012. Source Identification of Petroleum Hydrocarbons in Soil and Sediments from Iguaçú River Watershed, Paraná, Brazil Using the Chemsic Method (Chemometric Analysis of Selected Ion Chromatograms), *Journal of Chromatography A*, 1235: 149-158.
- Gardiner, W. W., Word, J. Q., Word, J. D., Perkins, R. A., McFarlin, K. M., Hester, B. W., Word, L. S. and Ray, C. M., 2013. The Acute Toxicity of Chemically and Physically Dispersed Crude Oil to Key Arctic Species under Arctic Conditions During the Open Water Season, *Environmental Toxicology and Chemistry*, 32(10): 2284-2300.
- Garo, J. P., Vantelon, J. P. and Fernandez-Pello, A. C., 1994. Boilover Burning of Oil Spilled on Water, *Symposium (International) on Combustion*, 25(1): 1481-1488.
- Garo, J. P., Vantelon, J. P. and Fernande-Pello, A. C., 1996. Effect of the Fuel Boiling Point on the Boilover Burning of Liquid Fuels Spilled on Water, *Symposium (International) on Combustion*, 26(1): 1461-1467.
- Garo, J. P., Gillard, P., Vantelon, J. P. and Fernandez-Pello, A. C., 1999a. Combustion of Liquid Fuels Spilled on Water. Prediction of Time to Start of Boilover, *Combustion Science and Technology*, 147(1-6): 39-59.
- Garo, J. P., Vantelon, J. P., Gandhi, S. and Torero, J. L., 1999b. Determination of the Thermal Efficiency of Pre-Boilover Burning of a Slick of Oil on Water, *Spill Science & Technology Bulletin*, 5(2): 141-151.

- Garrett, R. M., Guénette, C. C., Haith, C. E. and Prince, R. C., 2000. Pyrogenic Polycyclic Aromatic Hydrocarbons in Oil Burn Residues, *Environmental Science & Technology*, 34(10): 1934-1937.
- Garrett, W. D., 1969. Confinement and Control of Oil Pollution on Water with Monomolecular Surface Films, *International Oil Spill Conference Proceedings*, 1969(1): 257-261.
- Garrett, W. D. and Barger, W. R., 1970. Factors Affecting the Use of Monomolecular Surface Films to Control Oil Pollution on Water, *Environmental Science & Technology*, 4(2): 123-127.
- Gautier, D. L., Bird, K. J., Charpentier, R. R., Grantz, A., Houseknecht, D. W., Klett, T. R., Moore, T. E., Pitman, J. K., Schenk, C. J., Schuenemeyer, J. H., Sørensen, K., Tennyson, M. E., Valin, Z. C. and Wandrey, C. J., 2009. Assessment of Undiscovered Oil and Gas in the Arctic, *Science*, 324(5931): 1175-1179.
- Glassman, I. and Dryer, F. L., 1981. Flame Spreading across Liquid Fuels, *Fire Safety Journal*, 3(3): 123-138.
- Gottuk, D. T., Roby, R. J., Peatross, M. J. and Beyler, C. L., 1992. Carbon Monoxide Production in Compartment Fires, *Journal of Fire Protection Engineering*, 4(4): 133-150.
- Groenzin, H. and Mullins, O. C., 2000. Molecular Size and Structure of Asphaltenes from Various Sources, *Energy & Fuels*, 14(3): 677-684.
- Guénette, C. C., Sveum, P., Buist, I., Aunaas, T. and Godal, L., 1994. In-Situ Burning of Water-in-Oil Emulsions, Marine Spill Response Corporation, Washington D.C., 139 p.
- Guénette, C. C. and Sveum, P., 1995. In Situ Burning of Emulsions R&D in Norway, *Spill Science & Technology Bulletin*, 2(1): 75-77.
- Guénette, C. C., Sveum, P., Bech, C. M. and Buist, I. A., 1995. Studies of In Situ Burning of Emulsions in Norway, *International Oil Spill Conference Proceedings*, 1995(1): 115-122.
- Guénette, C. C. and Wighus, R., 1996. In-Situ Burning of Crude Oil and Emulsions in Broken Ice, in *Proceedings of the Nineteenth Arctic and Marine Oilspill Program (AMOP) Technical Seminar*, Environment Canada, Ottawa, Ontario, p. 895-906.
- Gulec, I. and Holdway, D. A., 1999. The Toxicity of Laboratory Burned Oil to the Amphipod *Allorchestes compressa* and the Snail *Polinices conicus*, *Spill Science & Technology Bulletin*, 5(2): 135-139.
- Hamins, A., Fischer, S. J., Kashiwagi, T., Klassen, M. E. and Gore, J. P., 1994. Heat Feedback to the Fuel Surface in Pool Fires, *Combustion Science and Technology*, 97(1-3): 37-62.
- Hamins, A., Kashiwagi, T. and Burch, R. R., 1995. *Characteristics of Pool Fire Burning*. Paper presented at the Fire Resistance of Industrial Fluids, ASTM International, Indianapolis, IN, p. 15-41.
- Heskestad, G., 1983. Luminous Heights of Turbulent Diffusion Flames, *Fire Safety Journal*, 5(2): 103-108.

- Heskestad, G., 2016. Fire Plumes, Flame Height, and Air Entrainment in *SFPE Handbook of Fire Protection Engineering*, M. J. Hurley, D. T. Gottuk, J. R. Hall Jr, K. Harada, E. D. Kuligowski, M. Puchovsky, J. L. Torero, J. M. Watts Jr and C. J. Wieczorek (Eds.), Springer New York, New York, NY, pp. 396-428.
- Holland-Bartels, L. and Pierce, B., 2011. An Evaluation of the Science Needs to Inform Decisions on Outer Continental Shelf Energy Development in the Chukchi and Beaufort Seas, Alaska, U.S. Geological Survey Circular 1370, 278 p.
- Hottel, H. C., 1958. Review - Certain Laws Governing Diffusive Burning of Liquids, by V. I. Blinov and G. N. Khudiakov, *Fire Research Abstracts and Reviews*, 1: 41-44.
- Hristov, J., Planas-Cuchi, E., Arnaldos, J. and Casal, J., 2004. Accidental Burning of a Fuel Layer on a Waterbed: A Scale Analysis of the Models Predicting the Pre-Boilover Time and Tests to Published Data, *International Journal of Thermal Sciences*, 43(3): 221-239.
- Ikegami, M., Xu, G., Ikeda, K., Honma, S., Nagaishi, H., Dietrich, D. L. and Takeshita, Y., 2003. Distinctive Combustion Stages of Single Heavy Oil Droplet under Microgravity, *Fuel*, 82(3): 293-304.
- ITOPF, 2016. The ITOPF Limited Handbook 2016/17, International Tanker Owners Pollution Federation, London, 55 p.
- Jacobsen, S., 2015. RPT-Statoil Hands Back Three Greenland Exploration Licences. Reuters, *Retrieved 3rd of January, 2017*, from [www.reuters.com/article/statoil-greenland-idUSL6NOUT33R20150114](http://www.reuters.com/article/statoil-greenland-idUSL6NOUT33R20150114).
- Kontogeorgis, G. and Kiil, S., 2016a. *Introduction to Applied Colloid and Surface Chemistry*, John Wiley & Sons, Ltd, 367 p.
- Kontogeorgis, G. M. and Kiil, S., 2016b. Surface and Interfacial Tensions – Principles and Estimation Methods in *Introduction to Applied Colloid and Surface Chemistry*, John Wiley & Sons, Ltd, pp. 34-73.
- Korsten, H., 2001. Viscosity of Liquid Hydrocarbons and Their Mixtures, *AIChE Journal*, 47(2): 453-462.
- Koseki, H. and Mulholland, G. W., 1991. The Effect of Diameter on the Burning of Crude Oil Pool Fires, *Fire Technology*, 27(1): 54-65.
- Lane, P., Newsom, P., Buist, I. A., Nedwed, T., Tidwell, A. and Flagg, K., 2012. Recent Efforts to Develop and Commercialize Oil Herders, in *Proceedings of the Thirty-fifth Arctic and Marine Oilspill Program (AMOP) Technical Seminar*, Environment Canada, Ottawa, ON, Canada, p. 472-479.
- Law, C. K., 1976. Multicomponent Droplet Combustion with Rapid Internal Mixing, *Combustion and Flame*, 26(0): 219-233.
- Law, C. K., 1977. A Model for the Combustion of Oil/Water Emulsion Droplets, *Combustion Science and Technology*, 17(1-2): 29-38.

Law, C. K., 1978. Internal Boiling and Superheating in Vaporizing Multicomponent Droplets, *AIChE Journal*, 24(4): 626-632.

Law, C. K., 2006. *Combustion Physics*, Cambridge University Press, New York, 722 p.

Lee, K., Nedwed, T., Prince, R. C. and Palandro, D., 2013. Lab Tests on the Biodegradation of Chemically Dispersed Oil Should Consider the Rapid Dilution That Occurs at Sea, *Marine Pollution Bulletin*, 73(1): 314-318.

Lee, R. F., 1999. Agents Which Promote and Stabilize Water-in-Oil Emulsions, *Spill Science & Technology Bulletin*, 5(2): 117-126.

Lewis, A., Daling, P. S., Strøm-Kristiansen, T., Nordvik, A. B. and Fiocco, R. J., 1995. Weathering and Chemical Dispersion of Oil at Sea, *International Oil Spill Conference Proceedings*, 1995(1): 157-164.

Lewis, A. and Daling, P. S., 2007. Evaluation of Dispersant Spray Systems and Platforms for Use on Spilled Oil in Seas with Ice Present, SINTEF, Trondheim, Norway, 12, 21 p.

Mackay, D., Stiver, W. and Tebeau, L. C. P. A., 1983. Testing of Crude Oils and Petroleum Products for Environmental Purposes, *International Oil Spill Conference Proceedings*, 1983(1): 331-337.

Mackay, D., 1987. Formation and Stability of Water-in-Oil Emulsions, Environment Canada, Ottawa, ON, 42 p.

Maersk Oil, 2005. DUC Crude Oil. Maersk Olie og Gas AS, Retrieved 1st of January, 2017, from [www.maerskoil.com/about-us/Documents/Sales/DUCassay.xls](http://www.maerskoil.com/about-us/Documents/Sales/DUCassay.xls).

Makino, A. and Law, C. K., 1988. On the Controlling Parameter in the Gasification Behavior of Multicomponent Droplets, *Combustion and Flame*, 73(3): 331-336.

Malmquist, L. M. V., Olsen, R. R., Hansen, A. B., Andersen, O. and Christensen, J. H., 2007. Assessment of Oil Weathering by Gas Chromatography–Mass Spectrometry, Time Warping and Principal Component Analysis, *Journal of Chromatography A*, 1164(1–2): 262-270.

Margesin, R. and Schinner, F., 2001. Biodegradation and Bioremediation of Hydrocarbons in Extreme Environments, *Applied Microbiology and Biotechnology*, 56(5): 650-663.

McGrattan, K. B., Putorti, A. D., Twilley, W. H. and Evans, D. D., 1993. Smoke Plume Trajectory from In Situ Burning of Crude Oil in Alaska, National Institute of Standards and Technology (NIST), Springfield, 65 p.

McGrattan, K. B., Walton, W. D. and Evans, D. D., 1997. Smoke Plumes from In-Situ Burning of Crude Oil, *International Oil Spill Conference Proceedings*, 1997(1): 137-147.

McLean, J. D. and Kilpatrick, P. K., 1997. Effects of Asphaltene Solvency on Stability of Water-in-Crude-Oil Emulsions, *Journal of Colloid and Interface Science*, 189(2): 242-253.

- McLeod, W. R. and McLeod, D. L., 1972. *Measures to Combat Offshore Arctic Oil Spills*. Offshore Technology Conference, p. 141-162.
- MLSA, 2016. List of Mineral and Petroleum Licences in Greenland, Mineral Licence and Safety Authority (MLSA), Nuuk, Greenland, 21 p.
- Moldestad, M. Ø. and Lewis, A., 2006. Oil Weathering and Oils Transported in the North Sea, SINTEF, Trondheim, Report No. 4, 129 p.
- MPE, 2016. Announcement 23rd Licensing Round Awards. Ministry of Petroleum and Energy (MPE), Retrieved 18th of October, 2016, from [www.regjeringen.no/en/aktuelt/announcement-23rd-licensing-round-awards/id2500936/](http://www.regjeringen.no/en/aktuelt/announcement-23rd-licensing-round-awards/id2500936/).
- Mudan, K. S., 1984. Thermal Radiation Hazards from Hydrocarbon Pool Fires, *Progress in Energy and Combustion Science*, 10(1): 59-80.
- Mulholland, G. W., Liggett, W. and Koseki, H., 1996. The Effect of Pool Diameter on the Properties of Smoke Produced by Crude Oil Fires, *Symposium (International) on Combustion*, 26(1): 1445-1452.
- Mullin, J., Belore, R. and Trudel, D. K., 2008. Cold Water Dispersant Effectiveness Experiments Conducted at Ohmsett with Alaskan Crude Oils Using Corexit 9500 and 9527 Dispersants, *International Oil Spill Conference Proceedings*, 2008(1): 817-822.
- Mullin, J., 2012. *The Oil and Gas Industry's Commitment to Responsible Arctic Operations: An Innovative Arctic Oil Spill Response Technology - Joint Industry Programme*. Paper presented at the Arctic Technology Conference, Offshore Technology Conference, Houston, TX, p. 1-6.
- National Research Council, 2005. *Oil Spill Dispersants: Efficacy and Effects*, The National Academies Press, Washington, DC, 400 p.
- National Research Council, 2014. *Responding to Oil Spills in the U.S. Arctic Marine Environment*, The National Academies Press, Washington, D.C., xiv + 195 p.
- Nedwed, T., Belore, R., Spring, W. and Blanchet, D., 2007. Basin-Scale Testing of ASD Icebreaker Enhanced Chemical Dispersion of Oil Spills, in *Proceedings of the Thirtieth Arctic and Marine Oilspill Program (AMOP) Technical Seminar*, Environment Canada, Ottawa, ON (Canada), p. 151-160.
- Nisbet, I. C. T. and LaGoy, P. K., 1992. Toxic Equivalency Factors (TEFs) for Polycyclic Aromatic Hydrocarbons (PAHs), *Regulatory Toxicology and Pharmacology*, 16(3): 290-300.
- Nolan, D. P., 2011. 4 - Physical Properties of Hydrocarbons in *Handbook of Fire and Explosion Protection Engineering Principles (Second Edition)*, William Andrew Publishing, Oxford, pp. 33-48.

NORCOR, Engineering & Research Ltd., 1975. The Interaction of Crude Oil with Arctic Sea Ice, Department of the Environment, Victoria, B.C., 145 p.

Nordvik, A. B., 1995. The Technology Windows-of-Opportunity for Marine Oil Spill Response as Related to Oil Weathering and Operations, *Spill Science & Technology Bulletin*, 2(1): 17-46.

Nordvik, A. B., Champ, M. A. and Bitting, K. R., 2003. Estimating Time Windows for Burning Oil at Sea: Processes and Factors, *Spill Science & Technology Bulletin*, 8(4): 347-359.

Nuka, Research & Planning Group, LLC., 2010. Oil Spill Prevention and Response in the U.S. Arctic Ocean: Unexamined Risks, Unacceptable Consequences, The PEW Environment Group, Washington, D.C., 136 p.

Osborne, N. S. and Ginnings, D. C., 1947. Measurements of Heat of Vaporization and Heat Capacity of a Number of Hydrocarbons, *Journal of Research of the National Institute of Standards and Technology*, 39: 453-477.

Peterson, C. H., Rice, S. D., Short, J. W., Esler, D., Bodkin, J. L., Ballachey, B. E. and Irons, D. B., 2003. Long-Term Ecosystem Response to the Exxon Valdez Oil Spill, *Science*, 302(5653): 2082.

Petty, S. E., 1983. Combustion of Crude Oil on Water, *Fire Safety Journal*, 5(2): 123-134.

Piacente, V., Fontana, D. and Scardala, P., 1994. Enthalpies of Vaporization of a Homologous Series of n-Alkanes Determined from Vapor Pressure Measurements, *Journal of Chemical & Engineering Data*, 39(2): 231-237.

Porter, D. J., Mayer, P. M. and Fingas, M., 2004. Analysis of Petroleum Resins Using Electrospray Ionization Tandem Mass Spectrometry, *Energy & Fuels*, 18(4): 987-994.

Potter, S., 2010a. Tests of Fire-Resistant Booms in Low Concentrations of Drift Ice - Field Experiments May 2008., SINTEF, Trondheim, Report No. 5, 23 p.

Potter, S., 2010b. Tests of Fire-Resistant Booms in Low Concentrations of Drift Ice - Field Experiments May 2009., SINTEF, Trondheim, Report No. 27, 17 p.

Potter, S., Buist, I. A., Trudel, B. K., Dickins, D. and Owens, E., 2012. Spill Response in the Arctic Offshore, American Petroleum Institute, Washington, D.C., 157 p.

Potter, S. G., Buist, I. A., Trudel, B. K., Walker, A. H., Brandvik, P. J., Fritt-Rasmussen, J. and Allen, A. A., 2013. In Situ Burning in Ice-Affected Waters: Status of Regulations in Arctic and Sub-Arctic Countries, *Arctic Response Technology*, 15 p.

Prosen, E. J. and Rossini, F. D., 1945. Heats of Combustion and Formation of the Paraffin Hydrocarbons at 25 C, *Journal of Research of the National Institute of Standards and Technology*, 34: 263-269.

Quintiere, J., 1981. A Simplified Theory for Generalizing Results from a Radiant Panel Rate of Flame Spread Apparatus, *Fire and Materials*, 5(2): 52-60.

- Quintiere, J. G., 2006. Ignition of Solids in *Fundamentals of Fire Phenomena*, John Wiley & Sons, Ltd, pp. 159-190.
- Randolph, A. L., Makino, A. and Law, C. K., 1988. Liquid-Phase Diffusional Resistance in Multicomponent Droplet Gasification, *Symposium (International) on Combustion*, 21(1): 601-608.
- Reijnhart, R. and Rose, R., 1982. Evaporation of Crude Oil at Sea, *Water Research*, 16(8): 1319-1325.
- Ross, J. L., Ferek, R. J. and Hobbs, P. V., 1996. Particle and Gas Emissions from an In Situ Burn of Crude Oil on the Ocean, *Journal of the Air & Waste Management Association*, 46(3): 251-259.
- Růžička, K. and Majer, V., 1994. Simultaneous Treatment of Vapor Pressures and Related Thermal Data between the Triple and Normal Boiling Temperatures for n-Alkanes C5–C20, *Journal of Physical and Chemical Reference Data*, 23(1): 1-39.
- Santodonato, J., Howard, P. and Basu, D., 1981. Health and Ecological Assessment of Polynuclear Aromatic Hydrocarbons, *Journal of Environmental Pathology and Toxicology*, 5(1): 1-364.
- Sartz, P. and Aggarwal, S., 2016. Gaseous Emissions from Herding Agent-Mediated In-Situ Burning for Arctic Oil Spills, in *Proceedings of the Thirty-ninth Arctic and Marine Oilspill Program (AMOP) Technical Seminar*, Environment and Climate Change Canada, Ottawa, ON, p. 735-750.
- Schuler, B., Meyer, G., Peña, D., Mullins, O. C. and Gross, L., 2015. Unraveling the Molecular Structures of Asphaltenes by Atomic Force Microscopy, *Journal of the American Chemical Society*, 137(31): 9870-9876.
- Seaton, W. H. and Keith Harrison, B., 1990. A New General Method for Estimation of Heats of Combustion for Hazard Evaluation, *Journal of Loss Prevention in the Process Industries*, 3(3): 311-320.
- Shell, 2011. Gasoline Safety Data Sheet, Shell Trading International Limited, 51 p.
- Shell, 2015. Shell Updates on Alaska Exploration. Royal Dutch Shell, Retrieved 18th of October, 2016, from [www.shell.com/media/news-and-media-releases/2015/shell-updates-on-alaska-exploration.html](http://www.shell.com/media/news-and-media-releases/2015/shell-updates-on-alaska-exploration.html).
- Shi, X., Bellino, P. W., Simeoni, A. and Rangwala, A. S., 2016. Experimental Study of Burning Behavior of Large-Scale Crude Oil Fires in Ice Cavities, *Fire Safety Journal*, 79: 91-99.
- Shigenaka, G., 2011. Effects of Oil in the Environment in *Oil Spill Science and Technology*, Chap. 27, M. Fingas (Ed.), Gulf Professional Publishing, Oxford, pp. 985-1024.
- Shigenaka, G., 2014. Twenty-Five Years after the *Exxon Valdez* Oil Spill: NOAA's Scientific Support, Monitoring and Research, NOAA Office of Response and Restoration, Seattle, 78 p.
- Short, J. W., Lindeberg, M. R., Harris, P. M., Maselko, J. M., Pella, J. J. and Rice, S. D., 2004. Estimate of Oil Persisting on the Beaches of Prince William Sound 12 Years after the Exxon Valdez Oil Spill, *Environmental Science & Technology*, 38(1): 19-25.

Siltech, 2012. Material Safety Data Sheet of Siltech OP-40, Siltech Corp., Toronto, ON, Canada, MSDS NR: 3120.4, 4 p.

Singsaas, I., Brandvik, P. J., Daling, P. S., Reed, M. and Lewis, A., 1994. Fate and Behaviour of Oils Spilled in the Presence of Ice - a Comparison of the Results from Recent Laboratory, Meso-Scale Flume and Field Tests, in *Proceedings of the seventeenth Arctic and Marine Oilspill Program (AMOP) Technical Seminar*, Environment Canada, p. 355-370.

Skoog, D. A., Holler, F. J. and Crouch, S. R., 2007. *Principles of Instrumental Analysis* (6th ed.), Thomson Brooks/Cole, 1039 p.

SL Ross, 2007. Mid-Scale Test Tank Research on Using Oil Herding Surfactants to Thicken Oil Slicks in Broken Ice, Bureau of Safety and Environmental Enforcement (BSEE), 67 p.

SL Ross, 2012. Research on Using Oil Herding Agents for Rapid Response In Situ Burning of Oil Slicks on Open Water, Bureau of Safety and Environmental Enforcement (BSEE), Washington D.C., 95 p.

SL Ross, Environmental Research Ltd. and DF Dickins, Associates Ltd., 1987. Field Research Spills to Investigate the Physical and Chemical Fate of Oil in Pack Ice, Environmental Studies Revolving Funds, Ottawa, Report No. 62, 118 p.

Spalding, D. B., 1955. *Some Fundamentals of Combustion*, Butterworths, London, 250 p.

Spalding, D. B., 1962. The Burning Rate of Liquid Fuels from Open Trays by Natural Convection, *Fire Research Abstracts and Reviews*, 4: 234-236.

Spring, W., Nedwed, T. and Belore, R., 2006. Icebreaker Enhanced Chemical Dispersion of Oil Spills, in *Proceedings of the Twenty-ninth Arctic and Marine Oilspill Program (AMOP) Technical Seminar*, Environment Canada, Ottawa, ON, p. 711-727.

Statoil, 2017. Grane Blend. Statoil, Retrieved 1st of January, 2017, from [www.statoil.com/en/OurOperations/TradingProducts/CrudeOil/Crudeoilassays/Downloads/GRANE%20BLEND%202017%2001.xls](http://www.statoil.com/en/OurOperations/TradingProducts/CrudeOil/Crudeoilassays/Downloads/GRANE%20BLEND%202017%2001.xls).

Sørheim, K. R. and Moldestad, M. Ø., 2008. Weathering Properties of the Goliat Kobbe and Two Goliat Blend of Kobbe and Realgrunnen Crude Oils, SINTEF, Trondheim, 95 p.

Sørstrøm, S. E., Brandvik, P. J., Buist, I. A., Daling, P. S., Dickins, D., Faksness, L.-G., Potter, S., Fritt-Rasmussen, J. and Singaas, I., 2010. Joint Industry Program on Oil Spill Contingency for Arctic and Ice-Covered Waters - Summary Report, SINTEF, Trondheim, Report No. 32, 40 p.

Tanaka, Y., Itani, Y., Kubota, H. and Makita, T., 1988. Thermal Conductivity of Five Normal Alkanes in the Temperature Range 283–373 K at Pressures up to 250 MPa, *International Journal of Thermophysics*, 9(3): 331-350.

- Tebeau, P. A., Meehan, T. M. and Saepoff, S. A., 1984. A Laboratory Study of Oil Spreading under Arctic Conditions, Environment Canada, Ottawa, ON, 22-34 p.
- Tewarson, A., 1982. Experimental Evaluation of Flammability Parameters of Polymeric Materials in *Flame - Retardant Polymeric Materials: Volume 3*, M. Lewin, S. M. Atlas and E. M. Pearce (Eds.), Springer New York, Boston, MA, pp. 97-153.
- Tewarson, A., Jiang, F. H. and Morikawa, T., 1993. Ventilation-Controlled Combustion of Polymers, *Combustion and Flame*, 95(1): 151-169.
- Torero, J., 2016. Flaming Ignition of Solid Fuels in *SFPE Handbook of Fire Protection Engineering*, M. J. Hurley, D. T. Gottuk, J. R. Hall Jr, K. Harada, E. D. Kuligowski, M. Puchovsky, J. L. Torero, J. M. Watts Jr and C. J. Wiecek (Eds.), Springer New York, New York, NY, pp. 633-661.
- Torero, J. L., Olenick, S. M., Garo, J. P. and Vantelon, J. P., 2003. Determination of the Burning Characteristics of a Slick of Oil on Water, *Spill Science & Technology Bulletin*, 8(4): 379-390.
- Vali, A., Nobes, D. S. and Kostiuik, L. W., 2015. Fluid Motion and Energy Transfer within Burning Liquid Fuel Pools of Various Thicknesses, *Combustion and Flame*, 162(4): 1477-1488.
- Vetere, A., 1979. New Correlations for Predicting Vaporization Enthalpies of Pure Compounds, *The Chemical Engineering Journal*, 17(2): 157-162.
- Walavalkar, A. Y. and Kulkarni, A. K., 2001. Combustion of Water-in-Oil Emulsion Layers Supported on Water, *Combustion and Flame*, 125(1-2): 1001-1011.
- Wang, C. H., Liu, X. Q. and Law, C. K., 1984. Combustion and Microexplosion of Freely Falling Multicomponent Droplets, *Combustion and Flame*, 56(2): 175-197.
- Wang, Z., Hollebone, B. P., Fingas, M., Fieldhouse, B., Sigouin, L., Landriault, M., Smith, P., Noonan, J., Thouin, G. and Weaver, J. W., 2003. Characteristics of Spilled Oils, Fuels and Petroleum Products: 1. Composition and Properties of Selected Oils, Environmental Protection Agency, Washington, D.C., 286 p.
- Wang, Z., Fingas, M., Yang, C. and Christensen, J. H., 2006. Crude Oil and Refined Product Fingerprinting: Principles in *Environmental Forensics*, Chap. 16, R. D. Morrison and B. L. Murphy (Eds.), Academic Press, Burlington, pp. 339-407.
- Westphal, P., Taylor, E. and Aurand, D., 1994. Human Health Risk Associated with Burning as a Spill Countermeasure, in *Proceedings of the Seventeenth Arctic and Marine Oil Spill Program (AMOP) Technical Seminar*, Environment Canada, Ottawa, ON, p. 685-705.
- Winoto, Loahardjo, N., Takamura, K. and Morrow, N. R., 2014. Spreading and Retraction of Spilled Crude Oil on Seawater, *International Oil Spill Conference Proceedings*, 2014(1): 1465-1473.

WMO, 2014. WMO Sea Ice Nomenclature, World Meteorological Organization, I-III: 121 p.

Woolfenden, E., 2010. Sorbent-Based Sampling Methods for Volatile and Semi-Volatile Organic Compounds in Air. Part 2. Sorbent Selection and Other Aspects of Optimizing Air Monitoring Methods, *Journal of Chromatography A*, 1217(16): 2685-2694.

Wu, N., Kolb, G. and Torero, J. L., 2000. The Effect of Weathering on the Flammability of a Slick of Crude Oil on a Water Bed, *Combustion Science and Technology*, 161(1): 269-308.

Yaws, C. L., 2015. Chapter 1 - Physical Properties – Organic Compounds in *The Yaws Handbook of Physical Properties for Hydrocarbons and Chemicals (Second Edition)*, Gulf Professional Publishing, Boston, pp. 1-683.

Zabetakis, M. G. and Burgess, D. S., 1961. Research on the Hazards Associated with the Production and Handling of Liquid Hydrogen, US Bureau of Mines, Pittsburgh, 50 p.

Zabetakis, M. G., 1965. Flammability Characteristics of Combustible Gases and Vapours, US Bureau of Mines, Bulletin 627, 213 p.

In-situ burning of spilled crude oil is a promising oil spill response method for potential oil spills in the Arctic. Forecasting the amount of oil that is removed during a crude oil fire on water (i.e. the burning efficiency) is, however, challenging due to a lack of theoretical understanding of the fundamental fire science behind crude oil fires on water. It is shown herein that the burning efficiency is primarily governed by the diameter of the crude oil pool fire and the complexity of the multicomponent fuel, both of which influence the ignition, flame spread and extinction processes.

**DTU Civil Engineering**  
Technical University of Denmark

Brovej, Bygning 118  
2800 Konges Lyngby

[www.byg.dtu.dk](http://www.byg.dtu.dk)

ISBN 9788778774644  
ISSN 1601-2917